

**The Missing Supernova Remnant Problem: Searching for Galactic  
Supernova Remnants with EMU & POSSUM**

by

Brianna Danielle Ball

A thesis submitted in partial fulfillment of the requirements for the degree of

Master of Science

Department of Physics  
University of Alberta

© Brianna Danielle Ball, 2023

# Abstract

Supernova remnants (SNRs) are an important part of the stellar feedback cycle that regulates star formation and influences the evolution of galaxies. They disperse the heavy elements formed in the cores of massive stars back into the interstellar medium, are responsible for forming and destroying large quantities of dust, and are believed to be the dominant source of Galactic cosmic rays. It is widely accepted that there is a significant discrepancy between the number of SNRs that have been discovered in our Galaxy and the number that models predict we should be able to detect at radio frequencies. This is often referred to as the “missing supernova remnant problem”. Most of the known Galactic SNR population has been observed in the radio and thus, discoveries of new Galactic SNRs have historically been driven by the development of more sophisticated radio telescopes. Improvements in the resolution and sensitivity of these telescopes allow us to detect smaller and/or fainter sources that likely would have been missed in previous surveys. Based on our current catalogues, the missing SNR population is believed to mostly consist of low surface brightness sources and sources located in regions with complex backgrounds and high concentrations of other Galactic radio sources, like HII regions. There may also be SNRs located at high latitudes that have been missed in previous surveys of the Galactic plane.

In this thesis, we present pilot data from the EMU and POSSUM sky surveys, conducted using the Australian Square Kilometre Array Pathfinder (ASKAP). We use this pilot data as a test case to assess the capabilities of these surveys to uncover new SNR candidates and to develop techniques that can be used to search for and study SNRs with the full surveys as data become available. The results show remark-

able success as we detect 21 SNR candidates in a field that previously only contained 7 known SNRs. If these candidates are confirmed, this will quadruple the number of SNRs in this small test field. By comparing our candidates to the known Galactic SNR population, we demonstrate that ASKAP should be capable of detecting many of the faint sources that likely comprise the majority of the missing SNR population. We believe that new SNRs discovered using these surveys will contribute to our understanding of the Galactic SNR population by allowing us to build a more complete census and conduct statistical studies of the distribution of SNRs in the Galaxy.

# Preface

This thesis is original work by Brianna D. Ball completed under the supervision of Dr. Roland Kothes and Dr. Erik Rosolowsky.

Chapter 2 has been published as Ball et al. (2023): “A catalogue of radio supernova remnants and candidate supernova remnants in the EMU/POSSUM Galactic pilot field”, *Monthly Notices of the Royal Astronomical Society*, Volume 524, Issue 1, September 2023, Pages 1396–1421, <https://doi.org/10.1093/mnras/stad1953>. I am the primary author of the paper and was responsible for writing all but Section 2.3.1. This section was written by Dr. Jennifer West and describes the data collection by ASKAP as part of the EMU and POSSUM surveys. The quality of the paper was improved by feedback from its co-authors.

*“It is of the nature of idea to be communicated: written, spoken, done. The idea is like grass. It craves light, likes crowds, thrives on crossbreeding, grows better for being stepped on.”*

–Ursula K. Le Guin, *The Dispossessed: An Ambiguous Utopia*

# Acknowledgements

First and foremost, I would like to acknowledge my supervisors Dr. Roland Kothes and Dr. Erik Rosolowsky for their support, guidance, and kindness throughout this process. I am thankful to my thesis examination committee members Dr. Rodrigo Fernández and Dr. Gregory Sivakoff for their feedback, which improved the quality of this work. I would also like to thank my collaborators from the EMU and POSSUM teams for contributing comments and ideas to the paper that became the core of this thesis.

I must acknowledge the contributions of the many individuals who worked to build ASKAP. This thesis would not be possible without the years of work that went into developing and constructing this instrument. ASKAP is located at Inyarrimanha Ilgari Bundara/the Murchison Radio-astronomy Observatory. Thus, I would also like to acknowledge the Wajarri Yamaji People as the Traditional Owners and native title holders of the Observatory site. My work was conducted at The University of Alberta, which is situated on Treaty 6 territory, traditional lands of First Nations and Métis people.

On a personal level, I would like to thank my parents for their unending support and love, and for attempting to understand my work. Finally, I would like to thank my best friend and partner, Nicholas Alger, for making every part of life infinitely better.

# Table of Contents

<b>1</b>	<b>Introduction</b>	<b>1</b>
1.1	Supernovae . . . . .	2
1.2	Supernova Remnants . . . . .	4
1.2.1	Stages of Evolution . . . . .	4
1.2.2	Morphology . . . . .	6
1.2.3	Pulsar Wind Nebulae . . . . .	8
1.3	Radio Emission from Supernova Remnants . . . . .	10
1.3.1	Synchrotron Emission from SNRs . . . . .	10
1.3.2	Polarization . . . . .	12
1.3.3	Studying SNRs in the Radio Band . . . . .	14
1.4	Emission from PWNe . . . . .	15
1.5	SNR Emission in Other Bands . . . . .	16
1.5.1	Infrared Emission . . . . .	16
1.5.2	Optical and UV Emission . . . . .	17
1.5.3	X-ray Emission . . . . .	18
1.5.4	Gamma Ray Emission . . . . .	19
1.6	The Galactic SNR Population . . . . .	20
1.6.1	The Missing SNR Problem . . . . .	20
1.6.2	Identifying Galactic SNRs . . . . .	21
1.6.3	The Distribution of Galactic SNRs . . . . .	21
1.7	ASKAP Observations with EMU & POSSUM . . . . .	24
1.7.1	The Australian Square Kilometre Array Pathfinder . . . . .	25
<b>2</b>	<b>A Catalogue of Radio Supernova Remnants and Candidate Supernova Remnants in the EMU/POSSUM Galactic Pilot Field</b>	<b>28</b>
2.1	Abstract . . . . .	28
2.2	Introduction . . . . .	29
2.3	Methods and Observations . . . . .	32
2.3.1	The EMU and POSSUM Observations with ASKAP . . . . .	32

2.3.2	Ancillary Data . . . . .	35
2.3.3	Flux Integration . . . . .	35
2.4	Results . . . . .	36
2.4.1	The EMU/POSSUM Galactic Pilot Field . . . . .	36
2.4.2	SNR Identification and Verification . . . . .	37
2.4.3	Characteristics of Known Supernova Remnants . . . . .	44
2.4.4	Spectral Indices of Known Remnants . . . . .	49
2.5	SNR Candidates . . . . .	52
2.5.1	Characteristics of SNR Candidates . . . . .	55
2.6	Discussion . . . . .	62
2.6.1	Estimating the SNR Density of the Galactic Disk . . . . .	62
2.6.2	The Known Galactic SNR Population . . . . .	64
2.7	Conclusions . . . . .	67
<b>3</b>	<b>Conclusions and Future Work</b>	<b>70</b>
3.1	Conclusions . . . . .	70
3.2	Future Work . . . . .	71
	<b>Bibliography</b>	<b>73</b>
	<b>Appendix A: Known Supernova Remnants</b>	<b>85</b>
	<b>Appendix B: Supernova Remnant Candidates</b>	<b>88</b>

# List of Tables

2.1	Known SNRs and SNR candidates in the EMU/POSSUM Galactic pilot II field. . . . .	54
-----	--	----

# List of Figures

1.1	Schematic view of a supernova remnant . . . . .	5
1.2	SNR Morphology Types . . . . .	7
1.3	Diagram of synchrotron emission . . . . .	10
1.4	The locations of known SNRs in the Galactic plane . . . . .	22
1.5	The Milky Way Galaxy . . . . .	27
2.1	The Galactic pilot field in total intensity and polarized intensity . . .	33
2.2	Faraday depth spectrum of J1551–5310 . . . . .	34
2.3	The Galactic pilot field in radio and MIR . . . . .	38
2.4	An HII region and SNR in radio and MIR . . . . .	44
2.5	Known SNRs . . . . .	45
2.6	Polarization of known SNRs . . . . .	47
2.7	Spectral indices of known SNRs . . . . .	50
2.8	SNR candidates . . . . .	56
2.9	Radio and MIR data for G327.1+0.9 . . . . .	60
2.10	Polarization data for G328.0+0.7 . . . . .	61
2.11	Comparing our SNR candidates to the known Galactic SNR population	65
A.1	Radio and MIR images of G323.5+0.1 . . . . .	85
A.2	G326.3–1.8 . . . . .	86
A.3	G327.1–1.1 . . . . .	86
A.4	G327.2–0.1 . . . . .	86
A.5	G327.4+0.4 . . . . .	87
A.6	G327.4+1.0 . . . . .	87
A.7	G328.4+0.2 . . . . .	87
B.1	Radio and MIR images of G323.2–1.0 . . . . .	88
B.2	G323.6–1.1, G323.6–0.8, G323.9–1.1 . . . . .	89
B.3	G323.7+0.0 . . . . .	89
B.4	G324.1–0.2 . . . . .	89
B.5	G324.1+0.0 . . . . .	90

B.6	G324.3+0.2	90
B.7	G324.4-0.4	90
B.8	G324.4-0.2	91
B.9	G324.7+0.0	91
B.10	G324.8-0.1	91
B.11	G325.0-0.5	92
B.12	G325.0-0.3	92
B.13	G325.0+0.2	92
B.14	G325.8-2.1	93
B.15	G325.8+0.3	93
B.16	G327.1+0.9	93
B.17	G328.0+0.7	94
B.18	G328.6+0.0	94
B.19	G330.2-1.6	94

# Chapter 1

## Introduction

Supernovae and their remnants play an important role in the formation and evolution of galaxies. They are responsible for ejecting large amounts of energy and matter into their surroundings, thereby enriching the interstellar medium (ISM) with heavy elements and playing an important role in ISM dynamics [1]. Thus, observations of supernova remnants (SNRs) and their properties are crucial in producing accurate models of interstellar phenomena, from the relatively small scale studies of molecular clouds to the large scale studies of galactic evolution.

Within our own Galaxy, we have currently only discovered 300–400 SNRs [2, 3] while various models indicate that we should be able to detect  $>1000$  at radio frequencies [4]. It is generally believed that this discrepancy is due to limitations in our observing capabilities, rather than in our understanding of the Galactic supernova rate or SNR evolution [5–7]. Indeed, while the exact size of the discrepancy is not well constrained, various modeling approaches agree that a significant discrepancy exists [4, 8–10]. Part of the solution to this “missing supernova remnant problem” lies in the detection of new Galactic SNRs using the latest generation of radio telescopes. Galactic SNRs are most often first observed at radio frequencies, so improvements in the resolution and sensitivity of these telescopes can drive new discoveries. The data used in this thesis come from one of these new telescopes, the Australian Square Kilometre Array Pathfinder (ASKAP) located in Western Australia.

This chapter will provide a brief overview to the physics governing supernova remnants as well as our current understanding of the Galactic SNR population. Section 1.1 outlines the supernova process in which SNRs are formed. Section 1.2 provides a basic introduction to supernova remnant evolution and morphology. In Sections 1.3–1.5, I describe SNR emission mechanisms across the electromagnetic spectrum and what we can learn from these multi-wavelength observations, with a focus on radio emission and how it is used to detect new SNRs. In Section 1.6, I discuss our current knowledge of the Galactic SNR population, the missing SNR problem, and how we can attempt to uncover some of these missing SNRs. Section 1.7 covers the role of the ASKAP telescope and the EMU and POSSUM radio sky surveys in our search for Galactic SNRs. Most of the research conducted for this thesis has been published in a paper, which is included as Chapter 2. Finally, in Chapter 3 I summarize our conclusions and plans for future work.

## 1.1 Supernovae

Supernova remnants are formed in the aftermath of stellar explosions known as supernovae (SNe). SNe are usually classified based on the mass of the progenitor star and the explosion mechanism. Iron core-collapse supernovae (CCSNe) occur in massive ( $\gtrsim 9 M_{\odot}$ ;  $1 M_{\odot} = 2 \times 10^{30}$  kg) stars when nuclear fusion in the core becomes insufficient to prevent gravitational collapse [11–13]. In intermediate mass stars ( $\sim 8 - 10 M_{\odot}$ ), core-collapse may occur at an earlier stage in the star’s evolution due to a process known as electron-capture. In these stars, electrons are captured by nuclei in the oxygen-neon-magnesium core, decreasing the electron degeneracy pressure that supports the core and resulting in gravitational collapse [14, 15]. In either of these cases, gravitational collapse will eventually be halted by the repulsive nuclear strong force, causing the core to rebound and send a shock wave into the infalling outer layers [16]. This shock loses energy as it propagates outward through the dissociation of heavy elements and the emission of neutrinos. As a result, the shock may

stall and must be revived through another mechanism [16].

A thermonuclear runaway (or Type Ia) supernova can occur when nuclear fusion is reignited in a white dwarf. There is not a single proposed progenitor model or explosion mechanism that can explain all observations of Type Ia SNe and different subclasses of this type of SN may exist [17]. The most prominent progenitor models are the single degenerate and double degenerate cases, though other possible progenitor scenarios have been proposed [18, 19]. In the single degenerate scenario, the white dwarf accretes matter from a larger companion star in a binary system, gaining mass until it approaches the Chandrasekhar mass limit ( $\sim 1.4 M_{\odot}$ ) [20] at which point nuclear fusion is reignited. The double degenerate scenario involves the merging of two white dwarfs in a binary system which triggers a thermonuclear explosion if the combined mass exceeds the Chandrasekhar limit. The exact explosion mechanism is currently not well understood and largely depends on whether white dwarfs explode at or below the Chandrasekhar limit [17].

Supernovae release huge amounts of energy ( $\sim 10^{51}$  erg) into the ISM. The result is an expanding shock wave that travels at supersonic speeds and sweeps up gas and dust, forming what is known as a supernova remnant. To be able to predict the number of SNRs we expect to be visible in the Galaxy, it is useful to have an estimate of the Galactic SN rate. CCSNe can occur on much faster timescales than Type Ia because massive stars have relatively short main sequence lifetimes of only a few million years. Because of this, in galaxies with active star formation, CCSNe are much more common [9]. Additionally, only white dwarfs that are in binary systems where they are able to accrete enough mass to exceed the Chandrasekhar limit will produce SNe. Thus, the SN rate depends on both the luminosity of a galaxy, which is related to the number of progenitor stars, and on its Hubble type, which is related to the galaxy's ratio of old stars to massive ones [9]. Because we have a reasonable understanding of our Galaxy's luminosity and Hubble type, we are able to make a good estimate of the Galactic SN rate. Based on these properties and observations of

other galaxies, a supernova is expected to occur in the Milky Way once every 30–50 years [9]. Statistics based on X-ray observations of Galactic SNRs appear to confirm this with an implied birth rate of 1 every 35 years [21].

## 1.2 Supernova Remnants

### 1.2.1 Stages of Evolution

A supernova remnant is formed following a supernova explosion when the cloud of expanding ejecta, traveling at supersonic velocities, interacts with the circumstellar/interstellar medium (CSM/ISM). This large release of energy forms a shock front that sweeps up interstellar material and magnetic fields as it travels. As the amount of swept up mass becomes comparable to the ejecta mass, the shock decelerates. Eventually, radiative losses become significant, the shock’s energy is dissipated, and the remnant merges with the surrounding ISM [22]. The lifespan of an SNR is generally broken up into the following phases.

**Ejecta-Dominated or Free Expansion phase:** In this phase, the remnant is able to expand freely, without significant deceleration, as the mass of the ejecta dominates over the mass swept up by the forward shock. The speed of the expansion is typically on the order of  $\sim 10,000$  km/s [23]. The swept up material, which is accelerated, compressed, and heated, pushes back on the ejecta and creates a reverse shock, which propagates inward in the frame of the expanding shock [24]. Between the forward shock and the reverse shock lies a contact discontinuity, separating the colder ejecta from the hotter shocked ISM, as shown in Figure 1.1. Most of the explosion’s kinetic energy is contained in the freely expanding, cold ejecta [25]. This phase typically lasts for a few hundred years, though this can vary depending on the density of the surrounding ISM [23]. SNRs can be difficult to detect in this phase as they are relatively small.

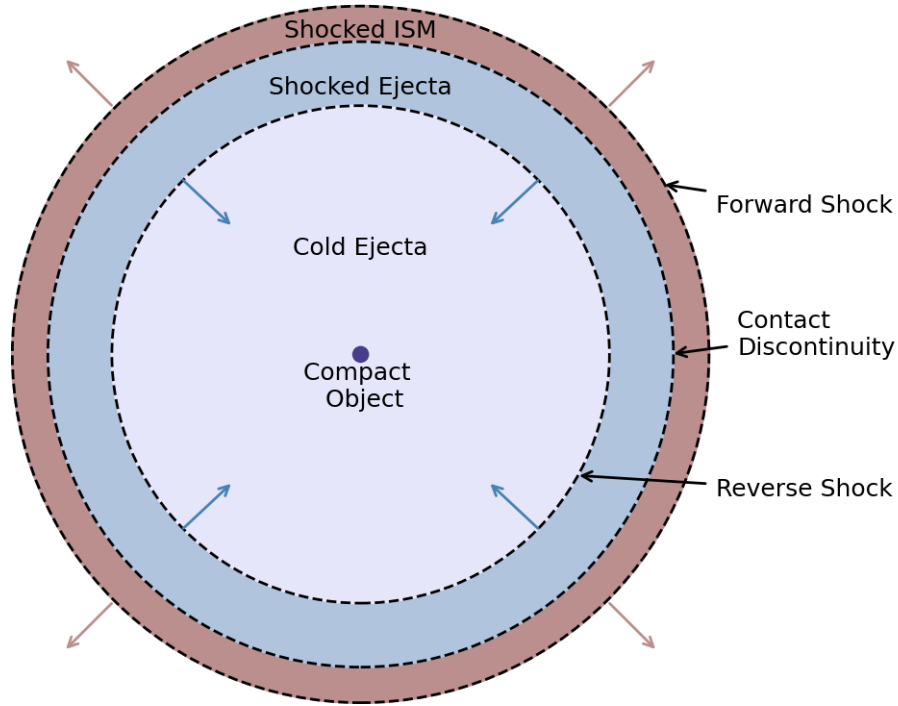


Figure 1.1: Schematic view of a supernova remnant. The forward shock expands into the ISM, sweeping up interstellar material as it travels. The reverse shock travels back into the remnant and heats the ejecta. CCSNe will also leave behind a compact object, typically a neutron star, that will initially be found near the remnant’s centre, though it may travel over time.

**Adiabatic or Sedov-Taylor (S-T) phase:** Eventually the swept up mass will begin to dominate over the ejecta mass, slowing the shock. The explosion energy is now mostly contained in the hot, expanding shell [25]. Radiative losses are still insignificant compared to the internal and kinetic energy of the shell, thus the expansion is considered to be adiabatic. This is referred to as the S-T phase because the shock wave can be well-described by a self-similar (Sedov-Taylor) solution [26]. The reverse shock propagates towards the centre of the remnant and results in the destruction of large quantities of dust. This phase typically lasts for 20–80 kyrs, though the exact timescale continues to depend on local ISM conditions [10].

**Radiative Pressure-Driven Snowplow:** When the shock velocity has decelerated to  $\sim 200$  km/s, radiative energy losses increase significantly [25]. This is because

the drop in the gas temperature allows electrons to recombine to form atoms, producing bright optical and ultraviolet emission in the form of recombination lines. This results in significant radiative losses, cooling the shock wave even further and resulting in a runaway feedback loop [23, 27]. The cool shell continues to expand, now pushing a significant amount of ISM material, like a snowplow. This phase is governed by conservation of momentum, as conservation of energy can no longer be assumed due to substantial radiative losses [25].

**Dissipation or Merging phase:** When the blast wave velocity approaches the sound speed of the surrounding gas, the shock wave slowly disappears, the shell expands subsonically, and eventually the remnant merges with the ISM [25]. This typically occurs after around 1 Myrs [23].

The amount of time an SNR spends in each phase mainly depends on the local environment, particularly the CSM/ISM density and the ambient magnetic field. Typically, SNRs are detected in the S-T phase, where they spend most of their radio visible lifetimes [10, 28, 29]. Once a remnant reaches the radiative phase, it is expected to lose energy quickly and fade, becoming undetectable. While SNRs may not fully merge with the ISM for 1 Myrs, they typically become undetectable within  $\sim 100$  kyrs.

### 1.2.2 Morphology

Determining the SN origin type of an SNR can be difficult and usually requires X-ray or optical spectroscopy to probe the ejecta composition [25]. Unless a neutron star or PWN is found within the remnant, it is generally not possible to infer the SN origin type from radio observations alone [30]. Therefore, supernova remnants are typically classified based on a more readily observable property, their radio morphology. There are four main types of radio SNR morphology:

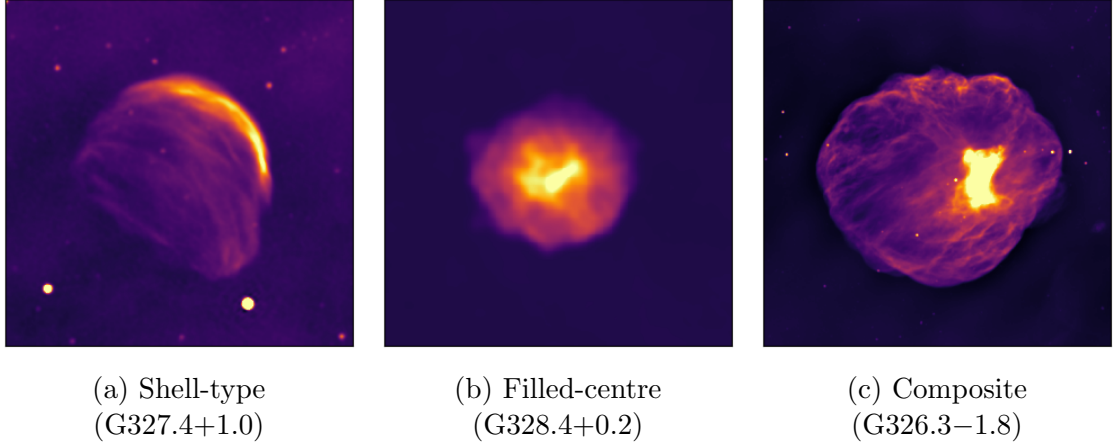


Figure 1.2: SNR images demonstrating radio SNR morphologies. These are radio images of known SNRs from the ASKAP pilot data at a frequency of 933 MHz.

1. Shell-type: These are the most common type of remnant, making up around 80% of the known Galactic SNR population [31]. Because we are seeing a two-dimensional projection of a spherical shell, the emission appears as a brightened outer ring with well-defined edges, produced by the shock. These shell structures are often asymmetric, as in the SNR shown in Figure 1.2a, due to variations in the surrounding gas density and interstellar magnetic fields [30]. The magnetic field inside the shell will be strongest where the SNR is expanding perpendicular to the ambient magnetic field and thus, the shell may exhibit a bilateral structure with brighter emission coming from regions where the magnetic field is stronger [32].
2. Filled-centre: For these remnants, there is no visible emission coming from the outer shell. Instead the emission comes from a smaller nebula located within the SNR, as seen in Figure 1.2b, known as a pulsar wind nebula (PWN, see Section 1.2.3). This type of SNR can only form when a pulsar is created in a core-collapse SN explosion. They are the rarest type of SNR, comprising only 3% of the Galactic SNR population [31]. The shell may be absent because it was never formed, due to a low ambient density, or it may have already disappeared,

fading into the surrounding ISM [30]. In some cases, the PWN may have already escaped its host SNR.

3. Composite (or Plerionic composite): As the name suggests, these sources are a composite of the shell-type and filled-centre type. Both the PWN and the outer shell are visible at radio frequencies, as illustrated in Figure 1.2c. Around 13% of known Galactic SNRs exhibit a composite morphology [31].
4. Mixed-Morphology (or Thermal composite): This class of remnants, first proposed by Rho & Petre [33], are sources that exhibit a shell-type morphology when viewed in the radio and a filled-centre morphology when viewed in X-rays. These remnants are typically found interacting with molecular or HI clouds [33]. The cause of this morphology is not well understood, but several hypotheses have been suggested to explain this phenomenon. One possibility is that they are remnants expanding in cloudy environments, where the X-ray emission is produced through the gas evaporated from these clouds [30]. Another hypothesis is that while the shell may have cooled so that it is no longer X-ray detectable, thermal conduction in the hot interior produces “fossil” radiation [33]. According to SNRcat [3], there are 45 mixed-morphology or possible mixed-morphology SNRs and SNR candidates.

### 1.2.3 Pulsar Wind Nebulae

A pulsar is a rapidly rotating, highly magnetized neutron star that can be created in a core-collapse supernova explosion. The pulsar emits a magnetized, relativistic wind that travels through the slower moving supernova ejecta. This forms a termination shock where electron-positron pairs can be re-accelerated to relativistic velocities, producing a synchrotron emitting nebula known as a pulsar wind nebula (PWN) [34]. PWNe appear soon after the creation of the pulsar. We expect young PWNe to appear in the radio as roughly spherical nebulae located near the center of a shell-

type remnant. However, in observations of young SNRs, we almost never see both the PWN and the shell [34].

Initially, the PWN expands supersonically through the cold, unshocked ejecta [35] and is not influenced by the SN shock. As discussed in Section 1.2.1, the deceleration of the forward SN shock leads to the formation of a reverse shock, which moves back through the remnant and heats up the ejecta. Eventually, typically after a few thousand years [36], the reverse shock will interact with the PWN, compressing the bubble and producing oscillations. Due to asymmetries in SN explosions, pulsars are often born with a velocity kick of several hundreds of km/s. As a result, by the time the reverse shock encounters the PWN, the PWN has usually traveled away from the remnant's center. Thus, this interaction typically occurs asymmetrically and over a period of time, with timescales of up to several kyrs [34]. The oscillations that are produced in the PWN can impact both its position and morphology, causing distortions in its previously spherical shape [35]. An example of a PWN that has been observed to have undergone this type of asymmetric interaction with the reverse shock of its host SNR, G327.1–1.1, can be found in Temim et al. [37].

After the reverse shock has passed, the pulsar continues to power the PWN, which continues to expand into the hot shocked SN ejecta, though now at subsonic speeds [35]. The next phase of the pulsar's life depends on its velocity and spin down luminosity [34]. If the pulsar has a high enough velocity, it may have traveled far enough that it has left behind its original wind bubble, leaving behind what is known as a relic PWN. In this case it may generate a new, smaller PWN at its current position [35]. Some pulsars have high enough velocities that they are able to escape their host SNRs entirely, traveling supersonically through the ISM. This scenario may produce what is known as a bow-shock nebula, where the pulsar drags a PWN along with it as it travels, leaving behind a long tail of radio emission.

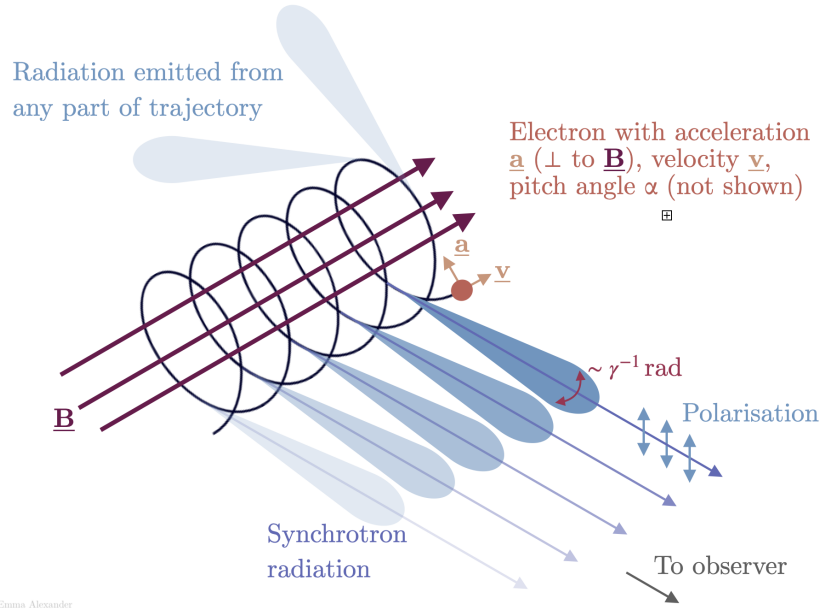


Figure 1.3: Diagram of synchrotron emission showing the helical path traveled by an electron around the magnetic field lines. An observer will only see the radiation emitted from the particle when the beam is aligned with the observer’s line of sight. Image by Emma Alexander. (Available from [https://commons.wikimedia.org/wiki/File:Emmaalexander\\_synchrotron.png](https://commons.wikimedia.org/wiki/File:Emmaalexander_synchrotron.png); CC-BY)

## 1.3 Radio Emission from Supernova Remnants

SNRs emit across all wavelengths, but they are most readily observed in the radio. Approximately 95% of the known Galactic SNR population has been observed in the radio [30]. Part of the challenge of finding new SNRs is distinguishing them from other radio-emitting nebulae, such as HII regions and planetary nebulae. Luckily, SNRs and HII regions produce radio emission through different mechanisms so we can identify SNRs by looking for signatures of nonthermal synchrotron emission. Extended Galactic radio sources with steeply decreasing spectra and linear polarization are almost definitely SNRs.

### 1.3.1 Synchrotron Emission from SNRs

Nonthermal synchrotron emission is created when charged particles moving at relativistic speeds interact with a magnetic field. The uniform circular motion caused by

the magnetic field combined with a particle’s velocity along the field lines causes the particle to move in a helical path around the magnetic field lines [38]. This acceleration results in the emission of photons with frequencies related to the energies of the particles.

Due to relativistic effects, in an observer’s frame of reference, synchrotron radiation from a single particle will appear to be beamed in the direction of the particle’s motion. The observer will only see significant radiation when the particle’s velocity vector lies within an angle of about  $1/\gamma$  to the observer’s line of sight, where  $\gamma$  represents the Lorentz factor [39]. This beaming effect is shown in Figure 1.3. The pitch angle  $\tilde{\alpha}$  refers to the angle between the magnetic field vector and the velocity vector of the particle. As the particle spirals along the magnetic field lines, the emitted radiation will be confined within an angle of  $1/\gamma$  to a “velocity cone” of half-angle  $\tilde{\alpha}$  [38].

In supernova remnants, charged particles are accelerated to relativistic speeds through multiple crossings at the shock front in a process known as diffusive shock acceleration (DSA) or first-order Fermi acceleration [30, 40]. The fast moving particles generate Alfvén waves, wave-like variations in the magnetic field, that the particles scatter off of, preventing them from escaping the shock front and allowing them to reach relativistic speeds [41, 42]. This acceleration mechanism results in an energy distribution of relativistic electrons that is well-approximated by a power-law distribution [39]:

$$n(E)dE \propto E^{-p}dE,$$

where  $n(E)$  represents the number of particles with energy  $E$ . This produces emission that also follows a power-law distribution:

$$S(\nu) \propto B^{(p+1)/2}\nu^{-(p-1)/2},$$

where  $S(\nu)$  is the flux density at frequency  $\nu$  and  $B$  represents the magnetic flux density [39]. Radio spectra are usually characterized by a spectral index  $\alpha$  relating

the frequency to the flux density as  $S(\nu) \propto \nu^\alpha$ . The synchrotron spectral index can then be written:

$$\alpha = -\frac{1}{2}(p - 1),$$

and thus depends only on the particle energy distribution. Most shell-type SNRs have spectral indices in the range  $\alpha = -0.5 \pm 0.2$  [30]. Because most SNRs have steep synchrotron indices, they are usually much brighter, and therefore easier to detect, at low radio frequencies.

### 1.3.2 Polarization

Synchrotron emission from SNRs can be distinguished from thermal radio emission by its characteristic linear polarization. The polarization state of light describes how the electric field waves are oriented in space. A set of values known as the Stokes parameters,  $I$ ,  $Q$ ,  $U$ , and  $V$ , can be used to characterize the polarization state of light. Stokes  $I$  represents the total intensity, Stokes  $Q$  and  $U$  describe the linear polarization, and Stokes  $V$  describes the circular polarization. In particular,  $Q$  represents the degree to which the light is horizontally ( $Q > 0$ ) or vertically ( $Q < 0$ ) polarized,  $U$  represents the light's tendency towards  $+45^\circ$  polarization ( $U > 0$ ) versus  $-45^\circ$  polarization ( $U < 0$ ), and  $V$  describes whether the light is more right-hand circularly polarized ( $V > 0$ ) or left-hand circularly polarized ( $V < 0$ ) [43]. The degree of polarization  $P$  can then be written as [38]:

$$P = \frac{\sqrt{Q^2 + U^2 + V^2}}{I}.$$

Polarization can carry information about how the light was created. Synchrotron emission from a population of particles along a highly-ordered magnetic field should be linearly polarized, meaning the electric field is confined to a plane along the direction of propagation. For a single relativistic particle, synchrotron emission is elliptically polarized. It may be right-handed or left-handed, depending on whether the line of sight lies just inside or outside the velocity cone [38]. For a population of high-

energy particles, the distribution of pitch angles is assumed to be isotropic [39]. When averaging over the distribution of particles (pitch angles), the elliptical components of the polarization cancel out as the emission cones will contribute equally from both sides of the line of sight [38]. This results in partial linear polarization.

The degree of linear polarization for a power-law energy distribution of electrons, as defined in Section 1.3.1, can be written as [39]:

$$\Pi = \frac{p + 1}{p + 7/3}.$$

Thus, for a typical SNR with a spectral index of  $\alpha = -0.5$  ( $p = 2$ ), we would expect the degree of polarization to be around 70%.

In reality, the emission will experience some amount of depolarization as it travels to the observer. When we are observing within our own Galaxy, these effects can be quite significant. Particularly of concern to us is differential Faraday rotation. A linearly polarized wave can be broken down into a right circular polarization component and a left circular polarization component. When passing through an external magnetic field, these components will travel with different velocities. This results in a rotation of the plane of polarization known as Faraday rotation [38]. The degree of rotation is proportional to the wavelength squared and thus, depolarization becomes more significant at low frequencies [39]. The strength of this effect is characterized by the rotation measure ( $RM$ ) [39]:

$$RM = 8.12 \times 10^3 \int_0^l N_e B_{\parallel} dl,$$

where  $N_e$  represents the electron number density in particles  $\text{m}^{-3}$ ,  $B_{\parallel}$  represents the parallel component of the ambient magnetic field in teslas, and integration is performed along the line of sight in units of parsecs. Observations have shown polarization of Galactic SNRs can be up to 70% [44]. We are more likely to detect polarization from sources that are nearby or that are located at a far distance from the Galactic plane, where the line of sight to the source traverses less interstellar

material. Because of the frequency-dependence of these effects, we are more likely to detect polarization when observing at higher radio frequencies.

### 1.3.3 Studying SNRs in the Radio Band

As discussed, radio observations are a powerful tool for detecting new supernova remnants, both within our own Galaxy and within other Local Group galaxies. In addition to making new discoveries, radio observations can be used to study properties of SNRs and their environments. For example, the most commonly used method for determining distances to SNRs is through the measurement of neutral hydrogen (HI) absorption spectra. Additionally, having a larger sample of remnants in the radio allows for statistical studies to be performed, analyzing population characteristics such as sizes, distances, ages, and spectral indices [45, 46].

Radio synchrotron emission can be used to study the shock front and its role as a particle acceleration mechanism, as well as the orientation and strength of interstellar magnetic fields [30]. As an example, while most SNRs have radio spectral indices around  $-0.5$ , consistent with the predictions of DSA, there are clear exceptions that cannot be accounted for by measurement errors. In particular, young remnants tend to have steeper radio spectra, while mixed-morphology remnants tend to have flatter spectra [25]. The causes of these trends are not currently well understood, but these outliers have prompted further research studying the SNR shock process. Potential explanations include differences in DSA efficiency, the amount of compression by the shock, and post-shock turbulent reacceleration [25]. Further insights into the synchrotron process at the shock front may be gained through studying these anomalies.

The magnetic field responsible for producing synchrotron emission in SNRs is the ambient interstellar field, which is compressed by the shock. The change in rotation measure across the remnant can be used to determine the orientation of the ambient magnetic field [32]. The energy from synchrotron radiation is primarily contained in the kinetic energy of the relativistic particles and in the magnetic field. Thus, if we

know the approximate energy requirements of a radio-emitting synchrotron source, we can make an estimate of the magnetic field strength [30]. Overall, radio observations have been particularly useful for studying SNR shocks and the environments they interact with, as well as for conducting larger population studies of SNR characteristics.

## 1.4 Emission from PWNe

PWNe also produce synchrotron emission at radio frequencies. The interaction of the pulsar wind with the supernova ejecta accelerates particles to relativistic speeds, in a similar but not identical process to that which occurs at the SN shock front, resulting in a different particle energy distribution. PWNe typically exhibit broken power-law spectra with flatter radio indices and steeper X-ray spectra [47]. A “cooling break” in the spectrum is expected because high-energy synchrotron-emitting particles have relatively short lifetimes compared to the lifetime of the PWNe. However, the breaks typically observed in PWNe spectra are not consistent with what is predicted by synchrotron cooling and thus are not well understood [34, 35]. Most PWNe have radio spectral indices within the range  $-0.3 < \alpha < 0.0$ , though in some cases they can be as steep as  $-0.7$  [34]. These steep spectra PWNe may have an additional acceleration mechanism, perhaps related to the reverse shock, that re-accelerates particles, but this is an open question [34].

As a PWN ages, it is thought that its spectrum shifts from being synchrotron dominated to being inverse Compton (IC) dominated. When relativistic electrons collide with low energy photons, they may transfer energy to the photon to produce X-ray or gamma ray emission in a process known as IC scattering. IC scattering is the dominant emission mechanism for PWN at high frequencies, and thus this shift represents a transition towards a gamma ray dominated spectrum [48]. In fact, it may be possible to classify the evolutionary state of PWNe based on their X-ray to gamma ray luminosity ratios [49].

## 1.5 SNR Emission in Other Bands

While supernova remnants are most often discovered in the radio, they emit across the entire electromagnetic spectrum. Although observations in other bands are generally not as useful for detecting new SNRs, they can be used to study SNR properties such as ejecta composition, dust production, density, temperature, and shock velocity.

### 1.5.1 Infrared Emission

Supernova remnants produce infrared (IR) emission mostly in the form of thermal continuum emission from heated dust grains and line emission from large molecules like polycyclic aromatic hydrocarbons (PAHs). For remnants that are very bright, synchrotron emission may also be detected at IR frequencies. The dominant emission mechanism for a particular remnant primarily depends on its evolutionary stage with emission from older remnants being dominated by line emission and emission from younger remnants being dominated by thermal continuum [50].

Core-collapse SNe and their remnants are known to produce significant quantities of dust. SNRs are also believed to be responsible for the destruction of large amounts of dust, as only a fraction of the dust survives the passage of the reverse shock. The balance between these processes has important implications for the impact of SNe on ISM evolution. The amount of dust that survives depends on properties like the characteristics of the explosion, the size distribution and composition of the dust grains, and the density of the surrounding ISM. Model predictions can vary greatly based on these variables from less than 1% to greater than 99% [51–54]. However, it should be noted that for SNRs in which significant dust masses have been observed, the dust found has not yet been processed by the reverse shock, indicating that the reverse shock likely plays a significant role in dust destruction [50]. It is generally believed that SNe are net destroyers of dust under standard ISM conditions [55, 56]. In addition, most of the dust that does survive is in a relatively cold state [56].

Most SNRs are not detectable at IR frequencies. Confusion with thermal emission from the ISM makes the IR detection of Galactic SNRs even more challenging. Because of this, IR surveys of Galactic SNRs use catalogues of known remnants, discovered in the radio, to search for IR counterparts. These studies have typically found detection rates of around 20–30%, with detections being more common in younger SNRs [57–59].

Perhaps the most well-studied SNR in the infrared is the core-collapse remnant G111.7–2.1, also known as Cassiopeia A (Cas A). Cas A is young ( $<400$  yrs [60]), relatively nearby, and bright making it an optimal candidate for IR observations. IR studies of Cas A have been an important link between models of dust formation and destruction in SNRs and observations [53, 61, 62]. For example, the IR emission from Cas A indicates that the dust production mostly occurred after the SN explosion, in the ejecta, and that this dust is mostly composed of silicates [25, 61]. Cas A also has a developed reverse shock meaning we are able to estimate pre- and post-shock dust masses and therefore dust destruction efficiency, which Priestley et al. [62] found to be around 92–98%. These types of findings are important for understanding the role that core-collapse SNe play in the Galactic dust budget. Generally, observations indicate that Type Ia SNe are not large producers of dust and that the dust grains they do produce are largely destroyed by the reverse shock [50].

### 1.5.2 Optical and UV Emission

Optical and ultraviolet (UV) emission from SNRs, in the form of spectral lines, can provide valuable information about remnants’ composition and evolutionary state, and can be used to estimate distances. This line emission comes from both the shock front itself and the cooling recombination zone downstream from the shock front [63]. There are at least 250 spectral lines in the IR to UV range that have been identified in SNRs [64]. For older SNRs that have entered the radiative phase, line emission from shocks plays an important role in cooling. When the primary shock encounters

denser regions in the ISM, secondary shocks with shorter cooling times are created in these denser regions [63]. These secondary shocks become radiative and their spectra contain information about parameters of the shock and the ISM.

SNR line emission typically has a filamentary or clumpy morphology, likely related to the distribution of dense gas [65]. Non-radiative shocks, shocks for which the radiative cooling time is long compared to dynamical timescales, appear in the optical as faint filaments of  $H\alpha$  emission [63]. These filaments are particularly of interest as the width of the  $H\alpha$  line can be used to obtain measurements of the shock velocity, which then can be used to obtain distance estimates.

Extinction effects make Galactic observations of SNRs in the optical and UV bands challenging and generally they are only possible for remnants that are nearby or located at latitudes far from the Galactic plane. Around 30% of known Galactic radio SNRs have been detected in the optical [31] and even fewer have been detected in the UV. Observations show that Galactic SNRs may be most successfully detected in the UV at high latitudes [66].

### 1.5.3 X-ray Emission

Approximately 40% of radio SNRs have also been detected in X-rays [31]. X-ray emission from SNRs can be produced both thermally, from the shock-heated plasmas, and non-thermally, from the shell in the form of synchrotron emission. The thermal emission is a combination of bremsstrahlung and line emission. For young remnants, line emission from alpha-elements (O, Ne, Mg, Si, S, Ar, Ca) and iron-group elements (mainly Fe, Ni) dominates and can provide useful information about the composition and spatial distribution of these heavy elements in SN ejecta [67]. Core-collapse and thermonuclear SN ejecta have different compositions and morphologies, which can be studied using their X-ray spectra.

For older SNRs, line emission becomes less prominent and X-ray spectra are dominated by emission from the shocked CSM/ISM [67]. The slowing of the shock re-

sults in cooling of the plasma and therefore the X-ray emission is softer. Eventually UV line emission dominates, resulting in runaway radiative cooling and the formation of filaments that are too cool to emit in X-rays. As discussed in Section 1.2.2, mixed-morphology SNRs are sources that appear to be shell-type in the radio but centre-filled in X-rays. One possible explanation for this is that the shell has become too cool to emit X-rays but the shocked ejecta in the interior is still hot enough to produce thermal X-ray emission.

X-ray synchrotron emission can be produced by PWNe and in the shells of young SNRs. The maximum energy particles obtain through acceleration at a shock front may be limited by either time or radiative losses. The corresponding synchrotron cut-off frequency is said to be either age-limited or loss-limited [68]. Because of this, high shock velocities ( $>2000$  km/s) are required and only the shells of young SNRs can produce X-ray synchrotron emission [69].

### 1.5.4 Gamma Ray Emission

Supernovae and their remnants are believed to be responsible for producing the majority of cosmic rays (CRs), highly energetic particles moving at ultra-relativistic speeds, particularly at energies below a spectral feature known as the “knee”, around  $10^{15}$  eV [70]. DSA at the shock front combined with magnetic field amplification is believed to be capable of accelerating protons to the necessary velocities [71]. These high energy protons interact with the ISM to produce pions, which then decay into gamma rays. Gamma radiation can also be produced through inverse Compton scattering between ultra-relativistic electrons and cosmic microwave photons, a process that is especially efficient at TeV energies [71]. Around 10% of radio SNRs have been detected in gamma rays using data from the Fermi Large Array Telescope [72].

The gamma ray spectra of SNRs can be very diverse with spectral shapes largely influenced by SNR evolutionary state and local ISM density. According to Yuan et al. [73], in low density environments IC emission dominates the gamma ray spectrum,

while in high density environments pion-decay dominates. Gamma radiation at GeV energies is detected in middle-aged SNRs that are interacting with molecular clouds. This emission is dominated by pion decay and is evidence of the acceleration of CRs in supernova shocks [71]. At TeV energies, we mostly detect young SNRs that have also been identified as sources of non-thermal X-ray emission [71].

Observations of the evolution of gamma ray spectra can also be used to study the DSA process and how acceleration efficiency changes as SNRs evolve [71]. Generally, acceleration efficiency decreases as the shock slows and the drop in the magnetic field allows particles to escape [74]. To account for the Galactic CR flux, around 10% of the SN energy must be converted to cosmic rays, and thus the efficiency of DSA is an important factor. While observations generally support SNRs as a dominant source of cosmic rays [75], there are still open questions related to acceleration efficiency and the maximum energy of shock-accelerated particles [71], whether SNRs truly are the dominant source of CRs up to the knee and potentially beyond [71, 76], and the role of line of sight effects when observing in our own Galaxy [76].

## 1.6 The Galactic SNR Population

### 1.6.1 The Missing SNR Problem

It is widely accepted that there is a discrepancy between the number of SNRs we have observed in the Galaxy and the number that are believed to exist [5, 77–79]. This discrepancy is difficult to exactly quantify due to challenges that arise from observing sources in the Galactic plane. Specifically, the radio visible lifetime of an SNR varies depending on local properties of the ISM, particularly the density and magnetic fields. Radio visibility is also affected by the presence of other radio-bright sources, mainly HII regions. Quantitative estimates of the size of the Galactic SNR population will be further explored in Section 2.2.

Based on X-ray observations, the young Galactic SNR population is believed to

be mostly complete [21]. Thus, we expect the missing SNR population to mainly be comprised of sources that are old and faint. These SNRs will vary in angular size, depending on the distance they are located at and the local ISM environment. It is also likely that we will find sources located at high latitudes, above or below the Galactic plane, that may not have been covered by previous surveys.

### 1.6.2 Identifying Galactic SNRs

Galactic supernova remnants are almost always detected in the radio. The biggest challenge is distinguishing them from other extended Galactic radio sources, most of which are HII regions. HII regions are clouds of hydrogen that have been ionized by hot, massive stars, and they can produce strong radio emission through thermal processes. To distinguish between SNRs and HII regions, we rely on the fact that they produce radio emission through different mechanisms that have distinct radio signatures. Generally, SNR candidates are first identified by comparing radio and mid-infrared (MIR) fluxes. As discussed in Section 1.5.1, most SNRs are not detectable in the IR and those that are detected are usually young and relatively faint. Contrarily, HII regions contain large quantities of hot dust and large IR-emitting molecules and are therefore IR bright. Therefore, a lack of IR emission indicates that a source is probably not an HII region. Additionally, because radio emission from SNRs is non-thermal synchrotron emission and radio emission from HII regions is thermal, we can also use polarization and spectral indices to distinguish between these two types of sources. Further descriptions of how we use these techniques to identify SNR candidates are provided in Section 2.4.2.

### 1.6.3 The Distribution of Galactic SNRs

We expect the distribution of core-collapse SNRs to be closely related to the distribution of young, massive stars and star forming regions. We expect a higher density of SNRs along spiral arms and that the remnants will mostly be confined to the Galactic

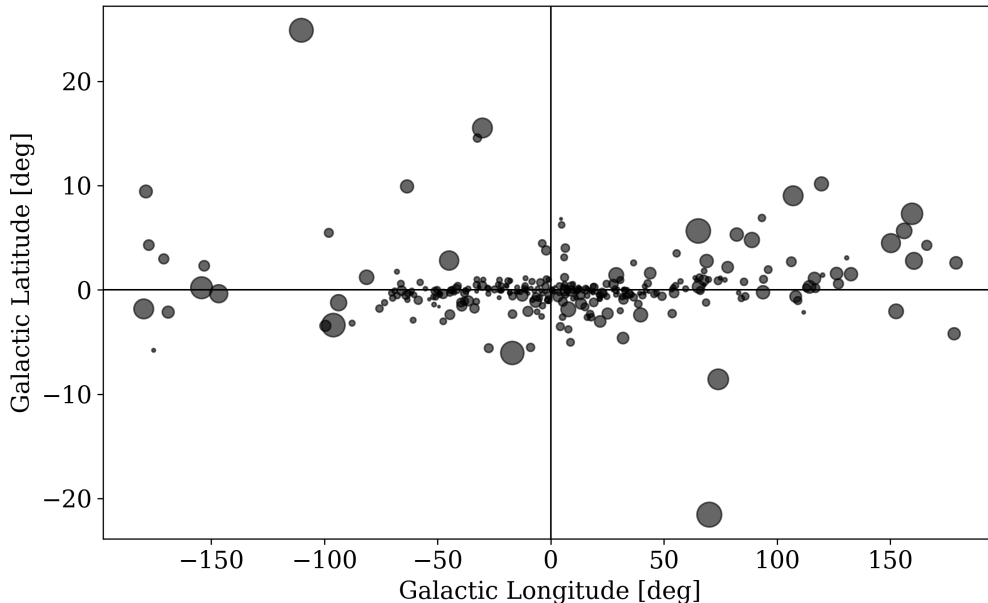


Figure 1.4: The locations of known SNRs in the Galactic plane. The sizes of the points are proportional to the radio angular sizes of the SNRs. Data are taken from Green [2].

plane. Type Ia remnants may be located at further distances, as their progenitors have had more time to travel through the ISM. From Figure 1.4 we see that indeed the majority of known remnants are located near the Galactic plane, though there are outliers at high latitudes. However, it is important to note that selection effects may also play a role here as surveys of the Galactic plane often do not cover these higher latitude regions. It is also true that the majority of known remnants are located in denser regions, particularly around the Galactic centre. Looking towards the Galactic centre we have a longer line of sight through the Galaxy, meaning that our field of view encompasses a larger volume of the Galaxy and thus a higher quantity of remnants.

### Determining Distances to Galactic SNRs

Having accurate distance measurements to Galactic SNRs is highly desirable, as they can provide information about other physical properties such as size, age, and lu-

minosity, and allow us to map the locations of SNRs within the Galactic disk. Determining distances to remnants is challenging and these estimates are often poorly constrained. Many different techniques for estimating SNR distances have been explored as there is no one method that can be applied to every source. The most reliable technique involves measuring radial velocities and proper motions [25]. The challenge with this method is that radial velocities are determined through the measurement of Doppler shifts of hydrogen emission lines and thus require optical observations, which cannot be obtained for most Galactic SNRs. Radio recombination lines (RRLs) cannot be used as RRLs from SNRs are expected to be very weak [80] and detection of RRLs indicates that the emission is likely thermal [6]. When RRLs are used for finding SNR distances, it is generally to determine the distance to an HII region that can be shown to be physically associated with the SNR, thus providing an indirect distance estimate [81].

Distances to Galactic SNRs are most commonly estimated by studying the 21 cm spectral line, created through absorption by clouds of neutral hydrogen (HI) [82]. The distance to the cloud can be determined through the shift in the absorption line. If this line is present in the SNR spectrum, then it must lie beyond the absorbing cloud. If it is not, it must be closer than the cloud. Thus, constraints can be placed on the locations of SNRs that lie between clouds of HI. However, as warm HI can also produce 21 cm emission, this technique only works if the SNR is bright enough that SNR absorption can be distinguished from HI self-absorption.

The radio surface brightness to diameter, or  $\Sigma - D$ , method assumes that the surface brightness of an SNR ( $\Sigma$ ) is related to its physical diameter ( $D$ ) through

$$\Sigma = AD^\beta$$

with constants  $A$  and  $\beta$  calibrated using SNRs with known distances [83]. The use of this technique is controversial, however, as SNR properties can be highly variable and there is a large scatter in the  $\Sigma - D$  data distribution. Additionally, observational

selection biases may mean that a non-representative sample was used for calibration [79]. In fact, when compared to more reliable methods, this technique has been shown to produce an average discrepancy of around 50% [46].

A variety of other techniques have been utilized to estimate SNR distances. These include HI emission at the shock front, interstellar X-ray or optical absorption, and association with an object of known distance such as a spiral arm, HII region, or molecular cloud [25]. All of these techniques can only be applied in the right conditions. As a result, only around half of Galactic SNRs have distance estimates included in the catalogues [2, 3]. This presents a huge challenge to studying SNRs and their properties, as well as their distribution throughout the Galaxy. Because we do not have a complete understanding of the properties of known Galactic SNRs, this limits our ability to characterize the missing SNR population.

## 1.7 ASKAP Observations with EMU & POSSUM

This thesis uses data from EMU (The Evolutionary Map of the Universe) and POSSUM (The Polarization Sky Survey of the Universe’s Magnetism), radio surveys of the southern sky that are being observed with ASKAP. EMU is a radio continuum survey centred around  $\sim 1$  GHz that aims to compile a census of radio sources [84]. POSSUM is a continuum polarization survey aimed at studying magnetic fields through the measurement of Faraday rotation measures [85]. The surveys are being observed commensally and should cover around 60% of the Galactic plane.

New SNR discoveries have generally been driven by technological improvements. In the northern sky, recent SNR candidate lists have been compiled using the THOR [6] and GLOSTAR [86] surveys, conducted with the VLA (Very Large Array). The last significant southern Galactic plane survey was the second epoch Molonglo Galactic Plane Survey (MGPS-2) conducted using MOST (the Molonglo Observatory Synthesis Telescope) [78], which uncovered 23 SNR candidates of angular sizes  $\geq 5'$ . More recently, GLEAM, a low-frequency southern sky survey, was used to perform follow-

up work on 101 candidates, definitively confirming 10 as SNRs, but this work was limited by its relatively poor angular resolution of  $2'$  [87]. The EMU and POSSUM surveys will offer improved resolution and sensitivity when compared to these previous southern sky radio surveys, allowing for the detection of smaller and fainter sources. ASKAP also was designed to have a large field of view and thus a fast survey speed without sacrificing sensitivity. This is important for detecting old (faint) SNRs as well as high latitude SNRs that are located at far distances from the Galactic plane.

### 1.7.1 The Australian Square Kilometre Array Pathfinder

ASKAP is an interferometer comprised of 36 12-meter dishes with baselines of up to 6 km. An interferometer is a type of telescope that combines the signals from a set of antennas to produce images with the angular resolution of a much larger telescope. The angular resolution of a single dish telescope can be approximated using the Rayleigh criterion as:

$$\theta \approx \frac{\lambda}{D}$$

where  $\lambda$  is the wavelength of light being observed,  $D$  is the diameter of the telescope, and  $\theta$  is the angular resolution with a smaller value indicating smaller sources can be resolved. Because radio wavelengths are long, this means large telescopes are required to achieve a high angular resolution, which presents practical construction challenges. For an interferometer, the resolution depends on the baseline, the separation between the antennas, rather than the size of the individual dishes. Thus, we are able to achieve the resolution of a much larger single dish telescope than we could ever realistically build. The main drawback to using interferometers is that, because there are gaps in the light collecting surface, they do not collect as much light as the single dish equivalent would. When we observe extended diffuse structures, missing short spacings as a result of incomplete coverage can create negative bowls of emission around bright peaks [88]. This presents a challenge to our work, in particular to the observations of large, faint remnants, which appear as extended diffuse sources. One solution

to this problem is to fill in the missing emission by supplementing interferometer data with observations from a single dish telescope [89, 90].

Each ASKAP antenna is equipped with a phased array feed (PAF), a checkerboard of 188 individual receivers. The PAF signals are digitized and combined to simultaneously form 36 separate beams [91]. This allows the telescope to collect more information from each antenna, increasing the field of view and therefore the survey speed. ASKAP has an instantaneous field of view of around  $30 \text{ deg}^2$  [91], making it a particularly effective tool for conducting large-scale, high resolution surveys at a fast speed.

ASKAP is a relatively young instrument, with pilot observations taking place from 2019–2022 and full operations commencing in late 2022. The data used in this thesis comes from the second pilot observations of the EMU and POSSUM surveys. The coverage of our small Galactic pilot field, which we use as a test case for work with the full data, is shown in Figure 1.5. The full surveys will take place over the next several years, with data being released as it is collected. We hope that the techniques and procedures developed in this project will serve as groundwork for future projects studying SNRs with the full surveys.

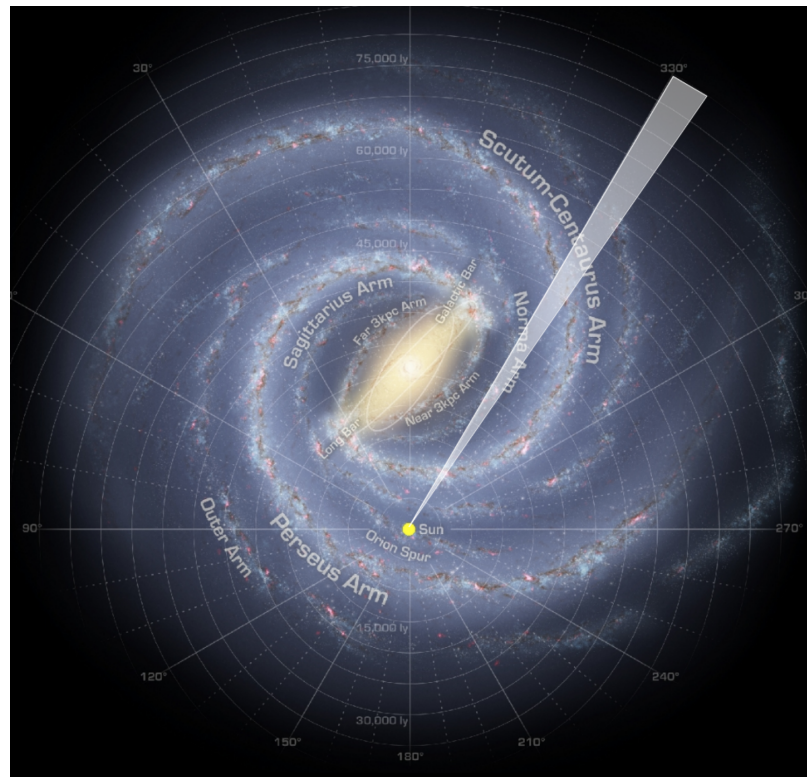


Figure 1.5: Diagram of the Milky Way Galaxy. The shaded region indicates the EMU/POSSUM pilot field, observed by ASKAP, that will be the focus of this thesis. Image adapted from NASA/JPL-Caltech/R. Hurt (SSC/Caltech). (Available from: <https://solarsystem.nasa.gov/resources/285/the-milky-way-galaxy/>)

## Chapter 2

# A Catalogue of Radio Supernova Remnants and Candidate Supernova Remnants in the EMU/POSSUM Galactic Pilot Field

This chapter has been published as Ball et al. (2023): “A catalogue of radio supernova remnants and candidate supernova remnants in the EMU/POSSUM Galactic pilot field”, *Monthly Notices of the Royal Astronomical Society*, Volume 524, Issue 1, September 2023, Pages 1396–1421, <https://doi.org/10.1093/mnras/stad1953>. The paper is reproduced here with changes made to only the formatting to match thesis guidelines. Appendices A and B of the paper have been moved to appear at the end of this work as appendices of the thesis.

### 2.1 Abstract

We use data from the pilot observations of the EMU/POSSUM surveys to study the “missing supernova remnant (SNR) problem”, the discrepancy between the number of Galactic SNRs that have been observed and the number that are estimated to exist. The Evolutionary Map of the Universe (EMU) and the Polarization Sky Survey of the Universe’s Magnetism (POSSUM) are radio sky surveys that are conducted using the

Australian Square Kilometre Array Pathfinder (ASKAP). We report on the properties of 7 known SNRs in the joint Galactic pilot field, with an approximate longitude and latitude of  $323^\circ \leq l \leq 330^\circ$  and  $-4^\circ \leq b \leq 2^\circ$  respectively, and identify 21 SNR candidates. Of these, 4 have been previously identified as SNR candidates, 3 were previously listed as a single SNR, 13 have not been previously studied, and 1 has been studied in the infrared. These are the first discoveries of Galactic SNR candidates with EMU/POSSUM and, if confirmed, they will increase the SNR density in this field by a factor of 4. By comparing our SNR candidates to the known Galactic SNR population, we demonstrate that many of these sources were likely missed in previous surveys due to their small angular size and/or low surface brightness. We suspect that there are SNRs in this field that remain undetected due to limitations set by the local background and confusion with other radio sources. The results of this paper demonstrate the potential of the full EMU/POSSUM surveys to uncover more of the missing Galactic SNR population.

## 2.2 Introduction

Supernovae and supernova remnants (SNRs) are the most significant sources of chemical enrichment in the interstellar medium (ISM) of our Galaxy. More than half of the material in the Milky Way has been processed by supernovae and their remnants [92]. Thus, our knowledge of the Galaxy and its evolution is necessarily informed by our understanding of the Galactic SNR population.

In this paper we seek to investigate the so-called “missing supernova remnant problem,” which refers to the discrepancy between the number of SNRs that are believed to exist in our Galaxy and the number that have been discovered [5, 77–79]. The exact size of the discrepancy is unknown, as accurately quantifying this problem is challenging due to variations in SNR density and radio visibility across the Galactic plane. Based on observations of extra-galactic supernovae, we know that in galaxies like ours a supernova should occur every 30 to 50 years [9]. We can combine this rate

with the expected SNR radio lifetime to obtain an estimate of the number of SNRs that should be detectable at radio wavelengths.

The radio-visible lifetime of a supernova remnant is difficult to estimate, however, as it likely varies based on local conditions and depends on the frequency of the observations. By studying associations between supernova remnants and pulsars, Frail et al. [93] estimated the mean radio SNR lifetime to be about 60,000 years. More recent work has shown that the majority of observed remnants in the Milky Way and Local Group galaxies are believed to be in the Sedov-Taylor (S-T) phase of evolution [29]. Thus, in many cases the S-T lifetime may serve as a useful proxy for the radio visible lifetime with a characteristic timescale of 20–80 kyrs dependent on the local ISM density [10]. However, adopting these age limits may result in estimates which are too conservative. Around 25% of known Galactic SNRs with age estimates are believed to be older than 20 kyrs [3]. Additionally, there have been discoveries of Galactic SNRs, observable at radio wavelengths, that are well beyond the S-T phase [44]. In comparing the Sarbadhicary et al. [10] model predictions to observations, Leahy et al. [94] found the model to be insufficient in reproducing observed radio emission.

According to Ranasinghe et al. [4], predictions for the total number of SNRs in the Galaxy should generally be  $>1000$ , so we adopt this as a lower limit. We form a conservative upper limit based on the supernova rate and S-T lifetime and estimate that at any given time, 1000 to 2700 radio supernova remnants should be detectable in our Galaxy. So far we have only discovered somewhere in the range of 300 to 400 [2, 3]. We aim to detect some of these missing SNRs and, by studying their properties, gain further insight into the nature of this discrepancy.

The majority of supernova remnants (approximately 95%) discovered in our Galaxy have been detected in the radio [30]. Thus, radio observations play an important role in the search for Galactic SNRs. Because of the limitations in working with radio data due to the relatively poor angular resolution and sensitivity when compared to obser-

vations at shorter wavelengths, sources with a small angular size and/or low surface brightness are more likely to be missed. It is therefore reasonable to expect that these types of sources may comprise a significant portion of the missing SNR population. This is especially true in regions of the Galaxy where radio emission is dominated by thermal sources, such as HII regions, and distinguishing SNRs becomes more difficult. X-ray observations of young Galactic SNRs are believed to be fairly complete with an implied Galactic SNR birth rate of  $\sim 1/35$  years, consistent with the supernova explosion rate [21]. Thus, we mostly expect to find old, faint SNRs of varying angular sizes, dependent on the distance to the source and the local environment.

Confusion with other extended radio sources, particularly HII regions, presents a significant challenge to confidently identifying SNR candidates. To address this, we adopt a commonly used methodology involving the comparison of radio and mid-infrared (MIR) fluxes. This technique has been used by many other Galactic SNR surveys, as well as in follow up studies of SNR candidates [5, 6, 77, 78, 86, 87, 95]. While SNRs and HII regions often have similar radio morphologies, HII regions produce strong MIR emission from warm dust and polycyclic aromatic hydrocarbons (PAHs). Conversely, SNRs have been found to produce little to no MIR emission [95–97]. The absence of an MIR counterpart is therefore evidence that a potential SNR candidate is not an HII region.

The Evolutionary Map of the Universe (EMU) and the Polarization Sky Survey of the Universe’s Magnetism (POSSUM) are radio surveys that will be observed together with the Australian Square Kilometre Array Pathfinder (ASKAP). Because of the improved resolution and sensitivity when compared to previous southern sky radio surveys, such as the MGPS-2 [78], the EMU/POSSUM surveys should be expected to uncover some of these small and faint sources. Additionally, ASKAP’s large field of view and good uv-coverage should allow for the detection of old SNRs that are large with low surface brightness. Here we utilize data from the pilot observations of these surveys to search for supernova remnants within a small field of the Galactic plane.

In this paper, we aim to (1) validate the quality of the EMU/POSSUM Galactic pilot field data by studying the properties of known supernova remnants in the field, (2) identify new supernova remnant candidates and uncover some of the missing SNR population, and (3) develop analysis techniques that can be used to study supernova remnants and search for new candidates with the full EMU/POSSUM sky survey data as they become available. Descriptions of the data used in this paper can be found in Section 2.3. In Section 2.4 we present the data and describe how SNR candidates were identified. We also discuss the known SNRs and their properties. In Section 2.5 we present our SNR candidates and in Section 2.6 we provide some analysis and comparison to the known Galactic SNR population. The conclusions are summarized in Section 2.7.

## **2.3 Methods and Observations**

### **2.3.1 The EMU and POSSUM Observations with ASKAP**

We use data from the ASKAP telescope [91], an interferometer with 36 12-meter dishes equipped with phased-array feeds (PAFs). These data were obtained during the commissioning phase of the telescope, specifically from the second pilot observations of the commensal EMU [84, 98] and POSSUM surveys [85, Gaensler in prep.]. These observations use a full 10-hour track having full Stokes with 288 MHz bandwidth, centred at 933 MHz. Imaging is performed using ASKAPsoft and the standard commensal EMU/POSSUM imaging parameter set [84], which produces both a multi-frequency synthesis (MFS) band-averaged Stokes I image for the EMU survey, and full Stokes I, Q, U, and V frequency cubes with 1 MHz channels for POSSUM. The cubes have been convolved to a common resolution of 18" across all PAF beams and all frequency channels. The observations for this particular pilot II survey field were observed on 06 November 2021 (Scheduling block 33284). Primary beam correction in all Stokes parameters are performed using beam models derived from standard ob-

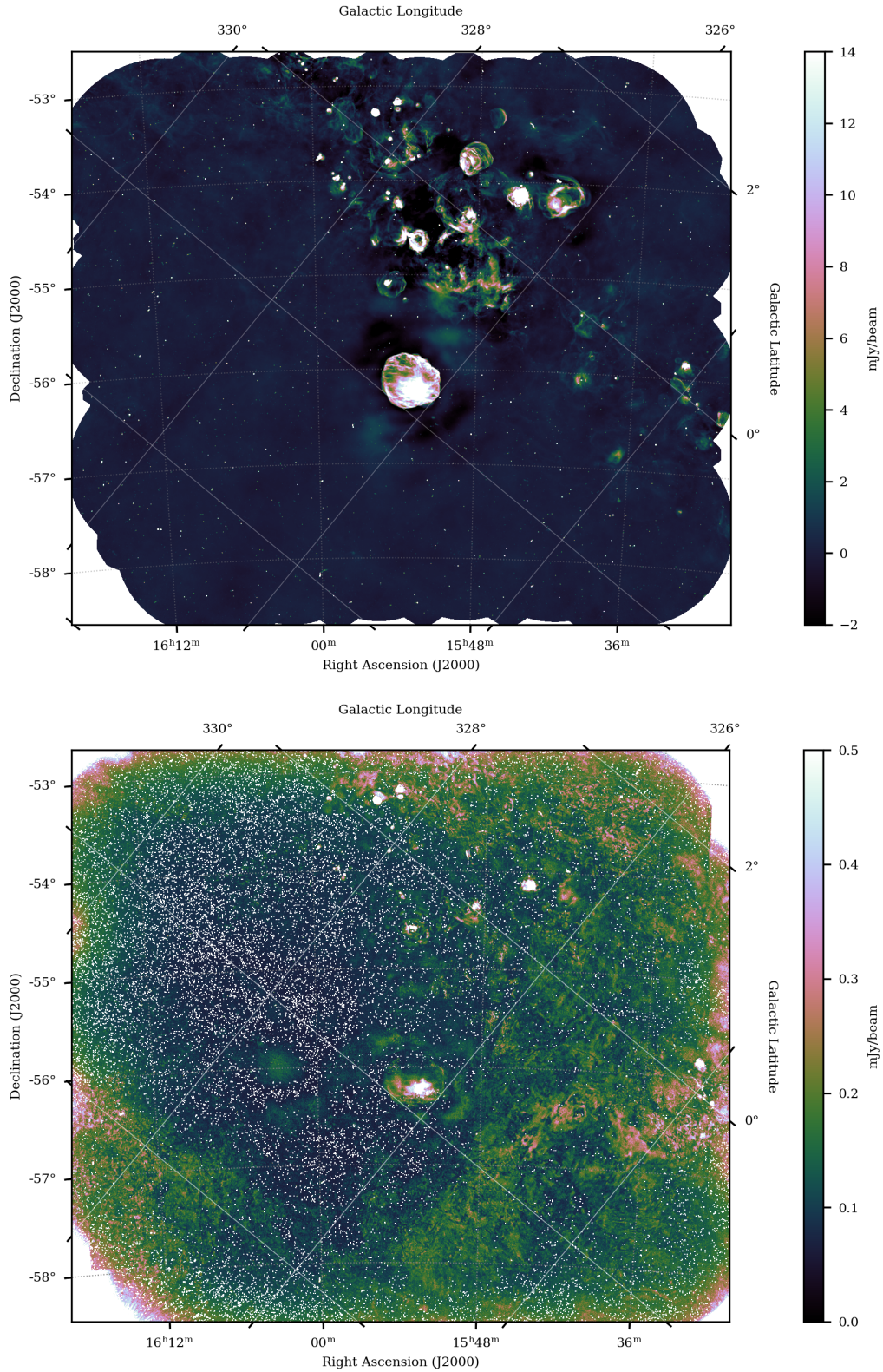


Figure 2.1: The top image shows the EMU/POSSUM Galactic pilot II field as observed by ASKAP at 933 MHz in total intensity with an angular resolution of  $18''$ . The bottom image shows the same field in polarized intensity.

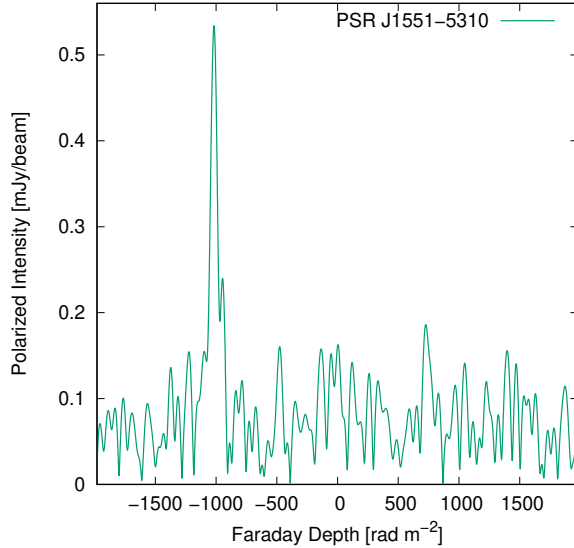


Figure 2.2: Faraday depth spectrum of the pulsar J1551–5310, which is located inside SNR candidate G328.0+0.7.

servatory holography observations from 20 June 2021 (Scheduling block 28162). The long period of time between the holography and the observations resulted in a poor leakage correction, and therefore this field was re-observed on 07 September 2022 (SB 43773). This field was corrected using holography observations from 28 July 2022 (SB 43057). This improved correction mitigates leakage from Stokes I into Stokes Q and U at around the 1% level or less over most of the field. The top image in Figure 2.1 shows the Stokes I image from the original pilot II observation and the bottom image shows the same field in polarized intensity (PI). The polarized intensity was taken from the peak of the Faraday depth (FD) function for each pixel.

For the known supernova remnants and our candidates, we did not use the FD cube from the POSSUM pipeline, but calculated them ourselves. We used the Q and U data cubes from scheduling block 43773. Instead of a Fourier transform, we de-rotated the Q and U data in each frequency channel for each rotation measure (RM). We probed an RM range from  $-2000$  to  $+2000$   $\text{rad m}^{-2}$  with a step size of  $1$   $\text{rad m}^{-2}$ . A sample FD function is shown in Figure 2.2. This was taken towards the pulsar PSR J1551–5310 inside our SNR candidate G328.0+0.7. The RM for this

pulsar is catalogued by Han et al. [99] to be  $-1023.3 \pm 6.3 \text{ rad m}^{-2}$ . In our data we find  $RM = -1017 \pm 5 \text{ rad m}^{-2}$ .

### 2.3.2 Ancillary Data

In addition to the radio data from ASKAP, we utilize images of the same field of the Galactic plane from two other sky surveys. Comparing radio and mid-infrared (MIR) fluxes is a commonly used technique for identifying supernova remnants. Thus, we make use of  $12 \mu\text{m}$  infrared data from WISE (Widefield Infrared Survey Explorer) [100] with an angular resolution of  $6.5''$  as part of the candidate identification process, further outlined in Section 2.4.2. We use  $12 \mu\text{m}$  data because it traces emission from hot dust and PAHs, both of which are expected to be abundant in HII regions [101] and largely destroyed in SNRs [55]. Pixel values in WISE data are measured in digital number (DN) units, which are designed for relative photometric measurements [102] and are sufficient for our purposes.

We use low frequency (198 MHz) data from GLEAM (The GaLactic and Extra-galactic All-sky MWA survey) [103] to calculate spectral indices for some remnants, the details of which are provided in Section 2.4.2. The angular resolution of the GLEAM data ( $\sim 169'' \times 149''$ ) is relatively poor compared to the resolution of ASKAP so while we are able to calculate spectral indices for six of the known remnants, we can obtain indices with these data for only two of our candidates.

### 2.3.3 Flux Integration

To calculate total intensity flux densities, we use a combined map that was created by averaging data from the two ASKAP second pilot observations. This was done to minimize the effect of background fluctuations.

Because of the complexity of the background, different methods for calculating flux densities and performing background subtraction were explored. Integrating over radial profiles using Karma software [104] did not allow us to properly account for

variations in the background or surrounding bright sources. Attempting to use a circular aperture to define the source with multiple circular apertures defining the background, as done by Anderson et al.[6], presented similar challenges and lacked consistency. Ultimately, flux integration was performed using the POLYGON\_FLUX software, which was developed by Hurley-Walker et al. [87] for the GLEAM survey to deal with extended sources that have complicated backgrounds. The software calculates the flux density within a chosen region, subtracts user-selected point sources, and performs background subtraction, allowing the user to select surrounding regions that should not be included as part of the background.

For each source, the calculations were performed multiple times in order to obtain a more accurate flux value and an error estimate. Three different definitions of the background were used to estimate the systematic uncertainty due to flux aperture definition. The calculations were run using backgrounds defined as 4 to 10, 10 to 16, and 16 to 22 pixels from the source (with a pixel size of 2"). Additionally, the source and background selection process was performed at least twice for each source to account for uncertainties resulting from the definition of the source perimeter. Thus, the flux density calculations were run at least six times per source. The flux densities in Table 2.1 were taken as the median values of these calculations and the errors were determined by the range between the extrema. Instrumental uncertainties in the fluxes were found to be relatively insignificant compared to the systematic estimates and were not included.

## 2.4 Results

### 2.4.1 The EMU/POSSUM Galactic Pilot Field

Figure 2.3 shows the EMU/POSSUM Galactic pilot II data as observed by ASKAP and the same field in the mid-infrared as observed by WISE [100]. The field looks across the Galactic plane, with an approximate longitude and latitude of  $323^\circ \leq l \leq$

$330^\circ$  and  $-4^\circ \leq b \leq 2^\circ$  respectively, along a tangent to the Norma arm and across several other spiral arms. This gives us a long line of sight through the inner Galaxy, up to distances of about 18 kpc.

The annotations shown in Figure 2.3 indicate the locations of the known SNRs (green) and HII regions (blue) within this field as well as the locations of our 21 SNR candidates (white). The known SNRs are taken from the Green [2] radio SNR catalogue and the HII regions come from the WISE Catalogue of Galactic HII regions [101]. There are 8 known SNRs in this field, including one that we believe should be reclassified as multiple sources (discussed further in Section 2.5). One of the known SNRs lies at the edge of the field and is only partially imaged in the combined map as shown.

This field was selected in part because it can be broken into two regions that are visually and meaningfully distinct in both the radio and MIR. The upper left part of the field looks along a tangent to the Norma arm and thus we see a high density of HII regions and thermal emission. The lower right part of the field is noticeably fainter with less background emission and a lower density of HII regions. This allows us to test our ability to detect SNR candidates in each of these regions. Since we are primarily expecting to find low surface brightness sources, it is probable that there are candidates in the upper left region of the Galactic plane that we are unable to detect due to the high concentration of thermal emission. The locations of the candidates in Figure 2.3 support this as they are clearly concentrated in areas with fewer HII regions and less background emission.

## 2.4.2 SNR Identification and Verification

A supernova remnant is formed in the aftermath of a stellar explosion as the ejected material expands into the ISM bounded by a supersonic shock wave that sweeps up interstellar material and magnetic fields as it travels. At the shock front, electrons are accelerated to relativistic speeds and interact with the magnetic field to produce

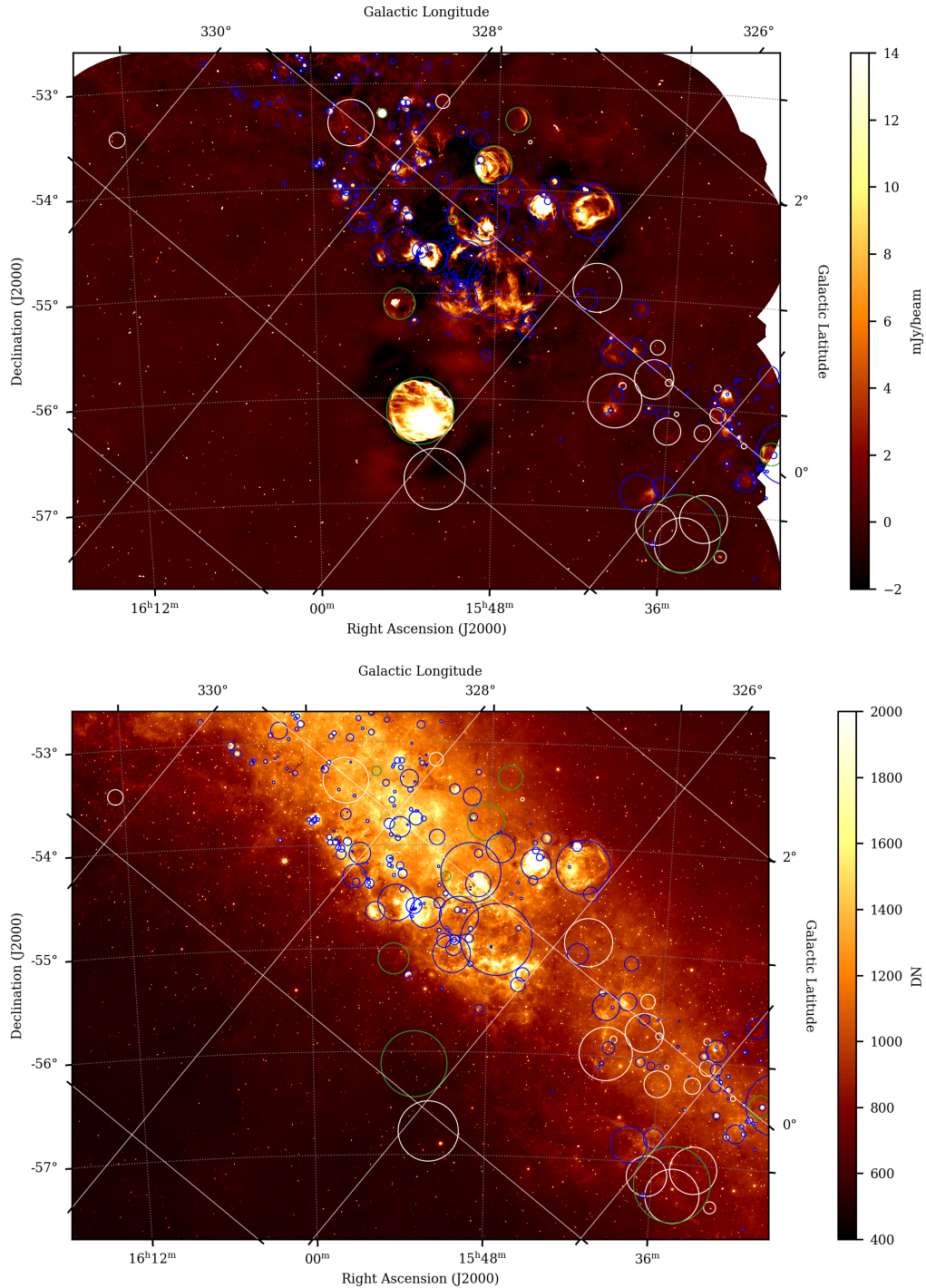


Figure 2.3: The top image shows the EMU/POSSUM Galactic pilot II field from ASKAP at 933 MHz in total intensity. The bottom image shows the same field in the mid-infrared from WISE ( $12 \mu\text{m}$ ). The green circles show the locations of known SNRs, taken from Green [2]. The blue circles indicate the locations of known HII regions, taken from WISE [101]. The white circles indicate the locations of our SNR candidates.

highly linearly polarized synchrotron emission that is best observed in the radio [105]. A supernova remnant can typically be identified by the distinctive shell-like structure that is formed through this interaction between the supernova shock and the ISM. The structural evolution of the remnant will depend on factors like the characteristics of the explosion, the density of the surrounding ISM, and the ambient magnetic field [24, 32, 106]. While these factors may result in asymmetries, we generally expect to see well-defined rounded edges, produced by the shock, with fainter emission coming from the remnant’s centre.

Here we identify supernova remnant candidates primarily by looking for radio-emitting shell-like structures that lack clear mid-infrared counterparts. After identifying candidates, we attempt to find further evidence that they are supernova remnants. First, the presence of a young pulsar indicates that a supernova explosion has recently occurred so spatial coincidence of a candidate with this type of star can significantly increase our confidence in its classification. Second, radio emission from SNRs is primarily non-thermal synchrotron emission that can be differentiated from thermal emission using polarization and spectral indices. Non-thermal synchrotron emission is associated with a steep negative spectral index and linear polarization while thermal optically thin free-free emission is associated with a flat, unpolarized spectrum. As we are observing at relatively low radio frequencies, we can also expect to find compact HII regions with optically thick free-free emission and steep positive spectral indices.

### **Radio and MIR Emission**

Comparing radio and MIR fluxes is a commonly used technique for distinguishing non-thermal SNR emission from thermally emitting sources like HII regions [6, 77, 78, 95]. HII regions produce MIR emission primarily through stochastic heating of small dust grains and the vibrational and bending modes of polycyclic aromatic hydrocarbons (PAHs) [107]. Supernovae are known to produce significant amounts of dust and

SNRs can also produce MIR emission through these thermal processes. However, this emission is relatively weak. This is in part because most dust ( $> 90\%$ ) found in SNRs is in the dense, cool gas phase, rather than the X-ray emitting plasmas, resulting in a spectral energy distribution that peaks at longer wavelengths than studied here [56]. Additionally, while the supernova shock can heat dust grains, it can also result in the destruction of a significant amount of dust and large molecules like PAHs [55]. According to Bianchi et al. [51], only 2–20% of the initial dust mass survives the passage of the reverse shock, depending on the density of the surrounding ISM. Therefore, dust emission from SNRs is typically expected to be weak, if it is detectable at all, and importantly it has been shown that SNRs have significantly lower MIR to radio flux ratios when compared to HII regions [95, 97]. Thus, while some SNRs do emit in the MIR, sources that lack MIR emission are unlikely to be HII regions.

We began our search for SNR candidates by comparing the radio data from ASKAP to MIR data from WISE. The images used can be found in Figure 2.3. Because of the small size of the field, we were able to perform a detailed search by eye, specifically looking for shell-like structures in the radio that do not have MIR counterparts. This was done separately by two of the authors before comparing results. To simplify the search, we eliminated sources that had already been classified as HII regions. The WISE Catalogue of Galactic HII Regions [101] was used to identify all known HII regions in the field. The catalogue was made using 12  $\mu\text{m}$  and 22  $\mu\text{m}$  data from WISE and includes over 8000 Galactic HII regions and HII region candidates. We use Version 2.2 of the catalogue, downloaded from <http://astro.phys.wvu.edu/wise/>, and include all listed entries. We did not find any sources in our field that we believe to be HII regions that were not already part of the WISE HII region catalogue. Specifically, we did not find any new extended sources that were clearly visible in both radio and MIR. Thus, the radio to MIR comparison was not used to rule out any potential candidates but instead served primarily as evidence that our candidates are not HII regions.

## Spectral Indices

Spectral indices can help to differentiate thermal and non-thermal emission. We assume the relation  $S(\nu) \propto \nu^\alpha$  where  $S$  represents the flux density,  $\nu$  represents the frequency, and  $\alpha$  represents the spectral index. The synchrotron spectral index is determined by the power-law energy distribution of relativistic particles which are accelerated through multiple crossings at the shock front in a process known as diffusive shock acceleration (DSA) [41, 42]. For a shell-type remnant, linear DSA predicts a spectral index of  $-0.5$  and observations show that most catalogued Galactic SNRs have a spectral index within the range  $\alpha = -0.5 \pm 0.2$  [108, 109]. However, there is significant uncertainty in many of the measured values and outliers do exist.

Thermally-emitting HII regions are expected to have flatter spectral indices for optically thin free-free emission, generally around  $-0.1$ , or steep inverse spectra, around  $+2$ , for optically thick. Pulsar wind nebulae (PWNe), or centre-filled supernova remnants, tend to have flatter spectra as well, usually within the range  $-0.3 \leq \alpha \leq 0.0$ , though in rare cases they can be as steep as  $-0.7$  [34]. PWNe accelerate relativistic particles through a different mechanism, the interaction of the pulsar wind with the supernova ejecta, which typically results in a flatter particle energy distribution. Thus, PWNe can be more difficult to distinguish from thermal sources when they do not have a visible shell component. This is not the only inherent bias against detecting these types of sources as they are also generally smaller and have a less visually distinct morphology. In fact, only 3% of catalogued Galactic SNRs are shell-less PWNe [30].

We calculate spectral indices using data from GLEAM [103] for sources that are large enough and bright enough to be detected in the highest frequency band of the GLEAM survey. These appear to be sources that are at least  $5'$  in diameter with a flux density of around 1 Jy in the GLEAM band. This includes all of the known supernova remnants in the field but only two of our SNR candidates. The GLEAM

flux densities were calculated using the method outlined in Section 2.3.3. These spectral indices can be found in Table 2.1 with errors based on the uncertainties of the flux densities. Attempts were made to calculate in-band spectral indices with the ASKAP pilot II data but the uncertainties were too significant to produce meaningful results. Follow up observations at a second frequency would be valuable in allowing for the calculation of spectral indices for sources that are not visible in the GLEAM survey.

### **Polarization**

Detection of linearly polarized radio emission is strong evidence that an extended Galactic radio nebula is a supernova remnant. SNRs emit highly linearly polarized synchrotron emission. The degree of polarization can be intrinsically more than 70%. For the SNR G181.1+9.5, in both the Effelsberg 5 GHz observations and 1.4 GHz observations with the synthesis telescope at the Dominion Radio Astrophysical Observatory (DRAO ST), Kothes et al. [44] find polarization of about 70%. G181.1+9.5 is a highly evolved SNR with a highly compressed and very regular magnetic field in its shell. Conversely, young SNRs typically have much lower intrinsic degrees of polarization as they display significant turbulence in their expanding shells. The lowest polarization observed at a high radio frequency in an SNR is possibly the 2% observed in SNR G11.2–1.1 at a frequency of 32 GHz [110].

EMU and POSSUM observe at radio frequencies between 800 and 1087 MHz. At these low frequencies, Faraday rotation strongly affects polarized signals. There is foreground Faraday rotation in the magneto-ionic medium between us and the nebula and there may be internal effects inside the SNR’s shell. In the SNR’s shell we find a mix of synchrotron emitting and Faraday rotating plasmas, which means that internally the synchrotron emission may be affected by different amounts of Faraday rotation depending on where the emission comes from within the shell. Integrating this emission along the line of sight through the emission region may lead to significant

depolarization. These effects become significantly worse at low frequencies as the amount of depolarization is inversely proportional to the frequency squared. Faraday rotation in the foreground ISM may also lead to depolarization, especially if the foreground path traverses turbulent ionized areas such as HII regions, or even spiral arms.

Because we are observing at a relatively low frequency, failure to detect polarization should not be considered evidence that a candidate is not an SNR, especially considering that many of our candidates are small or faint sources that may be located at far distances across the Galactic plane. The probability of detecting polarization from our SNR candidates is higher for high latitude sources, as their foreground likely does not contain any turbulent ionized regions. SNRs located close to the plane of the Galaxy may suffer from foreground depolarization caused by overlapping HII regions in the foreground or parts of a spiral arm between the SNR and us as spiral arms contain enhanced electron densities and magnetic fields.

Distinguishing between real and instrumental polarization is an additional challenge. As shown by the polarized intensity data in Figure 2.1, we see evidence of instrumental effects at the positions of known HII regions. Particularly for bright sources, we believe that polarization with a smooth structure that closely resembles what is seen in total power is potentially the result of Stokes I leakage. Polarization that has a speckled appearance is more likely to be real as this indicates a changing rotation measure, or intrinsic polarization angle, on small scales. For further evidence of real polarization, we look for structures that are contained entirely within the SNR and that appear similar in the polarized intensity and rotation measure maps. Real polarization from the SNR should be distinct from what is seen in the surrounding background in intensity and rotation measure.

We detect polarized signal significantly above the noise from all known SNRs in our field, but we are not convinced that all of it is real. Further details for each source are provided in Section 2.4.3. Similarly to Dokara et al. [111], we are mostly unsuccessful

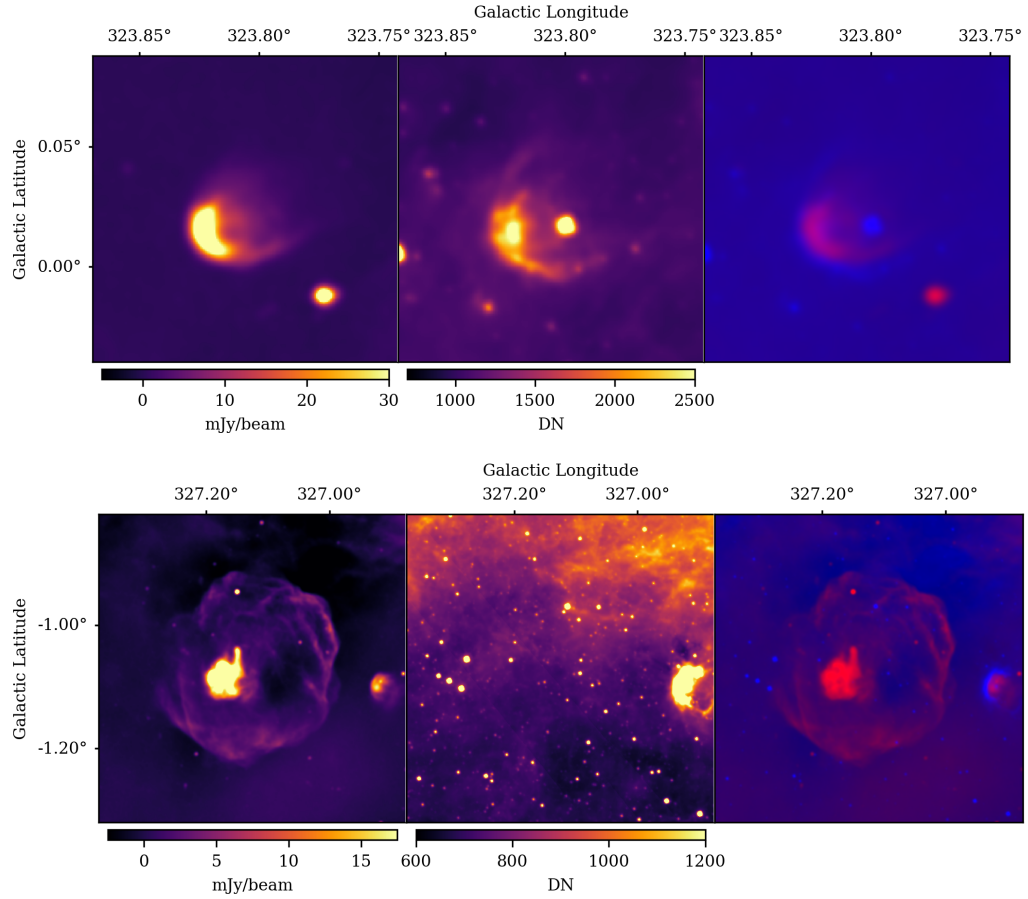


Figure 2.4: Comparing radio and MIR emission from an HII region and an SNR. From left to right, the top images show an HII region in radio (from ASKAP), MIR (from WISE), and a combined image with radio in red and MIR in blue. The bottom images show the same data for a known SNR, G327.1–1.1, and demonstrate the absence of an MIR counterpart.

in detecting polarization from Galactic SNR candidates. We are only able to detect what we believe to be real polarization from one of our SNR candidates, G328.0+0.7. The details of this can be found in the candidate description in Section 2.5.1.

### 2.4.3 Characteristics of Known Supernova Remnants

As discussed in Section 2.4.2, supernova remnants can be identified by looking for extended radio sources that lack a mid-infrared counterpart. The top images in Figure 2.4 show a known HII region that could potentially be misidentified as an SNR based solely on its radio morphology. The presence of a clear counterpart in

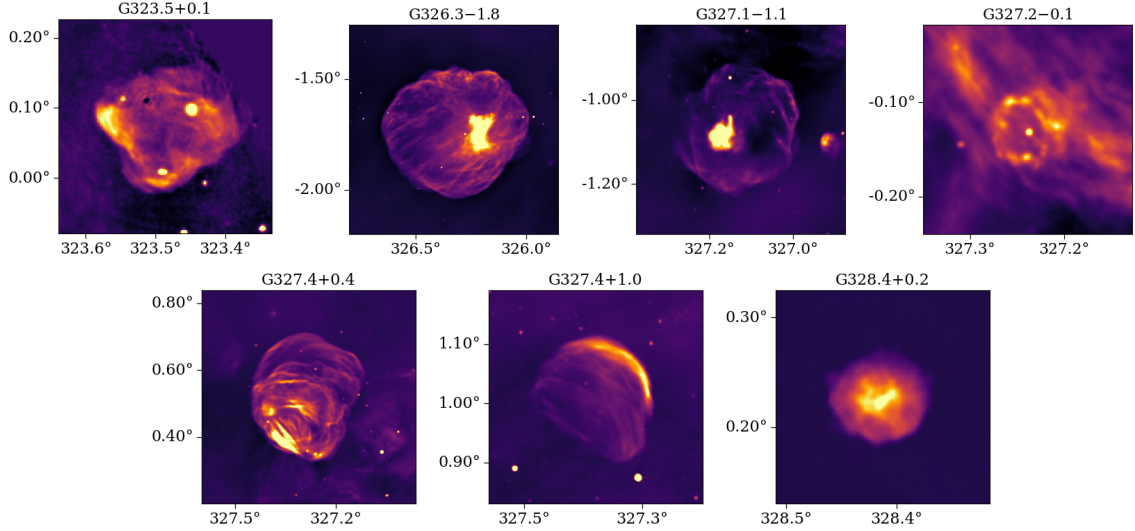


Figure 2.5: 933 MHz images of the 7 known SNRs with Galactic longitude on the x-axis and Galactic latitude on the y-axis. For more detailed images with colour bars, see Appendix A.

the MIR helps to correctly identify this source as an HII region. The bottom images in Figure 2.4 show a known SNR, G327.1–1.1, and its clear lack of MIR emission. A small HII region can be seen along the right edge of the SNR images in both the radio and the MIR, further illustrating this distinction.

There are eight known supernova remnants in the EMU/POSSUM Galactic pilot II field that appear in the Green [2] catalogue. We believe G323.7–1.0 should be reclassified as three separate sources so it is discussed under the candidates section. Our observations of the other seven known SNRs are discussed here. The 933 MHz ASKAP images of the SNRs can be found in Figure 2.5. More detailed images of the known SNRs in both radio and MIR, which include coordinate axes and colour bars, can be found in Appendix A.

**G323.5+0.1** This source is a shell-type supernova remnant that lies at the edge of our field. It is only fully imaged in the ASKAP data at low frequencies so it has not been studied here in-depth and thus does not appear in Table 2.1. Figure A.1 was made using a 48 MHz wide channel centred at 823.5 MHz since the source is not fully

visible in the higher frequency channels. The source overlaps with a bright HII region that can be seen in MIR.

**G326.3–1.8, MSH 15–56** This SNR is a composite source, a bright pulsar wind nebula with a well-defined radio shell. It is the largest supernova remnant in the field with a size of  $38'$ . Bright filamentary emission can be seen coming from the shell. The PWN is offset to the west of the remnant's centre and is elongated in the north-south direction (Figure A.2). The source is estimated to be at a distance of  $3.5 - 5.8$  kpc [4]. There is clear polarization, mostly concentrated around and extending from the PWN (Figure 2.6a). This can be seen in both the polarized intensity and rotation measure maps. There is also some polarization coming from the east side of the shell. We believe all of this polarization is real since it is not smooth and aligns with what is expected from total power without mirroring it exactly, which could indicate leakage. It also has a high negative RM and there is almost no polarized emission coming from the background in this part of the field it could be confused with.

**G327.1–1.1** This SNR is another composite source with a bright pulsar wind nebula and a relatively faint shell that is likely missing some short spacings in the ASKAP data. This is evidenced by the negative bowls of emission, seen in Figure A.3. There is a bright HII region located to the west of the SNR. The remnant is believed to be located at a distance of  $4.5 - 9$  kpc [112, 113], indicating it is likely located within or near the Norma arm. There is obvious polarization coming from the PWN but no clear polarization coming from the shell (Figure 2.6b). We believe this polarization to be real because it is contained entirely within the PWN and is not smooth.

**G327.2–0.1** This source is believed to be a shell-type remnant associated with a young magnetar, J1550-5418, located near its centre [114]. The magnetar has a characteristic age of 1.4 kyrs and a rotation measure of  $-1860 \pm 20$  rad/m<sup>2</sup> [115, 116]. Distance estimates for the shell are between  $4 - 5$  kpc [117] while the magnetar

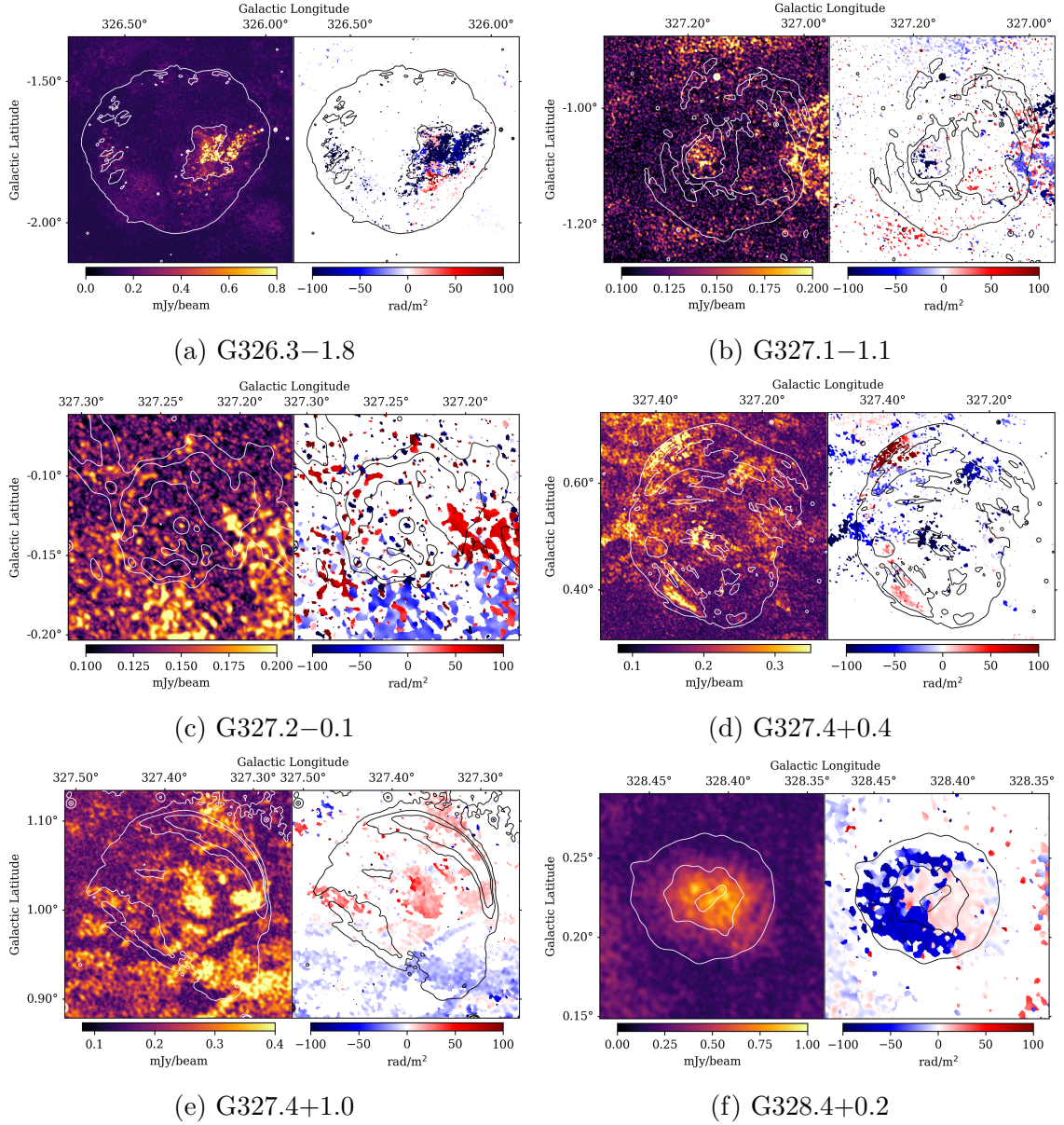


Figure 2.6: For each source, the left image shows polarized intensity and the right image shows Faraday rotation measure. The contours are used to indicate the total power structures.

has been estimated to be at a distance of 9 kpc [115]. The source lies on a larger filament of emission that is likely unrelated to the SNR (Figure A.4). While we were not able to detect any clear real polarization coming from the shell due to confusion with the background, there does seem to be real polarization coming from the centre (Figure 2.6c). Specifically, there are two peaks in the rotation measure for the central point source. We believe the first peak, around  $-1820 \text{ rad/m}^2$ , comes from the pulsar and we speculate that the second peak, around  $15 - 30 \text{ rad/m}^2$ , may come from a previously undetected pulsar wind nebula.

**G327.4+0.4, Kes 27** This shell-type SNR exhibits multiple shell structures and many internal filaments. There is a small overlapping HII region that can be seen in both radio and MIR (Figure A.5). HI absorption suggests the SNR is located at a distance of  $4.3 - 5.4 \text{ kpc}$  [118] while optical extinction suggests a distance of  $2.8 \text{ kpc}$  [112]. We detect polarization coming from several parts of the remnant (Figure 2.6d). We believe the polarization seen along the northeast edge of the remnant to be real as it is distinct from the total power structure, and thus cannot be leakage, and has a high positive rotation measure that is distinct from the RM found in the rest of the image. The polarization in the southeast may be real as well but this is not certain as the smoother appearance and flatter RM may indicate that it is instrumental. There is also some polarization near the centre of the remnant that has a high negative RM and may be real but this is also unclear.

**G327.4+1.0** This source is an asymmetrical shell that is brightest along the north-western edge. There is also some faint central emission with filaments that curve in the same direction as the shell (Figure A.6). There is potential polarization coming from the centre of the remnant but it is not strong enough to be definitively distinct from the background features seen in the south (Figure 2.6e). However, the positive RM seems to be mostly confined to the source with some extending to the north of

the remnant. This extension is somewhat mirrored in total power, possibly indicating that some of this polarization is real but this is not conclusive.

**G328.4+0.2, MSH 15–57** This SNR is believed to be the largest and most radio luminous pulsar wind nebula in our galaxy [119]. It has no visible shell but there is a central bar structure that runs in the southeast to northwest direction (Figure A.7). It is believed to be located at a distance of over 16.7 kpc [4] placing it along the outer edge of the Galaxy. The source appears to be polarized but because it is so bright we believe this is likely the result of leakage. In RM we see two components, a high negative component and a low positive component. The high negative component extends over the remnant and has a similar structure to what is seen in PI. The low positive component seems to be concentrated to the west side of the PWN (Figure 2.6f).

#### 2.4.4 Spectral Indices of Known Remnants

For each of the known SNRs, we calculate a spectral index using the 933 MHz flux density from ASKAP and the 198 MHz flux density value from GLEAM. These indices can be found in Table 2.1. Figure 2.7 shows the ASKAP and GLEAM flux densities calculated in this paper plotted with flux densities taken from Green’s catalogue[31] and references therein. The spectral indices seen on the plots are calculated using the slopes of the fit lines, which are made using the literature values as well as the ASKAP and GLEAM values. We use this second method of calculating spectral indices to evaluate whether or not the indices found using only the ASKAP and GLEAM data are reliable.

G326.3–1.8 is a composite source that has been shown to have an intermediate index ( $\sim -0.3$ ) with a flatter component coming from the PWN and a steeper component coming from the shell [120]. The values we obtain are in moderate agreement with each other and are consistent with the expected value for this source.

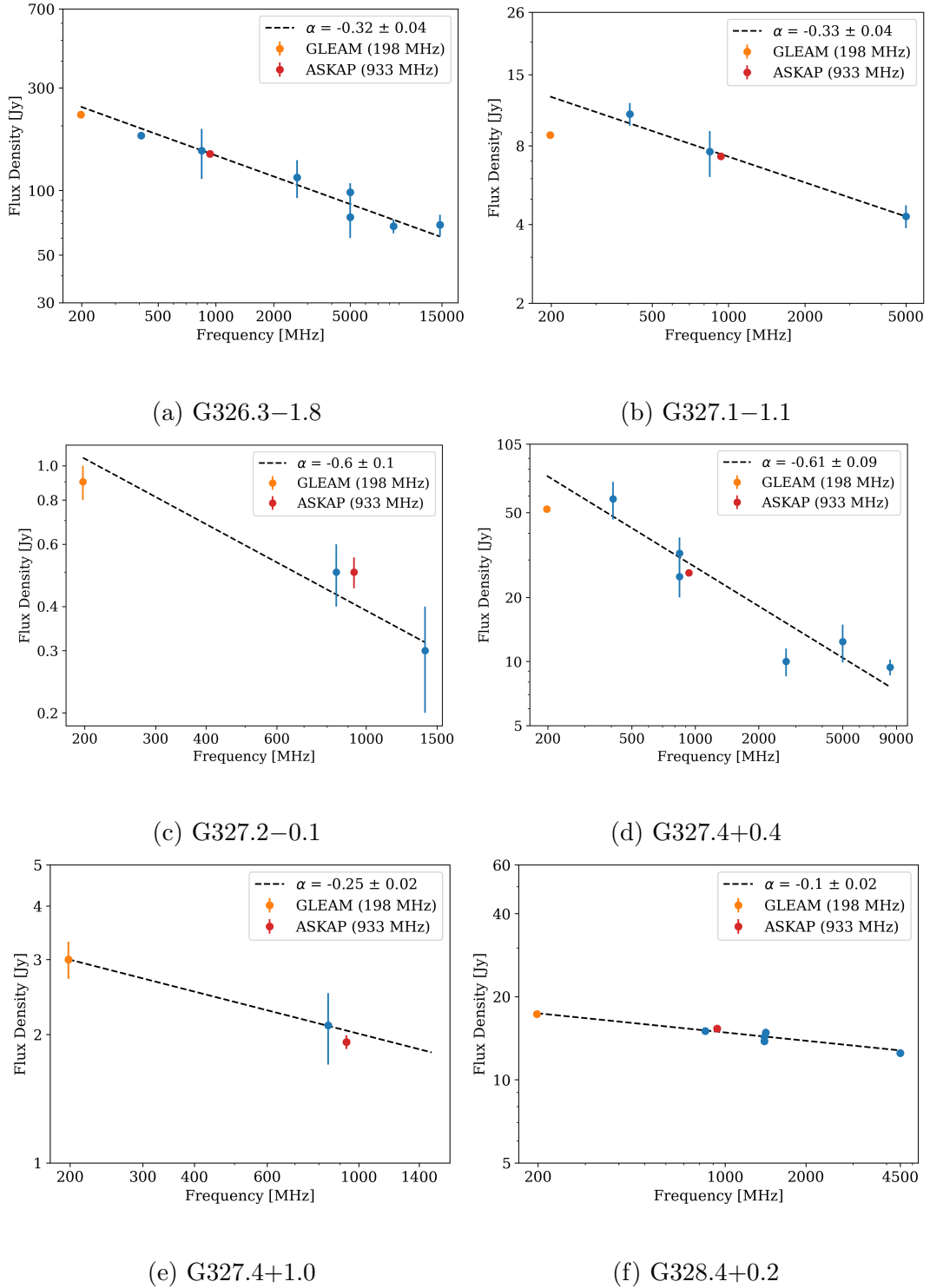


Figure 2.7: Flux densities of known SNRs. The red and orange data points are the values calculated in this paper using ASKAP and GLEAM data respectively. The blue data points represent the flux densities of known SNRs taken from Green’s catalogue [31] and references therein. 20% errors are assumed if none were given.  $\alpha$  represents the spectral index as determined by the slope of the linear fit.

G327.1–1.1 is also a composite source that is believed to have an intermediate index  $[-0.36, 121]$ . The flux value we obtain from the GLEAM data appears to be too low, as demonstrated by the plot, resulting in a spectral index that is likely too flat. The value obtained from the fit is consistent with what is expected and is likely more reliable.

G327.2–0.1 is believed to be a shell-type remnant though it is associated with a known magnetar and could be a composite source. The values we obtain are in moderate agreement though they have relatively large errors. Both are consistent with what is expected for non-thermal emission from a shell-type remnant.

G327.4+0.4 is also a shell-type remnant. The values we obtain are not in agreement though both are consistent with the expected index of a shell-type remnant. The plot appears to indicate that the GLEAM flux value may be too low.

G327.4+1.0 is a shell-type remnant for which there was previously only one flux measurement [95] so the spectral index derived from the linear fit may be less reliable. The values we obtain are consistent with each other and although they are flat for a shell-type remnant, they are not unreasonable for this type of source. Given that many of the GLEAM fluxes seem to be lower than expected, and because our fit is based on only three data points, the spectral index of this source may be steeper than the values we have calculated here.

G328.4+0.2 is a shell-less PWN that has been shown to have a flat spectral index [119, 122]. The values we obtain are consistent with each other and with what is expected for a typical pulsar wind nebula.

While the spectral indices we calculate using these two methods are generally in agreement with each other and with the expected values for the corresponding SNR types, many of these values have relatively large errors. The values obtained from the linear fit should be considered to be more reliable than the values provided in Table 2.1 as the deviations seem to mostly be the result of lower than expected values for the GLEAM fluxes, particularly for the fainter remnants. Thus, the spectral

indices we calculate for our candidates using this data should be viewed with a level of skepticism. High resolution data at a second frequency will likely be required to produce reliable spectral indices for the SNR candidates.

## 2.5 SNR Candidates

The locations of our SNR candidates are indicated in Figure 2.3. Notably, the candidates are highly concentrated in the lower right corner of the image. We believe we were able to detect more candidates in this part of the field because of the relatively low density of HII regions compared to the upper left half of the image. This may seem to contradict what is expected as the true SNR density is likely to be higher within spiral arms, not away from them. Thus, we believe it is highly probable that there are faint sources within the Norma arm region of the field that we were unable to detect due to the high concentration of thermal emission and HII regions.

Data collected for known and candidate supernova remnants is shown in Table 2.1. Right ascension and declination are determined by fitting an ellipse to the source using CARTA software [123] and taking the central coordinates of the ellipse. The sizes of the sources are determined by taking the major and minor axes of these ellipses.

Name	RA (J2000)	Dec (J2000)	Size [']	Flux Density [Jy at 933 MHz]	Surface Brightness [ $10^{-21}\text{Wm}^{-2}\text{Hz}^{-1}\text{sr}^{-1}$ ]	Polarization Detected	Spectral Index (with GLEAM)
Known SNRs							
G326.3−1.8	15:52:59	−56:07:27	38	$148 \pm 3$	$15.4 \pm 0.3$	Y	$-0.27 \pm 0.02$
G327.1−1.1	15:54:26	−55:05:59	18	$7.3 \pm 0.2$	$3.4 \pm 0.1$	Y	$-0.1 \pm 0.1$
G327.2−0.1	15:50:57	−54:18:00	5	$0.50 \pm 0.05$	$3.0 \pm 0.3$	Y?	$-0.4 \pm 0.1$
G327.4+0.4	15:48:23	−53:46:13	21	$26.1 \pm 0.4$	$8.9 \pm 0.1$	Y	$-0.44 \pm 0.01$
G327.4+1.0	15:46:53	−53:19:51	14	$1.92 \pm 0.07$	$1.47 \pm 0.05$	Y?	$-0.3 \pm 0.1$
G328.4+0.2	15:55:32	−53:17:02	5	$15.3 \pm 0.3$	$92 \pm 2$	N/A**	$-0.1 \pm 0.1$
SNR Candidates							
G323.2−1.0	15:31:40	−57:23:42	7	$0.32 \pm 0.01$	$0.97 \pm 0.04$	N	
G323.6−1.1*	15:34:03	−57:21:42	$34 \times 20$	N/A	N/A	N	
G323.6−0.8*	15:32:56	−57:02:53	$28 \times 23$	$< 1$	$< 0.3$	N	
G323.7+0.0	15:30:39	−56:19:26	3	$0.07 \pm 0.02$	$1.1 \pm 0.3$	N	
G323.9−1.1*	15:36:24	−57:08:45	$29 \times 18$	$< 1$	$< 0.3$	N	
G324.1−0.2	15:33:34	−56:13:59	$10 \times 9$	$0.26 \pm 0.03$	$0.43 \pm 0.06$	N	
G324.1+0.0	15:32:37	−56:03:05	$11 \times 7$	$1.0 \pm 0.1$	$1.9 \pm 0.2$	N	$-0.3 \pm 0.2$
G324.3+0.2	15:32:45	−55:47:45	4	$0.120 \pm 0.008$	$1.13 \pm 0.08$	N	
G324.4−0.4	15:36:00	−56:14:08	$18 \times 13$	$0.44 \pm 0.09$	$0.28 \pm 0.06$	N	

G324.4−0.2	15:35:26	−56:04:08	3 × 2	0.006 ± 0.001	0.14 ± 0.02	N	
G324.7+0.0	15:36:06	−55:46:29	4	0.055 ± 0.005	0.52 ± 0.04	N	
G324.8−0.1	15:37:07	−55:45:03	25 × 20	< 1	< 0.3	N	
G325.0−0.5	15:39:43	−55:58:29	34 × 28	< 6	< 0.9	N	
G325.0−0.3	15:39:14	−55:49:52	4	0.19 ± 0.01	1.7 ± 0.1	N	
G325.0+0.2	15:37:02	−55:26:56	5	0.11 ± 0.01	0.66 ± 0.08	N	
G325.8−2.1	15:52:03	−56:46:04	36 × 30	N/A	N/A	N	
G325.8+0.3	15:41:15	−54:54:26	28	N/A	N/A	N	
G327.1+0.9	15:45:59	−53:32:33	2	0.019 ± 0.004	0.7 ± 0.1	N	
G328.0+0.7	15:51:41	−53:10:11	8	0.50 ± 0.06	1.2 ± 0.1	Y?	
G328.6+0.0	15:57:31	−53:22:05	34 × 19	3.5 ± 0.9	0.8 ± 0.2	N	−0.75 ± 0.06
G330.2−1.6	16:12:32	−53:27:01	9	0.08 ± 0.02	0.14 ± 0.04	N	

Table 2.1: Known SNRs and SNR candidates in the EMU/POSSUM Galactic pilot II field. Surface brightnesses are given at 933 MHz. Spectral indices are calculated using the 933 MHz flux value from ASKAP and the 198 MHz flux value from GLEAM. \*Currently classified as a single source (G323.7−1.0). \*\*Leakage.

### 2.5.1 Characteristics of SNR Candidates

Here we list 21 supernova remnant candidates, three times the number of known SNRs in this field. We believe some of these sources to be strong SNR candidates while others are weaker and will require further observations to determine if they are indeed SNRs. We define the strength of our candidates based on whether or not we are able to find evidence of other expected SNR properties, such as polarization or a steep negative spectral index. Only two of the candidates were visible in the GLEAM data, allowing us to calculate spectral indices, and only one shows clear evidence of real polarization. The 933 MHz images of the candidates can be found in Figure 2.8. More detailed images of the SNR candidates in both radio and MIR, which include coordinate axes and colour bars, can be found in Appendix B.

**G323.2–1.0** This source has the morphology of a pulsar wind nebula with a very faint shell. As shown in Figure B.1, there is an infrared source that overlaps with the PWN but the IR source has a different morphology and has been identified as a star by Cutri et al. [0]. The shell is roughly circular and the PWN has a similar shape to the PWN of G326.3–1.8, but elongated along the east-west axis. This source was listed as an SNR candidate by Whiteoak et al. [95] but was not confirmed and no image was provided.

**G323.6–1.1, G323.6–0.8, G323.9–1.1** This object is currently classified as a single source in Green’s catalogue, G323.7–1.0 [78]. The ASKAP observations have revealed faint filamentary structures that were previously not visible, leading us to believe that it is actually three separate overlapping sources. As shown in Figure B.2, there are two brighter, elliptically shaped sources, one located to the northwest (G323.6–0.8) and the other to the southeast (G323.9–1.1). The third source (G323.6–1.1) appears to lie behind the other two sources and only a faint southwestern edge can be seen. Because this source is very faint and overlaps with the

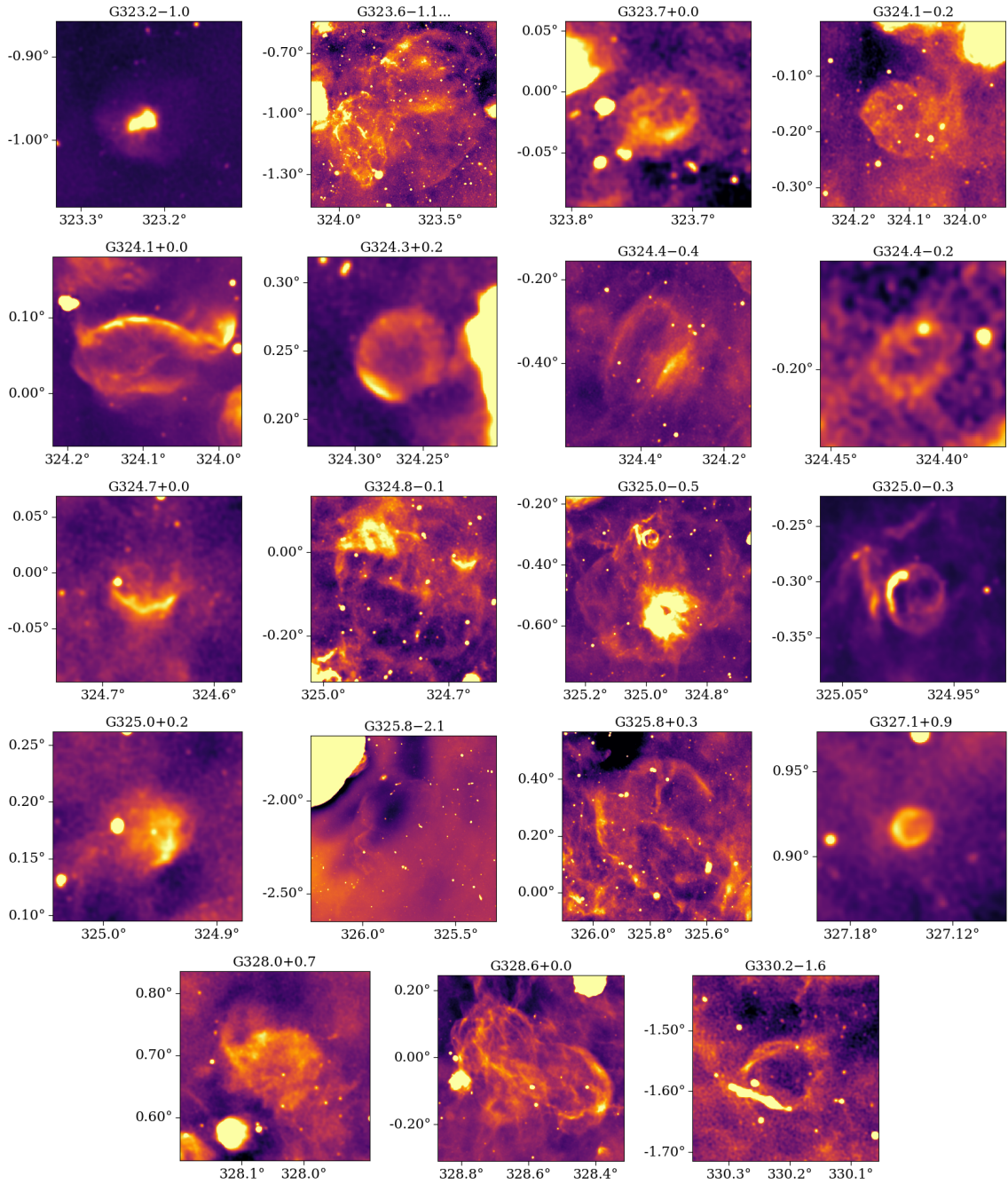


Figure 2.8: 933 MHz images of the 7 known SNRs with Galactic longitude on the x-axis and Galactic latitude on the y-axis. For more detailed images with colour bars, see Appendix B.

other sources, it was not possible to obtain a flux estimate. For the two brighter sources, only rough upper limits could be obtained for the flux densities. It is unclear if all three sources are supernova remnants but none of them has an obvious MIR counterpart.

**G323.7+0.0** The source shown in Figure B.3 is a small shell-like structure that is roughly circular and brightest along the southern edge. There is a small amount of overlap with a known HII region in the southeast and a larger HII region can be seen to the northeast. There is some faint MIR emission to the east that could be related to the radio emission. Since the emission is faint and the relation is not entirely clear, we include the source in our list of candidates.

**G324.1–0.2** This candidate does not have a clear shell-structure but it has a roughly circular shape with well-defined rounded edges, characteristic of a shock front (Figure B.4). There are several overlapping point sources and a bright HII region can be seen in the northwest. There is no clear MIR counterpart.

**G324.1+0.0** This source was originally identified as an SNR candidate by Whiteoak et al. [95] but an image was not included. Green et al. [78] have also listed it as a candidate and provided an image but there was insufficient evidence for it to be included in the Green [2] catalogue. The source, seen in Figure B.5, is an elliptical shell, elongated in the east-west direction, with the brightest emission coming from the north and a fainter shell visible in the south. Multiple HII regions can be seen in the image and there is some overlap between the SNR candidate and HII regions in the northwest and northeast. This candidate is visible in the GLEAM data and a spectral index of  $-0.3 \pm 0.2$  was determined. The index indicates the emission may be nonthermal but the uncertainty is too large to be conclusive. Because this source has been studied previously and has a very clear shell-like morphology, we believe it should be classified as an SNR.

**G324.3+0.2** The source shown in Figure B.6 has a shell structure that is almost perfectly circular, with some brightening towards the southeast. Based on the distinct morphology and clear lack of an MIR counterpart, we believe this candidate should be classified as an SNR. A large, bright HII region can be seen to the west of the source.

**G324.4–0.4** In Figure B.7 we see an elliptical shell with brightening along the southwest edge. There are many overlapping point sources and a couple of known HII regions located to the northeast. There is overlapping emission in the MIR but nothing that clearly mirrors the shell structure seen in the radio.

**G324.4–0.2** The source shown in Figure B.8 is a very small, faint shell-like structure with an overlapping point source. It is located just north of G324.4–0.4 and can also be seen in Figure B.7. There is no obvious MIR counterpart.

**G324.7+0.0** This candidate is a partial shell that arcs in the southern direction with no clear northern counterpart though some faint emission can be seen extending north from the southern shell (Figure B.9). There is a bright overlapping point source in the east. Several bright point sources can be seen in the MIR but the shell has no counterpart.

**G324.8–0.1** As shown in Figure B.10, this source consists of faint filaments that form a large ellipse. The source overlaps with G324.7+0.0 and with a large HII region in the northeast. Because of this overlap, only a rough upper limit could be obtained for the flux. The rounded filaments do not appear to have an MIR counterpart.

**G325.0–0.5** This candidate, shown in Figure B.11, is composed of filaments that form a roughly elliptical structure. Many overlapping sources can be seen, including G325.0–0.3 and several HII regions. A long filament, which can be seen in MIR

and is thus likely thermal, runs from the northeast to the southwest. The filaments that form the edges of the ellipse are not visible in MIR. Because of the overlapping emission, only an upper limit could be obtained for the flux.

**G325.0–0.3** This candidate was originally identified by Whiteoak et al. [95] (with no image) and later studied by Green et al. [78] who provided an image but the source is not included in the Green [2] catalogue. In Figure B.12 a clear shell structure can be seen that is brightest to the east. A filament of emission can be seen to the east of the candidate but it is likely thermal and unrelated. The candidate has no MIR counterpart. Based on our observations and the previous studies, we believe this source should be classified as an SNR.

**G325.0+0.2** This source consists of roughly circular emission that is brightened to the west where the edge of the source is the most well-defined (Figure B.13). A bright overlapping point source can be seen to the east. Emission can be seen in the MIR but it does not have the same rounded structure as the radio source.

**G325.8–2.1** This object is composed of very faint filaments of emission found to the southwest of the bright known SNR G326.3–1.8. As shown in Figure B.14 the source overlaps with negative bowls of emission, likely caused by missing short spacings. The filaments can be seen most clearly in the southeast but some faint structures are also visible in the northwest. This source is only visible because it is located at a far distance from the Galactic plane and there is little thermal emission. The source was too faint to obtain an estimate of the flux density.

**G325.8+0.3** This candidate is composed of rounded filamentary structures that can be seen to the north and southeast in Figure B.15. The source overlaps with a large HII region and many point sources. Missing short interferometer spacings generate a negative bowl around these strong emitters. Because of this, and because

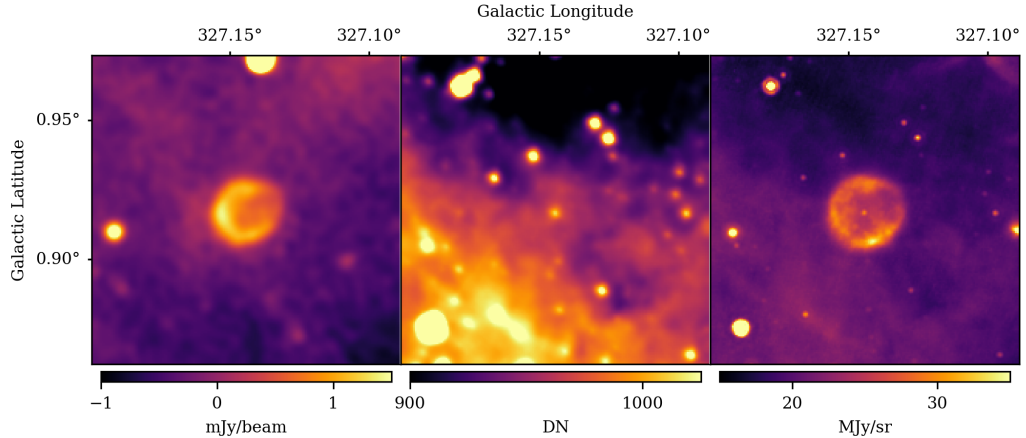


Figure 2.9: 933 MHz ASKAP data, 12  $\mu\text{m}$  WISE data, and 24  $\mu\text{m}$  MIPS data for G327.1+0.9.

the filaments are so faint, we were unable to obtain a flux estimate for the source.

**G327.1+0.9** This candidate is a small, roughly circular source that appears to have a brightened shell-like edge to the east (Figure B.16). This is our smallest source with a size of 2' and we believe that this marks the approximate lower size limit of sources in which we would be able to detect a shell-like structure, given the resolution of our data. This source appears in Gvaramadze et al. [0] in their table of 24  $\mu\text{m}$  nebulae compiled using data from the Multiband Imaging Photometer for Spitzer (MIPS). There is a circular MIR nebula at 24  $\mu\text{m}$  (diameter of 1.6') with a total flux of 1.4 Jy [0], with a compact source in the infrared visible at the centre. Since there is no counterpart at the WISE 12  $\mu\text{m}$  image (see Figure 2.9,  $F_{12} < 0.05$  Jy), the source meets our criteria for a candidate. However, Gvaramadze et al. [0] identify this source as a possible wind driven bubble around a Wolf-Rayet (WR) star. The dusty nebulae around WR stars can be bright at 22  $\mu\text{m}$  and relatively faint at  $\sim 12$   $\mu\text{m}$ , with spectroscopy studies suggesting that most emission toward WR nebulae at  $\sim 12$   $\mu\text{m}$  comes from material along the line of sight [e.g., 0]. Since the winds from Wolf-Rayet stars can be detected in the 1.4 GHz radio continuum [e.g., 0], this candidate could be a dusty WR nebula. However, G327.1+0.9 is an extended shell-like radio source and

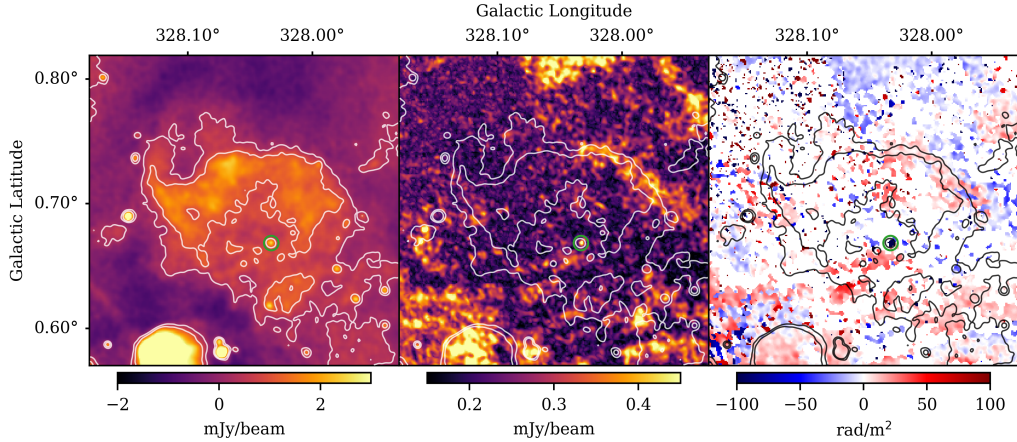


Figure 2.10: Total power, PI, and RM maps for G328.0+0.7 with total power contours to indicate where emission overlaps. The green circle indicates the location of the young pulsar, which is polarized and has a high rotation measure.

the radio emission from Wolf-Rayet winds is typically centrally peaked and does not extend much further than 1000 stellar radii [0]. In this case we propose that there are three possible explanations for G327.1+0.9. The first would be a late stage HII region produced by the central Wolf-Rayet star. The second would be a planetary nebula [0]. Finally, it could be the SNR of a supernova that exploded in a binary system. Follow-up polarimetric observations at high radio frequencies with ATCA should help to solve this mystery, as only the SNR would show linearly polarized radio emission.

**G328.0+0.7** The source shown in Figure B.17 is composed of roughly circular emission with a well-defined edge that is brightest in the northern part of the shell. There is a point source located near the centre of the candidate that coincides with the location of the known young ( $\sim 37$  kys) pulsar J1551–5310 [0]. Several HII regions can be seen in the south. There is possibly polarization associated with the northwest edge of the shell but it cannot be definitely differentiated from the background emission, as shown in Figure 2.10. We do see clear polarization coming from the central pulsar with a rotation measure of  $-1017 \pm 5$  rad/m<sup>2</sup>, consistent with the catalogued value of  $-1023.3 \pm 6.3$  rad/m<sup>2</sup> [99]. Because of the possible association with a young

pulsar and detectable polarization, we believe this source should be classified as a supernova remnant.

**G328.6+0.0** This source was observed by McClure et al. [118] and is listed by Green [2] as an SNR candidate but it does not appear in the actual catalogue. Here we see elongated filaments that form a roughly elliptical shape, which could be two separate sources (Figure B.18). There is a well-defined shell-like edge in the southwest and less defined shell-like filaments in the northeast. There are several overlapping HII regions and an unidentified bright point source located near the geometric centre of the southwest arc that may be polarized. The very bright source to the northwest of the image is G328.4+0.2. This source is visible in the GLEAM data and a steep negative spectral index of  $-0.75 \pm 0.06$  was determined, indicating the emission is likely nonthermal. We believe this source should also be classified as a supernova remnant.

**G330.2-1.6** This source, shown in Figure B.19, is very faint but it is located at a far distance from the Galactic plane making it detectable. It has a clear circular shell-like structure with little to no emission coming from the centre and no obvious MIR counterpart. The filamentary emission seen in the southeast appears to be unrelated and may instead be a radio galaxy, with a bright core, two external bright spots, and internal lobes, indicating jet precession.

## 2.6 Discussion

### 2.6.1 Estimating the SNR Density of the Galactic Disk

Based on our estimate of the size of the Galactic SNR population, we can roughly estimate the theoretical SNR surface density of the Galactic disk. Since most SNRs should be found within the star-forming disk, we assume a Galactic radius of 12.5 kpc, which encompasses 95% of the stellar mass of the Milky Way disk [0]. We

estimate that the Milky Way should have at least 1000–2700 radio-bright SNRs. This corresponds to an average Galactic SNR surface density between 2.0–5.5 SNRs/kpc<sup>2</sup>. We can compare this range of values to the density of known Galactic SNRs. The University of Manitoba’s SNRcat [3] currently lists 383 SNRs and SNR candidates. Of these, 369 have been detected in the radio. Thus, the Galaxy has an average known SNR surface density of only 0.75 radio-bright SNRs/kpc<sup>2</sup>.

To gain further insight into the missing SNR population, we can analyze how the known SNRs are distributed within the Galaxy by quadrant. Quadrants I and IV look towards the Galactic centre and encompass a larger, but denser, part of the Galactic plane. Quadrants II and III look away from the Galactic centre with shorter lines of sight and less emission. The known SNR surface density distribution can be broken down by quadrant as follows:

- Quadrant I ( $0^\circ \leq l < 90^\circ$ ): 0.74 SNRs/kpc<sup>2</sup>
- Quadrant II ( $90^\circ \leq l < 180^\circ$ ): 1.23 SNRs/kpc<sup>2</sup>
- Quadrant III ( $180^\circ \leq l < 270^\circ$ ): 0.63 SNRs/kpc<sup>2</sup>
- Quadrant IV ( $270^\circ \leq l < 360^\circ$ ): 0.72 SNRs/kpc<sup>2</sup>

We see that Quadrant II has a noticeably higher density of known SNRs than the other quadrants. It is likely higher than Quadrants I and IV because SNRs in Quadrant II are closer (on average) and there is less thermal emission in this direction. Quadrant II is also relatively well-surveyed which may explain why it has a higher density of known SNRs than Quadrant III.

The EMU/POSSUM Galactic pilot II field ( $323^\circ \leq l < 330^\circ$ ) has 7 known SNRs giving it an SNR surface density of 0.34 SNRs/kpc<sup>2</sup>, around a factor of 2 lower than the Quadrant IV average. To achieve the theoretical average Galactic SNR density of 2.0 – 5.5 SNRs/kpc<sup>2</sup> we would need to find 34 – 106 new SNRs in this field. If

we include our 21 SNR candidates, the density of known SNRs is brought up to 1.36 SNRs/kpc<sup>2</sup>, which is comparable to the SNR density we see in Quadrant II.

## 2.6.2 The Known Galactic SNR Population

Figure 2.11 shows how the angular sizes and flux densities of our SNR candidates compare to the known Galactic SNR population, not including the candidates for which we were unable to determine a reliable flux density. This plot was made using data from Green’s catalogue [2], omitting sources where no flux estimate was given. It should be noted that 1 GHz flux densities are provided in Green’s catalogue and our 933 MHz values were not adjusted to this frequency since we do not have spectral indices for most of the candidates. However, given the small frequency difference relative to the scale of the plot, the changes in the positions of the points are insignificant, even for sources with steep spectra.

The shaded regions of the plot indicate what we estimate to be the limits of what can be detected with our data. The minimum size was chosen to be 2’ as this is the size of our smallest source and we believe it would be difficult to detect shell-like structures for smaller sources given the 18” resolution. The minimum surface brightness was based on an estimate of the minimal thermal noise (taken to be  $\sigma = 40 \mu\text{Jy}/\text{beam}$ ), though variations across the image likely set different limits for different regions. The grey dotted lines in the plot represent the  $\sigma$  and  $3\sigma$  surface brightness limits. Because we are studying extended sources, rather than point sources, we are able to detect sources below the theoretical thermal noise limit.

Our results support that there is likely still a large population of undetected supernova remnants within our Galaxy. Figure 2.11 demonstrates that many of our candidates are smaller and fainter than most known SNRs. This may be evidence that some of the missing SNR population was missing because it was previously undetectable. Improvements in the angular resolution and sensitivity of radio telescopes should then allow for the detection of some of these SNRs in future sky surveys. It

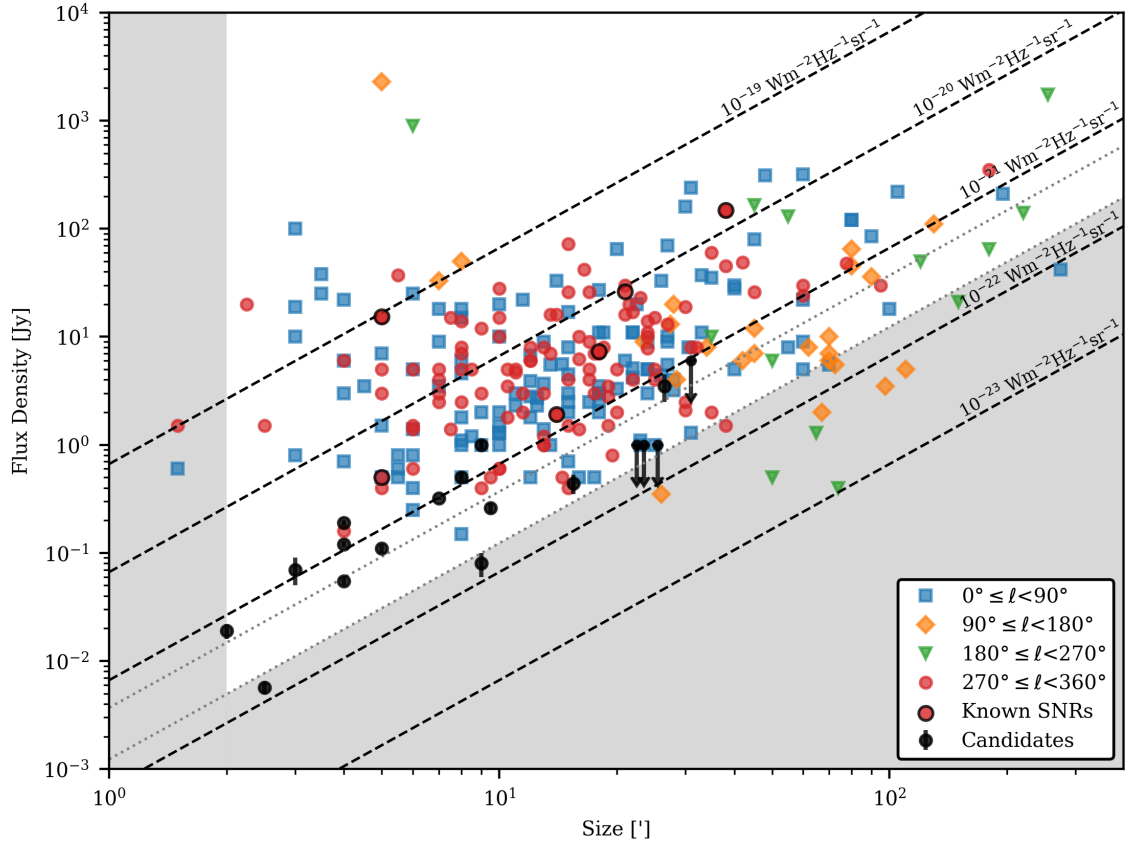


Figure 2.11: Sizes and flux densities of our SNR candidates compared with the known SNR population as a function of quadrant (data from Green’s catalogue [2], sources without flux estimates omitted). The “Known SNRs” are the six SNRs that are fully imaged in our field. The “Candidates” are the 18 SNR candidates listed in this paper for which we were able to obtain flux estimates. Note that for some candidates the error bars are too small to be visible and others have arrows to indicate that the values should be taken as upper limits. The dashed lines are lines of constant surface brightness. Shaded regions indicate the approximate limits of what we believe we should be able to detect with ASKAP at this frequency. The grey dotted lines represent the  $\sigma$  and  $3\sigma$  thermal noise limits.

may be that improvements in angular resolution are more important as the technological surface brightness lower limit is approaching the limit set by the background emission [6, 7]. However, future improvements in angular resolution may also have limited impact in Galactic SNR observations. Given that we have shown we are capable of detecting shell-like structures in sources as small as  $2'$ , even at the farthest Galactic distances within this field ( $\sim 18$  kpc) we should be able to detect sources with linear sizes as small as 10 pc. Based on observations of other Local Group galaxies [28, 0] and given that X-ray observations of young (small) Galactic SNRs are believed to be fairly complete [21], it is unlikely that there are many undetected sources below this size limit. Thus, any remaining missing SNRs in this field are most likely obscured by superimposed radio-bright sources, particularly HII regions.

The impact of background emission on SNR detection can be further demonstrated by the fact that we were not able to detect new sources in the brighter part of the field that we believe to be associated with the Norma arm. In fact, almost all of our candidates are in the lower right corner of the field, as shown in Figure 2.3. Theoretically, there should be a higher density of supernova remnants within and near spiral arms. If we compare the bright upper left half of the image to the lower right half, including our candidates the former has an SNR density of  $\sim 1$  SNR/kpc<sup>2</sup> while the latter has a density of  $\sim 2$  SNRs/kpc<sup>2</sup>, which is the theoretical lower limit we derived in Section 2.6.1. While the actual SNR density should be higher in the upper left half, we find the observed SNR density to be higher in the lower right half. This indicates there is likely still a population of SNRs within the bright part of the field that we were unable to detect. Further, this demonstrates the impact of background emission in setting detectability limits and supports that technological improvements in sensitivity may no longer be as effective for detecting new radio SNRs in these types of regions.

## 2.7 Conclusions

In this paper we used pilot data from ASKAP to study the known supernova remnant population in a small field of the Galactic plane. We also found 21 SNR candidates, three times the number of known SNRs in this field. Of the candidates, 13 have not been previously studied, 4 have been studied as SNR candidates, 3 classed as a single SNR, and 1 studied as an MIR nebula. For most candidates, observations at a second, ideally higher, frequency are required to confirm the sources as SNRs as these observations would likely provide more information about polarization and spectral indices.

The results of this paper demonstrate the potential for the full EMU/POSSUM surveys, taking place over the next few years, to fill in some of the missing Galactic supernova remnant population through the detection of small and/or faint sources. We were able to detect sources that seem to have been missed in previous surveys due to their small angular size and/or low surface brightness. Comparing the properties of our candidates to the known Galactic SNR population further supports this. Future work using ASKAP data to expand upon the size of the surveyed Galactic field will likely detect more of these types of sources, allowing for a better characterization of the Galactic SNR population. In this field we have uncovered approximately 1 new SNR/kpc<sup>2</sup>. The full EMU/POSSUM surveys will cover roughly 60% of the Galactic plane meaning they could hypothetically uncover around 300 new SNRs. However, it is important to note the impact of background emission and the challenges we faced in detecting low surface brightness SNRs in complex regions. Because a significant portion of the surveyed area will be in the direction of the Galactic centre, it is unlikely that we will be as successful in these denser, brighter fields.

The missing supernova remnant problem and the size of the Galactic SNR population remain difficult problems to exactly quantify. While technological advancements have continued to lead to new SNR detections, there is likely a population of SNRs

that will never be observed due to detection limits set by the local background. Estimates of the size of the Galactic SNR discrepancy should then exclude these types of sources as they may be considered undetectable. In future work we hope to further explore this problem, utilizing the full EMU/POSSUM surveys to study variations in SNR detectability across the Galactic plane.

## Acknowledgements

We are grateful to an anonymous referee whose comments improved the quality of the paper. This scientific work uses data obtained from Inyarrimanha Ilgari Bundara / the Murchison Radio-astronomy Observatory. We acknowledge the Wajarri Yamaji People as the Traditional Owners and native title holders of the Observatory site. CSIRO's ASKAP radio telescope is part of the Australia Telescope National Facility (<https://ror.org/05qajvd42>). Operation of ASKAP is funded by the Australian Government with support from the National Collaborative Research Infrastructure Strategy. ASKAP uses the resources of the Pawsey Supercomputing Research Centre. Establishment of ASKAP, Inyarrimanha Ilgari Bundara, the CSIRO Murchison Radio-astronomy Observatory and the Pawsey Supercomputing Research Centre are initiatives of the Australian Government, with support from the Government of Western Australia and the Science and Industry Endowment Fund. The POSSUM project (<https://possum-survey.org>) has been made possible through funding from the Australian Research Council, the Natural Sciences and Engineering Research Council of Canada (NSERC), the Canada Research Chairs Program, and the Canada Foundation for Innovation. This publication makes use of data products from the Wide-field Infrared Survey Explorer, which is a joint project of the University of California, Los Angeles, and the Jet Propulsion Laboratory/California Institute of Technology, funded by the National Aeronautics and Space Administration. RK acknowledges the support of NSERC, funding reference number RGPIN-2020-04853. ER acknowledges the support of NSERC, funding reference number RGPIN-2022-03499. The

Dunlap Institute is funded through an endowment established by the David Dunlap family and the University of Toronto. B.M.G. acknowledges the support of NSERC through grant RGPIN-2022-03163, and of the Canada Research Chairs program. DL acknowledges the support of NSERC.

# Chapter 3

## Conclusions and Future Work

### 3.1 Conclusions

While the missing SNR problem remains difficult to exactly quantify, there are clearly still Galactic SNRs left to be discovered. Historically, these discoveries have been driven by technological advancement and the invention of better radio telescopes. Based on our results, this appears to still be the case. In this work we have shown that ASKAP is capable of detecting many new SNR candidates in the southern sky, sources that probably would not have been detected with previous instruments. However, we may be reaching the point where improvements in radio telescopes will be less effective for detecting new Galactic SNRs. The resolution of telescopes like ASKAP, MeerKAT, and the VLA are good enough that we should be able to detect all but the smallest, and thus youngest, Galactic SNRs. As the young SNR population is believed to be mostly complete, future improvements in angular resolution may have limited impact.

We expect the remaining missing SNRs to have low surface brightness, as bright sources have most likely already been discovered. This is consistent with our findings in this work, as our candidates have relatively low surface brightnesses when compared to the rest of the Galactic SNR population. This is clearly evidenced in Figure 2.11. These faint sources are challenging to detect, particularly in regions with complex backgrounds. Most Galactic SNRs should be created in core-collapse

SNe, meaning we expect to find them near regions of active star formation, and thus within a high concentration of HII regions. As we demonstrate here, most of our candidates are located in the faint part of our field, even though we expect the true SNR density should be higher in the bright part. This indicates that the complexity of the background may now play an important role in determining what is detectable. Confusion from the diffuse background emission is also likely to make future detections more challenging. It may be that with instruments like ASKAP, detections of high latitude, probably large and faint, SNRs become more common, as confusion with the Galactic background is less of an issue. ASKAP is well-suited to observing these types of sources due to its large field of view.

## 3.2 Future Work

In this thesis, we used pilot data from ASKAP to demonstrate its capabilities for detecting new SNR candidates. In future work, we aim to apply the methods developed for this project to the full EMU/POSSUM surveys. We hope that with the new data we will be able to make better use of polarization and spectral indices as techniques for SNR identification, potentially utilizing data in a second frequency band, as collected by POSSUM. With these surveys, we should be able to help build a more complete census of the Galactic SNR population through the detection of low surface brightness, and possibly high latitude, sources. Identifying a larger sample of sources will allow us to conduct statistical studies of the distribution of SNRs in the Galaxy and their environments. This should help to refine parameters and models that go into the SNR radio evolutionary simulations. It will also help to tie SNRs to regions of star formation and the distribution of massive stars in our Galaxy. Understanding these factors may help to put constraints on our estimates of the missing Galactic SNR population.

It is also important to acknowledge that some Galactic SNRs will never be detected because of where they are located in the Galactic plane. SNRs in regions with high

densities of thermal emission, and particularly those located near the Galactic centre, will be difficult, if not impossible, to detect. Thus, it is important that our predictions of the number of radio-detectable SNRs account for this. Putting better constraints on SNR distances and thus locations, possibly using HI data, will help to develop these models. Perhaps data from WALLABY, an HI sky survey being conducted with ASKAP, could be useful in this endeavor. Ultimately, an improved understanding of the locations of known SNRs will allow us to better characterize their sizes, ages, luminosities, and the relationships they have to their surrounding environments. This will not only help us to understand the known SNR population but also allow us to make better predictions about what kinds of Galactic SNRs are missing from our surveys and the reasons why.

# Bibliography

- [1] K. M. Fierlinger *et al.*, “Stellar feedback efficiencies: supernovae versus stellar winds,” *Monthly Notices of the Royal Astronomical Society*, vol. 456, no. 1, pp. 710–730, Feb. 2016. DOI: 10.1093/mnras/stv2699. arXiv: 1511.05151 [astro-ph.GA].
- [2] D. A. Green. “A catalogue of galactic supernova remnants (2022 december version).” (2022), [Online]. Available: <https://www.mrao.cam.ac.uk/surveys/snrs/index.html> (visited on 01/16/2023).
- [3] G. Ferrand and S. Safi-Harb, “A census of high-energy observations of Galactic supernova remnants,” *Advances in Space Research*, vol. 49, no. 9, pp. 1313–1319, May 2012. DOI: 10.1016/j.asr.2012.02.004. arXiv: 1202.0245 [astro-ph.HE].
- [4] S. Ranasinghe and D. Leahy, “Distances, Radial Distribution, and Total Number of Galactic Supernova Remnants,” *The Astrophysical Journal*, vol. 940, no. 1, 63, p. 63, Nov. 2022. DOI: 10.3847/1538-4357/ac940a. arXiv: 2209.04570 [astro-ph.HE].
- [5] C. L. Brogan, J. D. Gelfand, B. M. Gaensler, N. E. Kassim, and T. J. W. Lazio, “Discovery of 35 New Supernova Remnants in the Inner Galaxy,” *The Astrophysical Journal Letters*, vol. 639, no. 1, pp. L25–L29, Mar. 2006. DOI: 10.1086/501500. arXiv: astro-ph/0601451 [astro-ph].
- [6] L. D. Anderson *et al.*, “Galactic supernova remnant candidates discovered by THOR,” *Astronomy & Astrophysics*, vol. 605, A58, A58, Sep. 2017. DOI: 10.1051/0004-6361/201731019. arXiv: 1705.10927 [astro-ph.GA].
- [7] R. Dokara *et al.*, “A global view on star formation: The GLOSTAR Galactic plane survey. VII. Supernova remnants in the Galactic longitude range  $28^\circ < l < 36^\circ$ ,” *arXiv e-prints*, arXiv:2211.13811, arXiv:2211.13811, Nov. 2022. arXiv: 2211.13811 [astro-ph.GA].
- [8] Z. Li, J. C. Wheeler, F. N. Bash, and W. H. Jefferys, “A Statistical Study of the Correlation of Galactic Supernova Remnants and Spiral Arms,” *The Astrophysical Journal*, vol. 378, p. 93, Sep. 1991. DOI: 10.1086/170409.
- [9] G. A. Tammann, W. Loeffler, and A. Schroeder, “The Galactic Supernova Rate,” *The Astrophysical Journal Supplement*, vol. 92, p. 487, Jun. 1994. DOI: 10.1086/192002.

- [10] S. K. Sarbadhicary, C. Badenes, L. Chomiuk, D. Caprioli, and D. Huizenga, “Supernova remnants in the Local Group - I. A model for the radio luminosity function and visibility times of supernova remnants,” *Monthly Notices of the Royal Astronomical Society*, vol. 464, no. 2, pp. 2326–2340, Jan. 2017. DOI: 10.1093/mnras/stw2566. arXiv: 1605.04923 [astro-ph.HE].
- [11] S. Woosley and T. Janka, “The physics of core-collapse supernovae,” *Nature Physics*, vol. 1, no. 3, pp. 147–154, Dec. 2005. DOI: 10.1038/nphys172. arXiv: astro-ph/0601261 [astro-ph].
- [12] S. J. Smartt, “Progenitors of Core-Collapse Supernovae,” *Annual Reviews of Astronomy & Astrophysics*, vol. 47, no. 1, pp. 63–106, Sep. 2009. DOI: 10.1146/annurev-astro-082708-101737. arXiv: 0908.0700 [astro-ph.SR].
- [13] T. Sukhbold, T. Ertl, S. E. Woosley, J. M. Brown, and H. T. Janka, “Core-collapse Supernovae from 9 to 120 Solar Masses Based on Neutrino-powered Explosions,” *The Astrophysical Journal*, vol. 821, no. 1, 38, p. 38, Apr. 2016. DOI: 10.3847/0004-637X/821/1/38. arXiv: 1510.04643 [astro-ph.HE].
- [14] K. Nomoto, “Evolution of 8-10 solar mass stars toward electron capture supernovae. I - Formation of electron-degenerate O + NE + MG cores.,” *The Astrophysical Journal*, vol. 277, pp. 791–805, Feb. 1984. DOI: 10.1086/161749.
- [15] D. Hiramatsu *et al.*, “The electron-capture origin of supernova 2018zd,” *Nature Astronomy*, vol. 5, pp. 903–910, Jun. 2021. DOI: 10.1038/s41550-021-01384-2. arXiv: 2011.02176 [astro-ph.HE].
- [16] H. T. Janka and A. Bauswein, “Dynamics and Equation of State Dependencies of Relevance for Nucleosynthesis in Supernovae and Neutron Star Mergers,” *arXiv e-prints*, arXiv:2212.07498, arXiv:2212.07498, Dec. 2022. DOI: 10.48550/arXiv.2212.07498. arXiv: 2212.07498 [astro-ph.HE].
- [17] Z.-W. Liu, F. K. Röpke, and Z. Han, “Type Ia Supernova Explosions in Binary Systems: A Review,” *Research in Astronomy and Astrophysics*, vol. 23, no. 8, 082001, p. 082001, Aug. 2023. DOI: 10.1088/1674-4527/acd89e. arXiv: 2305.13305 [astro-ph.HE].
- [18] W. Hillebrandt and J. C. Niemeyer, “Type IA Supernova Explosion Models,” *Annual Reviews of Astronomy & Astrophysics*, vol. 38, pp. 191–230, Jan. 2000. DOI: 10.1146/annurev.astro.38.1.191. arXiv: astro-ph/0006305 [astro-ph].
- [19] D. Maoz, F. Mannucci, and G. Nelemans, “Observational Clues to the Progenitors of Type Ia Supernovae,” *Annual Reviews of Astronomy & Astrophysics*, vol. 52, pp. 107–170, Aug. 2014. DOI: 10.1146/annurev-astro-082812-141031. arXiv: 1312.0628 [astro-ph.CO].
- [20] P. A. Mazzali, F. K. Röpke, S. Benetti, and W. Hillebrandt, “A Common Explosion Mechanism for Type Ia Supernovae,” *Science*, vol. 315, no. 5813, p. 825, Feb. 2007. DOI: 10.1126/science.1136259. arXiv: astro-ph/0702351 [astro-ph].

- [21] D. A. Leahy, S. Ranasinghe, and M. Gelowitz, “Evolutionary Models for 43 Galactic Supernova Remnants with Distances and X-Ray Spectra,” *The Astrophysical Journal Supplement*, vol. 248, no. 1, 16, p. 16, May 2020. DOI: 10.3847/1538-4365/ab8bd9. arXiv: 2003.08998 [astro-ph.HE].
- [22] L. Woltjer, “Supernova Remnants,” *Annual Reviews of Astronomy & Astrophysics*, vol. 10, p. 129, Jan. 1972. DOI: 10.1146/annurev.aa.10.090172.001021.
- [23] A. Bamba and B. J. Williams, “Supernova Remnants: Types and Evolution,” in *Handbook of X-ray and Gamma-ray Astrophysics. Edited by Cosimo Bambi and Andrea Santangelo*, 2022, 77, p. 77. DOI: 10.1007/978-981-16-4544-0-88-1.
- [24] J. K. Truelove and C. F. McKee, “Evolution of Nonradiative Supernova Remnants,” *The Astrophysical Journal Supplement*, vol. 120, no. 2, pp. 299–326, Feb. 1999. DOI: 10.1086/313176.
- [25] J. Vink, *Physics and Evolution of Supernova Remnants*. 2020. DOI: 10.1007/978-3-030-55231-2.
- [26] L. I. Sedov, *Similarity and Dimensional Methods in Mechanics*. 1959.
- [27] D. F. Cioffi, C. F. McKee, and E. Bertschinger, “Dynamics of Radiative Supernova Remnants,” *The Astrophysical Journal*, vol. 334, p. 252, Nov. 1988. DOI: 10.1086/166834.
- [28] C. Badenes, D. Maoz, and B. T. Draine, “On the size distribution of supernova remnants in the Magellanic Clouds,” *Monthly Notices of the Royal Astronomical Society*, vol. 407, no. 2, pp. 1301–1313, Sep. 2010. DOI: 10.1111/j.1365-2966.2010.17023.x. arXiv: 1003.3030 [astro-ph.GA].
- [29] C. Albert and V. V. Dwarkadas, “An exploration of X-ray Supernova remnants in the Milky Way and nearby galaxies,” *Monthly Notices of the Royal Astronomical Society*, vol. 514, no. 1, pp. 728–743, Jul. 2022. DOI: 10.1093/mnras/stac1288. arXiv: 2205.05103 [astro-ph.HE].
- [30] G. Dubner, “Radio Emission from Supernova Remnants,” in *Handbook of Supernovae*, A. W. Alsabti and P. Murdin, Eds., 2017, p. 2041. DOI: 10.1007/978-3-319-21846-5\_91.
- [31] D. A. Green, “A revised catalogue of 294 Galactic supernova remnants,” *Journal of Astrophysics and Astronomy*, vol. 40, no. 4, 36, p. 36, Aug. 2019. DOI: 10.1007/s12036-019-9601-6. arXiv: 1907.02638 [astro-ph.GA].
- [32] R. Kothes and J.-A. Brown, “Probing interstellar magnetic fields with Supernova remnants,” in *Cosmic Magnetic Fields: From Planets, to Stars and Galaxies*, K. G. Strassmeier, A. G. Kosovichev, and J. E. Beckman, Eds., vol. 259, Apr. 2009, pp. 75–80. DOI: 10.1017/S1743921309030087. arXiv: 0812.3392 [astro-ph].
- [33] J. Rho and R. Petre, “Mixed-Morphology Supernova Remnants,” *The Astrophysical Journal Letters*, vol. 503, no. 2, pp. L167–L170, Aug. 1998. DOI: 10.1086/311538.

- [34] R. Kothes, “Radio Properties of Pulsar Wind Nebulae,” in *Modelling Pulsar Wind Nebulae*, D. F. Torres, Ed., ser. Astrophysics and Space Science Library, vol. 446, Jan. 2017, p. 1. DOI: 10.1007/978-3-319-63031-1\_1.
- [35] B. M. Gaensler and P. O. Slane, “The Evolution and Structure of Pulsar Wind Nebulae,” *Annual Reviews of Astronomy & Astrophysics*, vol. 44, no. 1, pp. 17–47, Sep. 2006. DOI: 10.1146/annurev.astro.44.051905.092528. arXiv: astro-ph/0601081 [astro-ph].
- [36] E. van der Swaluw, T. P. Downes, and R. Keegan, “An evolutionary model for pulsar-driven supernova remnants. A hydrodynamical model,” *Astronomy & Astrophysics*, vol. 420, pp. 937–944, Jun. 2004. DOI: 10.1051/0004-6361:20035700. arXiv: astro-ph/0311388 [astro-ph].
- [37] T. Temim, P. Slane, C. Kolb, J. Blondin, J. P. Hughes, and N. Bucciantini, “Late-Time Evolution of Composite Supernova Remnants: Deep Chandra Observations and Hydrodynamical Modeling of a Crushed Pulsar Wind Nebula in SNR G327.1-1.1,” *The Astrophysical Journal*, vol. 808, no. 1, 100, p. 100, Jul. 2015. DOI: 10.1088/0004-637X/808/1/100. arXiv: 1506.03069 [astro-ph.HE].
- [38] G. B. Rybicki and A. P. Lightman, *Radiative Processes in Astrophysics*. 1986.
- [39] M. S. Longair, *High Energy Astrophysics*. 2011.
- [40] R. Blandford and D. Eichler, “Particle acceleration at astrophysical shocks: A theory of cosmic ray origin,” *Physics Reports*, vol. 154, no. 1, pp. 1–75, Oct. 1987. DOI: 10.1016/0370-1573(87)90134-7.
- [41] A. R. Bell, “The acceleration of cosmic rays in shock fronts - I.,” *Monthly Notices of the Royal Astronomical Society*, vol. 182, pp. 147–156, Jan. 1978. DOI: 10.1093/mnras/182.2.147.
- [42] R. D. Blandford and J. P. Ostriker, “Particle acceleration by astrophysical shocks.,” *The Astrophysical Journal Letters*, vol. 221, pp. L29–L32, Apr. 1978. DOI: 10.1086/182658.
- [43] B. Schaefer, E. Collett, R. Smyth, D. Barrett, and B. Fraher, “Measuring the Stokes polarization parameters,” *American Journal of Physics*, vol. 75, no. 2, pp. 163–168, Feb. 2007. DOI: 10.1119/1.2386162.
- [44] R. Kothes, P. Reich, T. J. Foster, and W. Reich, “G181.1+9.5, a new high-latitude low-surface brightness supernova remnant,” *Astronomy & Astrophysics*, vol. 597, A116, A116, Jan. 2017. DOI: 10.1051/0004-6361/201629848. arXiv: 1612.01956 [astro-ph.HE].
- [45] J.-W. Xu, X.-Z. Zhang, and J.-L. Han, “Statistics of Galactic Supernova Remnants,” *Chinese Journal of Astronomy and Astrophysics*, vol. 5, no. 2, pp. 165–174, Apr. 2005. DOI: 10.1088/1009-9271/5/2/007.
- [46] S. Ranasinghe and D. Leahy, “A Statistical Analysis of Galactic Radio Supernova Remnants,” *The Astrophysical Journal Supplement*, vol. 265, no. 2, 53, p. 53, Apr. 2023. DOI: 10.3847/1538-4365/acc1de. arXiv: 2302.06593 [astro-ph.GA].

- [47] S. Xu, N. Klingler, O. Kargaltsev, and B. Zhang, “On the Broadband Synchrotron Spectra of Pulsar Wind Nebulae,” *The Astrophysical Journal*, vol. 872, no. 1, 10, p. 10, Feb. 2019. DOI: 10.3847/1538-4357/aafb2e. arXiv: 1812.10827 [astro-ph.HE].
- [48] S. J. Tanaka and F. Takahara, “A Model of the Spectral Evolution of Pulsar Wind Nebulae,” *The Astrophysical Journal*, vol. 715, no. 2, pp. 1248–1257, Jun. 2010. DOI: 10.1088/0004-637X/715/2/1248. arXiv: 1004.3098 [astro-ph.HE].
- [49] B.-T. Zhu, L. Zhang, and J. Fang, “Multiband nonthermal radiative properties of pulsar wind nebulae,” *Astronomy & Astrophysics*, vol. 609, A110, A110, Jan. 2018. DOI: 10.1051/0004-6361/201629108.
- [50] B. J. Williams and T. Temim, “Infrared Emission from Supernova Remnants: Formation and Destruction of Dust,” in *Handbook of Supernovae*, A. W. Alsabti and P. Murdin, Eds., 2017, p. 2105. DOI: 10.1007/978-3-319-21846-5\_94.
- [51] S. Bianchi and R. Schneider, “Dust formation and survival in supernova ejecta,” *Monthly Notices of the Royal Astronomical Society*, vol. 378, no. 3, pp. 973–982, Jul. 2007. DOI: 10.1111/j.1365-2966.2007.11829.x. arXiv: 0704.0586 [astro-ph].
- [52] D. W. Silvia, B. D. Smith, and J. M. Shull, “Numerical Simulations of Supernova Dust Destruction. I. Cloud-crushing and Post-processed Grain Sputtering,” *The Astrophysical Journal*, vol. 715, no. 2, pp. 1575–1590, Jun. 2010. DOI: 10.1088/0004-637X/715/2/1575. arXiv: 1001.4793 [astro-ph.GA].
- [53] F. Kirchschrager, F. D. Schmidt, M. J. Barlow, E. L. Fogerty, A. Bevan, and F. D. Priestley, “Dust survival rates in clumps passing through the Cas A reverse shock - I. Results for a range of clump densities,” *Monthly Notices of the Royal Astronomical Society*, vol. 489, no. 4, pp. 4465–4496, Nov. 2019. DOI: 10.1093/mnras/stz2399. arXiv: 1908.10875 [astro-ph.SR].
- [54] F. D. Priestley, H. Chawner, M. Matsuura, I. De Looze, M. J. Barlow, and H. L. Gomez, “Revisiting the dust destruction efficiency of supernovae,” *Monthly Notices of the Royal Astronomical Society*, vol. 500, no. 2, pp. 2543–2553, Jan. 2021. DOI: 10.1093/mnras/staa3445. arXiv: 2011.00937 [astro-ph.GA].
- [55] J. D. Slavin, E. Dwek, and A. P. Jones, “Destruction of Interstellar Dust in Evolving Supernova Remnant Shock Waves,” *The Astrophysical Journal*, vol. 803, no. 1, 7, p. 7, Apr. 2015. DOI: 10.1088/0004-637X/803/1/7. arXiv: 1502.00929 [astro-ph.GA].
- [56] F. D. Priestley, H. Chawner, M. J. Barlow, I. De Looze, H. L. Gomez, and M. Matsuura, “Properties of shocked dust grains in supernova remnants,” *Monthly Notices of the Royal Astronomical Society*, vol. 516, no. 2, pp. 2314–2325, Oct. 2022. DOI: 10.1093/mnras/stac2408. arXiv: 2208.11137 [astro-ph.GA].
- [57] J. M. Saken, R. A. Fesen, and J. M. Shull, “An IRAS Survey of Galactic Supernova Remnants,” *The Astrophysical Journal Supplement*, vol. 81, p. 715, Aug. 1992. DOI: 10.1086/191703.

- [58] W. T. Reach *et al.*, “A Spitzer Space Telescope Infrared Survey of Supernova Remnants in the Inner Galaxy,” *The Astronomical Journal*, vol. 131, no. 3, pp. 1479–1500, Mar. 2006. DOI: 10.1086/499306. arXiv: astro-ph/0510630 [astro-ph].
- [59] H. Chawner *et al.*, “A complete catalogue of dusty supernova remnants in the Galactic plane,” *Monthly Notices of the Royal Astronomical Society*, vol. 493, no. 2, pp. 2706–2744, Apr. 2020. DOI: 10.1093/mnras/staa221. arXiv: 2001.05504 [astro-ph.GA].
- [60] J. R. Thorstensen, R. A. Fesen, and S. van den Bergh, “The Expansion Center and Dynamical Age of the Galactic Supernova Remnant Cassiopeia A,” *The Astronomical Journal*, vol. 122, no. 1, pp. 297–307, Jul. 2001. DOI: 10.1086/321138. arXiv: astro-ph/0104188 [astro-ph].
- [61] J. Rho *et al.*, “Freshly Formed Dust in the Cassiopeia A Supernova Remnant as Revealed by the Spitzer Space Telescope,” *The Astrophysical Journal*, vol. 673, no. 1, pp. 271–282, Jan. 2008. DOI: 10.1086/523835. arXiv: 0709.2880 [astro-ph].
- [62] F. D. Priestley, M. Arias, M. J. Barlow, and I. De Looze, “Dust destruction and survival in the Cassiopeia A reverse shock,” *Monthly Notices of the Royal Astronomical Society*, vol. 509, no. 3, pp. 3163–3171, Jan. 2022. DOI: 10.1093/mnras/stab3195. arXiv: 2111.01151 [astro-ph.GA].
- [63] W. P. Blair and J. C. Raymond, “Ultraviolet and Optical Insights into Supernova Remnant Shocks,” in *Handbook of Supernovae*, A. W. Alsabti and P. Murdin, Eds., 2017, p. 2087. DOI: 10.1007/978-3-319-21846-5\_93.
- [64] R. A. Fesen and A. P. Hurford, “A Catalog of Ultraviolet, Optical, and Near-Infrared Emission Lines Identified in Supernova Remnants,” *The Astrophysical Journal Supplement*, vol. 106, p. 563, Oct. 1996. DOI: 10.1086/192348.
- [65] E. I. Makarenko *et al.*, “How do supernova remnants cool? – I. Morphology, optical emission lines, and shocks,” *arXiv e-prints*, arXiv:2305.07652, arXiv:2305.07652, May 2023. DOI: 10.48550/arXiv.2305.07652. arXiv: 2305.07652 [astro-ph.HE].
- [66] R. A. Fesen *et al.*, “Far-UV and Optical Emissions from Three Very Large Supernova Remnants Located at Unusually High Galactic Latitudes,” *The Astrophysical Journal*, vol. 920, no. 2, 90, p. 90, Oct. 2021. DOI: 10.3847/1538-4357/ac0ada. arXiv: 2102.12599 [astro-ph.HE].
- [67] J. Vink, “X-Ray Emission Properties of Supernova Remnants,” in *Handbook of Supernovae*, A. W. Alsabti and P. Murdin, Eds., 2017, p. 2063. DOI: 10.1007/978-3-319-21846-5\_92.
- [68] E. A. Helder, J. Vink, A. M. Bykov, Y. Ohira, J. C. Raymond, and R. Terrier, “Observational Signatures of Particle Acceleration in Supernova Remnants,” *Space Science Reports*, vol. 173, no. 1-4, pp. 369–431, Nov. 2012. DOI: 10.1007/s11214-012-9919-8. arXiv: 1206.1593 [astro-ph.HE].

- [69] J. Vink, “Supernova remnants: the X-ray perspective,” *Astronomy & Astrophysics Reports*, vol. 20, 49, p. 49, Dec. 2012. DOI: 10.1007/s00159-011-0049-1. arXiv: 1112.0576 [astro-ph.HE].
- [70] A. M. Bykov, D. C. Ellison, A. Marcowith, and S. M. Osipov, “Cosmic Ray Production in Supernovae,” *Space Science Reports*, vol. 214, no. 1, 41, p. 41, Feb. 2018. DOI: 10.1007/s11214-018-0479-4. arXiv: 1801.08890 [astro-ph.HE].
- [71] S. Funk, “High-Energy Gamma Rays from Supernova Remnants,” in *Handbook of Supernovae*, A. W. Alsabti and P. Murdin, Eds., 2017, p. 1737. DOI: 10.1007/978-3-319-21846-5\_12.
- [72] F. Acero *et al.*, “The First Fermi LAT Supernova Remnant Catalog,” *The Astrophysical Journal Supplement*, vol. 224, no. 1, 8, p. 8, May 2016. DOI: 10.3847/0067-0049/224/1/8. arXiv: 1511.06778 [astro-ph.HE].
- [73] Q. Yuan, S. Liu, and X. Bi, “An Attempt at a Unified Model for the Gamma-Ray Emission of Supernova Remnants,” *The Astrophysical Journal*, vol. 761, no. 2, 133, p. 133, Dec. 2012. DOI: 10.1088/0004-637X/761/2/133. arXiv: 1203.0085 [astro-ph.HE].
- [74] D. Caprioli, “Cosmic-ray acceleration in supernova remnants: non-linear theory revised,” *Journal of Cosmology and Physics*, vol. 2012, no. 7, 038, p. 038, Jul. 2012. DOI: 10.1088/1475-7516/2012/07/038. arXiv: 1206.1360 [astro-ph.HE].
- [75] H. Zeng, Y. Xin, and S. Liu, “Evolution of High-energy Particle Distribution in Supernova Remnants,” *The Astrophysical Journal*, vol. 874, no. 1, 50, p. 50, Mar. 2019. DOI: 10.3847/1538-4357/aaf392. arXiv: 1811.12644 [astro-ph.HE].
- [76] J. Becker Tjus and L. Merten, “Closing in on the origin of Galactic cosmic rays using multimessenger information,” *Physics Reports*, vol. 872, pp. 1–98, Aug. 2020. DOI: 10.1016/j.physrep.2020.05.002. arXiv: 2002.00964 [astro-ph.HE].
- [77] D. J. Helfand, R. H. Becker, R. L. White, A. Fallon, and S. Tuttle, “MAGPIS: A Multi-Array Galactic Plane Imaging Survey,” *The Astronomical Journal*, vol. 131, no. 5, pp. 2525–2537, May 2006. DOI: 10.1086/503253.
- [78] A. J. Green, S. N. Reeves, and T. Murphy, “The Second Epoch Molonglo Galactic Plane Survey: Images and Candidate Supernova Remnants,” *Publications of the Astronomical Society of Australia*, vol. 31, e042, e042, Nov. 2014. DOI: 10.1017/pasa.2014.37. arXiv: 1410.8247 [astro-ph.GA].
- [79] D. A. Green, “Constraints on the distribution of supernova remnants with Galactocentric radius,” *Monthly Notices of the Royal Astronomical Society*, vol. 454, no. 2, pp. 1517–1524, Dec. 2015. DOI: 10.1093/mnras/stv1885. arXiv: 1508.02931 [astro-ph.HE].
- [80] T. Foster, R. Kothes, X. H. Sun, W. Reich, and J. L. Han, “ $10^{51}$  erg less: the Galactic H II region OA 184,” *Astronomy & Astrophysics*, vol. 454, no. 2, pp. 517–526, Aug. 2006. DOI: 10.1051/0004-6361:20064881.

- [81] S. Ranasinghe, D. Leahy, and W. W. Tian, “Distance and Evolutionary States of Supernova Remnant G18.9-1.1 and Candidate G28.6+0.0,” *arXiv e-prints*, arXiv:1910.05407, arXiv:1910.05407, Oct. 2019. DOI: 10.48550/arXiv.1910.05407. arXiv: 1910.05407 [astro-ph.HE].
- [82] D. Leahy and W. Tian, “Distances to Supernova Remnants from H I Absorption Spectra,” in *The Dynamic Interstellar Medium: A Celebration of the Canadian Galactic Plane Survey*, R. Kothes, T. L. Landecker, and A. G. Willis, Eds., ser. Astronomical Society of the Pacific Conference Series, vol. 438, Dec. 2010, p. 365.
- [83] G. L. Case and D. Bhattacharya, “A New  $\Sigma$ -D Relation and Its Application to the Galactic Supernova Remnant Distribution,” *The Astrophysical Journal*, vol. 504, no. 2, pp. 761–772, Sep. 1998. DOI: 10.1086/306089. arXiv: astro-ph/9807162 [astro-ph].
- [84] R. P. Norris *et al.*, “The Evolutionary Map of the Universe pilot survey,” *Publications of the Astronomical Society of Australia*, vol. 38, e046, e046, Sep. 2021. DOI: 10.1017/pasa.2021.42. arXiv: 2108.00569 [astro-ph.CO].
- [85] B. M. Gaensler, T. L. Landecker, A. R. Taylor, and POSSUM Collaboration, “Survey Science with ASKAP: Polarization Sky Survey of the Universe’s Magnetism (POSSUM),” in *American Astronomical Society Meeting Abstracts #215*, ser. American Astronomical Society Meeting Abstracts, vol. 215, Jan. 2010, 470.13, p. 470.13.
- [86] R. Dokara *et al.*, “A global view on star formation: The GLOSTAR Galactic plane survey. II. Supernova remnants in the first quadrant of the Milky Way,” *Astronomy & Astrophysics*, vol. 651, A86, A86, Jul. 2021. DOI: 10.1051/0004-6361/202039873. arXiv: 2103.06267 [astro-ph.GA].
- [87] N. Hurley-Walker *et al.*, “Candidate radio supernova remnants observed by the GLEAM survey over  $345^\circ \leq l \leq 60^\circ$  and  $180^\circ \leq l \leq 240^\circ$ ,” *Publications of the Astronomical Society of Australia*, vol. 36, e048, e048, Nov. 2019. DOI: 10.1017/pasa.2019.33. arXiv: 1911.08124 [astro-ph.HE].
- [88] S. Stanimirovic, “Short-Spacings Correction from the Single-Dish Perspective,” in *Single-Dish Radio Astronomy: Techniques and Applications*, S. Stanimirovic, D. Altschuler, P. Goldsmith, and C. Salter, Eds., ser. Astronomical Society of the Pacific Conference Series, vol. 278, Dec. 2002, pp. 375–396. DOI: 10.48550/arXiv.astro-ph/0205329. arXiv: astro-ph/0205329 [astro-ph].
- [89] E. Bajaja and G. D. van Albada, “Complementing aperture synthesis radio data by short spacing components from single dish observations.,” *Astronomy & Astrophysics*, vol. 75, no. 1-2, pp. 251–254, May 1979.
- [90] R. Braun and R. A. M. Walterbos, “A solution to the short spacing problem in radio interferometry.,” *Astronomy & Astrophysics*, vol. 143, pp. 307–312, Feb. 1985.

- [91] A. W. Hotan *et al.*, “Australian square kilometre array pathfinder: I. system description,” *Publications of the Astronomical Society of Australia*, vol. 38, e009, e009, Mar. 2021. DOI: 10.1017/pasa.2021.1. arXiv: 2102.01870 [astro-ph.IM].
- [92] T. Padmanabhan, *Theoretical Astrophysics - Volume 2, Stars and Stellar Systems*. 2001, vol. 2. DOI: 10.2277/0521562414.
- [93] D. A. Frail, W. M. Goss, and J. B. Z. Whiteoak, “The Radio Lifetime of Supernova Remnants and the Distribution of Pulsar Velocities at Birth,” *The Astrophysical Journal*, vol. 437, p. 781, Dec. 1994. DOI: 10.1086/175038. arXiv: astro-ph/9407031 [astro-ph].
- [94] D. A. Leahy, F. Merrick, and M. Filipović, “Radio Emission from Supernova Remnants: Model Comparison with Observations,” *Universe*, vol. 8, no. 12, p. 653, Dec. 2022. DOI: 10.3390/universe8120653.
- [95] J. B. Z. Whiteoak and A. J. Green, “The MOST supernova remnant catalogue (MSC).,” *Astronomy & Astrophysics Supplement*, vol. 118, pp. 329–380, Aug. 1996.
- [96] E. Fuerst, W. Reich, and Y. Sofue, “The identification of galactic radio sources based on a comparison of radio-continuum and infrared emission,” *Astronomy & Astrophysics Supplement*, vol. 71, no. 1, pp. 63–67, Oct. 1987.
- [97] D. Pinheiro Gonçalves, A. Noriega-Crespo, R. Paladini, P. G. Martin, and S. J. Carey, “The MIPS GAL View of Supernova Remnants in the Galactic Plane,” *The Astronomical Journal*, vol. 142, no. 2, 47, p. 47, Aug. 2011. DOI: 10.1088/0004-6256/142/2/47. arXiv: 1104.2894 [astro-ph.GA].
- [98] R. P. Norris *et al.*, “EMU: Evolutionary Map of the Universe,” *Publications of the Astronomical Society of Australia*, vol. 28, no. 3, pp. 215–248, Aug. 2011. DOI: 10.1071/AS11021. arXiv: 1106.3219 [astro-ph.CO].
- [99] J. L. Han, R. N. Manchester, W. van Straten, and P. Demorest, “Pulsar Rotation Measures and Large-scale Magnetic Field Reversals in the Galactic Disk,” *The Astrophysical Journal Supplement*, vol. 234, no. 1, 11, p. 11, Jan. 2018. DOI: 10.3847/1538-4365/aa9c45. arXiv: 1712.01997 [astro-ph.GA].
- [100] E. L. Wright *et al.*, “The Wide-field Infrared Survey Explorer (WISE): Mission Description and Initial On-orbit Performance,” *The Astronomical Journal*, vol. 140, no. 6, pp. 1868–1881, Dec. 2010. DOI: 10.1088/0004-6256/140/6/1868. arXiv: 1008.0031 [astro-ph.IM].
- [101] L. D. Anderson *et al.*, “The WISE Catalog of Galactic H II Regions,” *The Astrophysical Journal Supplement*, vol. 212, no. 1, 1, p. 1, May 2014. DOI: 10.1088/0067-0049/212/1/1. arXiv: 1312.6202 [astro-ph.GA].
- [102] R. M. Cutri *et al.*, *Explanatory Supplement to the AllWISE Data Release Products*, Explanatory Supplement to the AllWISE Data Release Products, by R. M. Cutri *et al.* Nov. 2013.

- [103] R. B. Wayth *et al.*, “GLEAM: The GaLactic and Extragalactic All-Sky MWA Survey,” *Publications of the Astronomical Society of Australia*, vol. 32, e025, e025, Jun. 2015. DOI: 10.1017/pasa.2015.26. arXiv: 1505.06041 [astro-ph.IM].
- [104] R. Gooch, “Space and the Spaceball,” in *Astronomical Data Analysis Software and Systems IV*, R. A. Shaw, H. E. Payne, and J. J. E. Hayes, Eds., ser. Astronomical Society of the Pacific Conference Series, vol. 77, 1995, p. 144.
- [105] H. van der Laan, “Intense shell sources of radio emission,” *Monthly Notices of the Royal Astronomical Society*, vol. 124, p. 179, Jan. 1962. DOI: 10.1093/mnras/124.2.179.
- [106] J. B. Whiteoak and F. F. Gardner, “A Supernova Remnant in Centaurus,” *The Astrophysical Journal*, vol. 154, p. 807, Dec. 1968. DOI: 10.1086/149803.
- [107] B. T. Draine, *Physics of the Interstellar and Intergalactic Medium*. 2011.
- [108] S. P. Reynolds, B. M. Gaensler, and F. Bocchino, “Magnetic Fields in Supernova Remnants and Pulsar-Wind Nebulae,” *Space Science Reports*, vol. 166, no. 1-4, pp. 231–261, May 2012. DOI: 10.1007/s11214-011-9775-y. arXiv: 1104.4047 [astro-ph.GA].
- [109] G. Dubner and E. Giacani, “Radio emission from supernova remnants,” *Astronomy & Astrophysics Reports*, vol. 23, 3, p. 3, Sep. 2015. DOI: 10.1007/s00159-015-0083-5. arXiv: 1508.07294 [astro-ph.HE].
- [110] R. Kothes and W. Reich, “A high frequency radio study of G11.2-0.3, a historical supernova remnant with a flat spectrum core,” *Astronomy & Astrophysics*, vol. 372, pp. 627–635, Jun. 2001. DOI: 10.1051/0004-6361:20010407. arXiv: astro-ph/0104384 [astro-ph].
- [111] R. Dokara *et al.*, “Confirmation Of Two Galactic Supernova Remnant Candidates Discovered by THOR,” *The Astrophysical Journal*, vol. 866, no. 1, 61, p. 61, Oct. 2018. DOI: 10.3847/1538-4357/aadc0c. arXiv: 1808.06628 [astro-ph.GA].
- [112] S. Wang *et al.*, “Distances to the supernova remnants in the inner disk,” *Astronomy & Astrophysics*, vol. 639, A72, A72, Jul. 2020. DOI: 10.1051/0004-6361/201936868. arXiv: 2005.08270 [astro-ph.GA].
- [113] M. Sun, Z.-r. Wang, and Y. Chen, “X-Ray Observation and Analysis of the Composite Supernova Remnant G327.1-1.1,” *The Astrophysical Journal*, vol. 511, no. 1, pp. 274–281, Jan. 1999. DOI: 10.1086/306656. arXiv: astro-ph/9808339 [astro-ph].
- [114] J. D. Gelfand and B. M. Gaensler, “The Compact X-Ray Source 1E 1547.0-5408 and the Radio Shell G327.24-0.13: A New Proposed Association between a Candidate Magnetar and a Candidate Supernova Remnant,” *The Astrophysical Journal*, vol. 667, no. 2, pp. 1111–1118, Oct. 2007. DOI: 10.1086/520526. arXiv: 0706.1054 [astro-ph].

- [115] F. Camilo, S. M. Ransom, J. P. Halpern, and J. Reynolds, “1E 1547.0-5408: A Radio-emitting Magnetar with a Rotation Period of 2 Seconds,” *The Astrophysical Journal Letters*, vol. 666, no. 2, pp. L93–L96, Sep. 2007. DOI: 10.1086/521826. arXiv: 0708.0002 [astro-ph].
- [116] F. Camilo, J. Reynolds, S. Johnston, J. P. Halpern, and S. M. Ransom, “The Magnetar 1E 1547.0-5408: Radio Spectrum, Polarimetry, and Timing,” *The Astrophysical Journal*, vol. 679, no. 1, pp. 681–686, May 2008. DOI: 10.1086/587054. arXiv: 0802.0494 [astro-ph].
- [117] A. Tiengo *et al.*, “The Dust-scattering X-ray Rings of the Anomalous X-ray Pulsar 1E 1547.0-5408,” *The Astrophysical Journal*, vol. 710, no. 1, pp. 227–235, Feb. 2010. DOI: 10.1088/0004-637X/710/1/227. arXiv: 0911.3064 [astro-ph.HE].
- [118] N. M. McClure-Griffiths, A. J. Green, J. M. Dickey, B. M. Gaensler, R. F. Haynes, and M. H. Wieringa, “The Southern Galactic Plane Survey: The Test Region,” *The Astrophysical Journal*, vol. 551, no. 1, pp. 394–412, Apr. 2001. DOI: 10.1086/320095. arXiv: astro-ph/0012302 [astro-ph].
- [119] B. M. Gaensler, J. R. Dickel, and A. J. Green, “G328.4+0.2: A Large and Luminous Crab-like Supernova Remnant,” *The Astrophysical Journal*, vol. 542, no. 1, pp. 380–385, Oct. 2000. DOI: 10.1086/309522. arXiv: astro-ph/0003342 [astro-ph].
- [120] J. R. Dickel, D. K. Milne, and R. G. Strom, “Radio Emission from the Composite Supernova Remnant G326.3-1.8 (MSH 15-56),” *The Astrophysical Journal*, vol. 543, no. 2, pp. 840–849, Nov. 2000. DOI: 10.1086/317160. arXiv: astro-ph/0007230 [astro-ph].
- [121] D. H. Clark, J. L. Caswell, and A. J. Green, “408 and 5000 MHz Observations of 28 New Galactic Supernova Remnants,” *Australian Journal of Physics Astrophysical Supplement*, vol. 37, pp. 1–38, Sep. 1975.
- [122] J. D. Gelfand, B. M. Gaensler, P. O. Slane, D. J. Patnaude, J. P. Hughes, and F. Camilo, “The Radio Emission, X-Ray Emission, and Hydrodynamics of G328.4+0.2: A Comprehensive Analysis of a Luminous Pulsar Wind Nebula, Its Neutron Star, and the Progenitor Supernova Explosion,” *The Astrophysical Journal*, vol. 663, no. 1, pp. 468–486, Jul. 2007. DOI: 10.1086/518498. arXiv: 0704.0219 [astro-ph].
- [123] A. Comrie *et al.*, *CARTA: The Cube Analysis and Rendering Tool for Astronomy*, version 2.0.0, Jun. 2021. DOI: 10.5281/zenodo.4905459. [Online]. Available: <https://doi.org/10.5281/zenodo.4905459>.
- [0] R. M. Cutri *et al.*, “VizieR Online Data Catalog: 2MASS All-Sky Catalog of Point Sources (Cutri+ 2003),” *VizieR Online Data Catalog*, II/246, pp. II/246, Jun. 2003.

- [0] V. V. Gvaramadze, A. Y. Kniazev, and S. Fabrika, “Revealing evolved massive stars with Spitzer,” *Monthly Notices of the Royal Astronomical Society*, vol. 405, no. 2, pp. 1047–1060, Jun. 2010. DOI: 10.1111/j.1365-2966.2010.16496.x. arXiv: 0909.0458 [astro-ph.SR].
- [0] D. R. Mizuno *et al.*, “A Catalog of MIPS GAL Disk and Ring Sources,” *The Astronomical Journal*, vol. 139, no. 4, pp. 1542–1552, Apr. 2010. DOI: 10.1088/0004-6256/139/4/1542. arXiv: 1002.4421 [astro-ph.GA].
- [0] J. A. Toalá, M. A. Guerrero, G. Ramos-Larios, and V. Guzmán, “WISE morphological study of Wolf-Rayet nebulae,” *Astronomy & Astrophysics*, vol. 578, A66, A66, Jun. 2015. DOI: 10.1051/0004-6361/201525706. arXiv: 1503.06878 [astro-ph.SR].
- [0] M. Güdel, “Stellar Radio Astronomy: Probing Stellar Atmospheres from Protostars to Giants,” *Annual Reviews of Astronomy & Astrophysics*, vol. 40, pp. 217–261, Jan. 2002. DOI: 10.1146/annurev.astro.40.060401.093806. arXiv: astro-ph/0206436 [astro-ph].
- [0] A. Ingallinera *et al.*, “High-resolution Very Large Array observations of 18 MIPS GAL bubbles,” *Monthly Notices of the Royal Astronomical Society*, vol. 463, no. 1, pp. 723–739, Nov. 2016. DOI: 10.1093/mnras/stw2053. arXiv: 1609.00003 [astro-ph.GA].
- [0] G. Hobbs *et al.*, “The Parkes multibeam pulsar survey - IV. Discovery of 180 pulsars and parameters for 281 previously known pulsars,” *Monthly Notices of the Royal Astronomical Society*, vol. 352, no. 4, pp. 1439–1472, Aug. 2004. DOI: 10.1111/j.1365-2966.2004.08042.x. arXiv: astro-ph/0405364 [astro-ph].
- [0] R. N. Manchester, G. B. Hobbs, A. Teoh, and M. Hobbs, “The Australia Telescope National Facility Pulsar Catalogue,” *The Astronomical Journal*, vol. 129, no. 4, pp. 1993–2006, Apr. 2005. DOI: 10.1086/428488. arXiv: astro-ph/0412641 [astro-ph].
- [0] J. Binney and E. Vasiliev, “Self-consistent models of our Galaxy,” *Monthly Notices of the Royal Astronomical Society*, vol. 520, no. 2, pp. 1832–1847, Apr. 2023. DOI: 10.1093/mnras/stad094. arXiv: 2206.03523 [astro-ph.GA].
- [0] K. S. Long *et al.*, “The Chandra ACIS Survey of M33: X-ray, Optical, and Radio Properties of the Supernova Remnants,” *The Astrophysical Journal Supplement*, vol. 187, no. 2, pp. 495–559, Apr. 2010. DOI: 10.1088/0067-0049/187/2/495. arXiv: 1002.1839 [astro-ph.GA].

# Appendix A: Known Supernova Remnants

This appendix is a reproduction of Appendix A from Ball et al. (2023). In Figures A.1 to A.7 we present images of the known SNRs in the EMU/POSSUM Galactic pilot II field. Here we show the 933 MHz radio images from ASKAP, the same region in the MIR at 12  $\mu\text{m}$  using data from WISE, and a composite image with radio emission shown in red and MIR in blue.

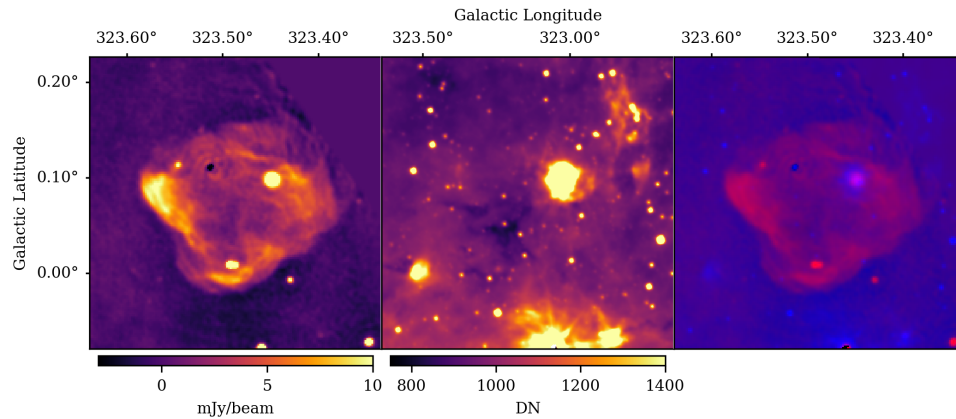


Figure A.1: G323.5+0.1

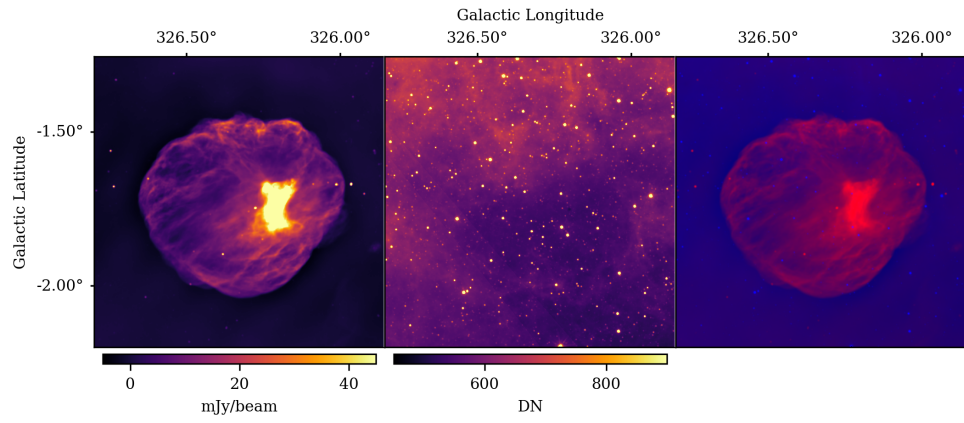


Figure A.2: G326.3–1.8

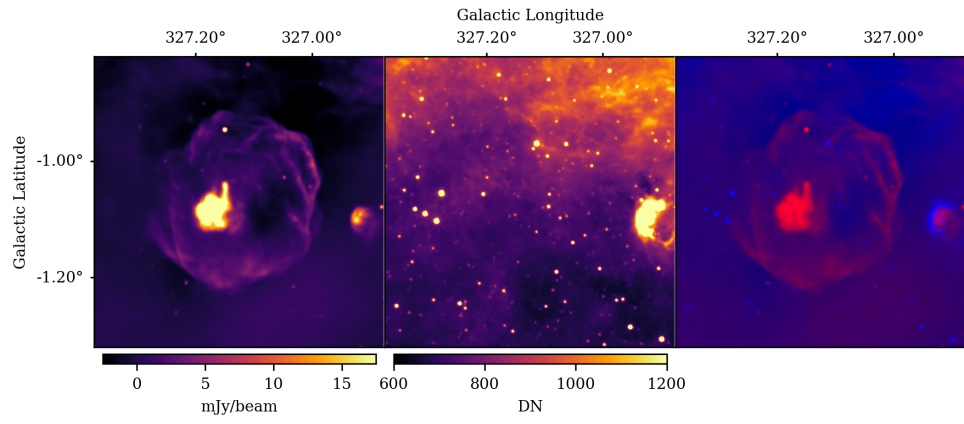


Figure A.3: G327.1–1.1

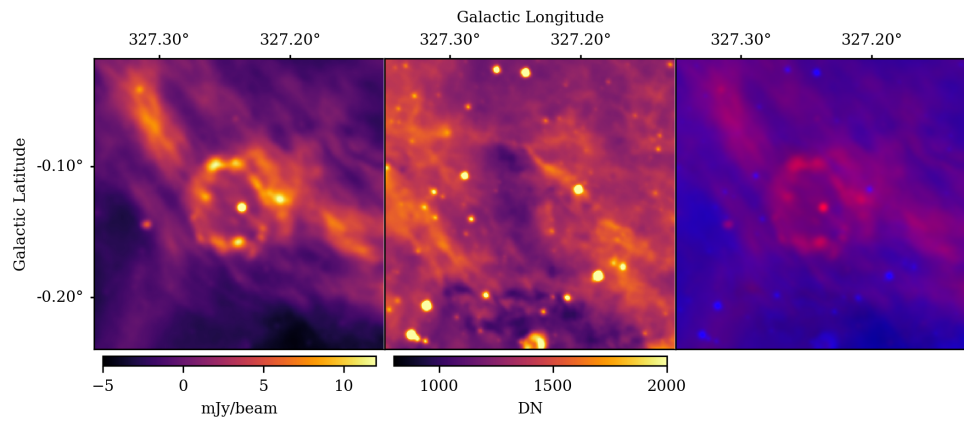


Figure A.4: G327.2–0.1

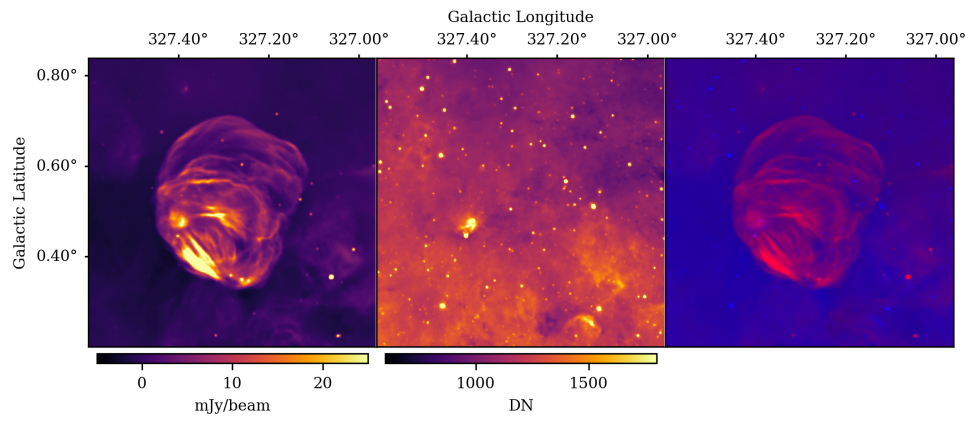


Figure A.5: G327.4+0.4

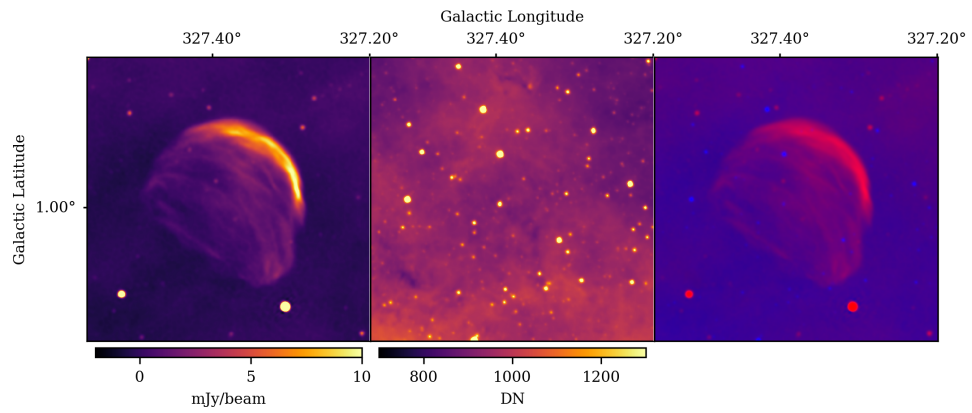


Figure A.6: G327.4+1.0

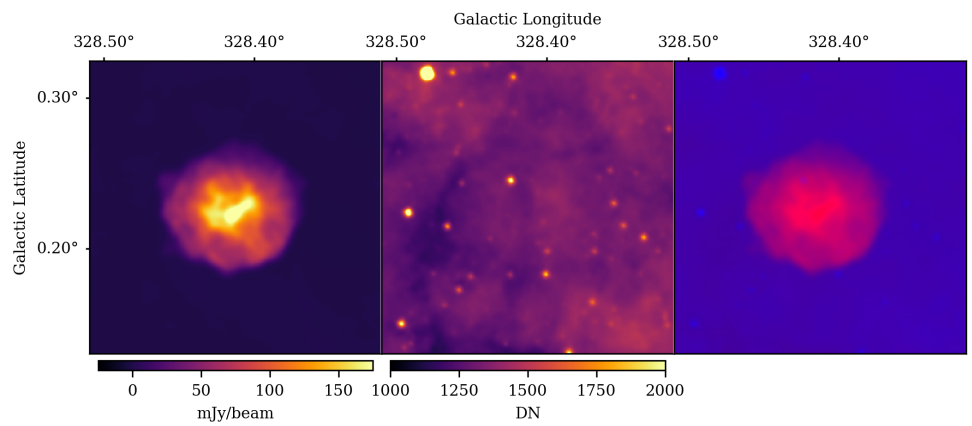


Figure A.7: G328.4+0.2

# Appendix B: Supernova Remnant Candidates

This appendix is a reproduction of Appendix B from Ball et al. (2023). In Figures B.1 to B.19 we present images of the SNR candidates in the EMU/POSSUM Galactic pilot II field using the same format described in Appendix A. These are sources that do not appear in the Green [2] radio SNR catalogue.

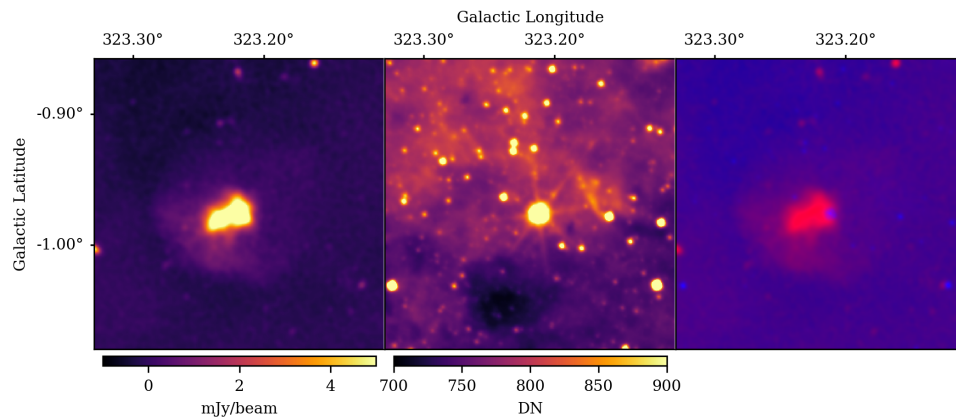


Figure B.1: G323.2-1.0

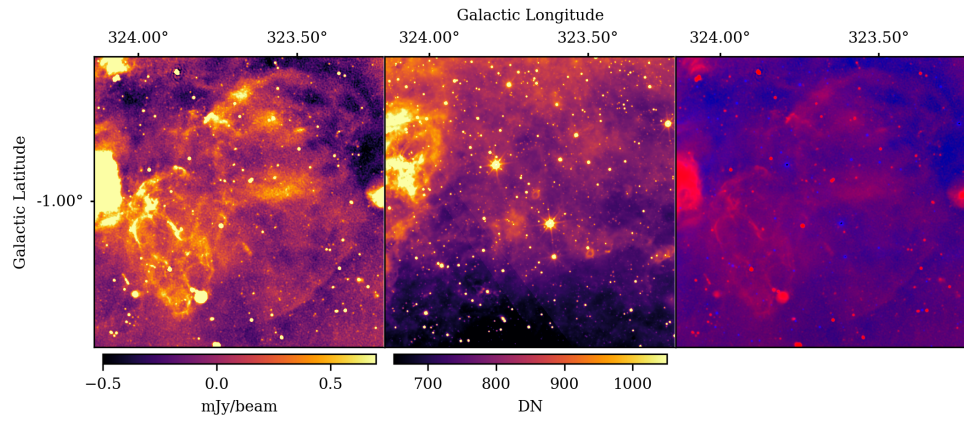


Figure B.2: G323.6-1.1, G323.6-0.8, G323.9-1.1

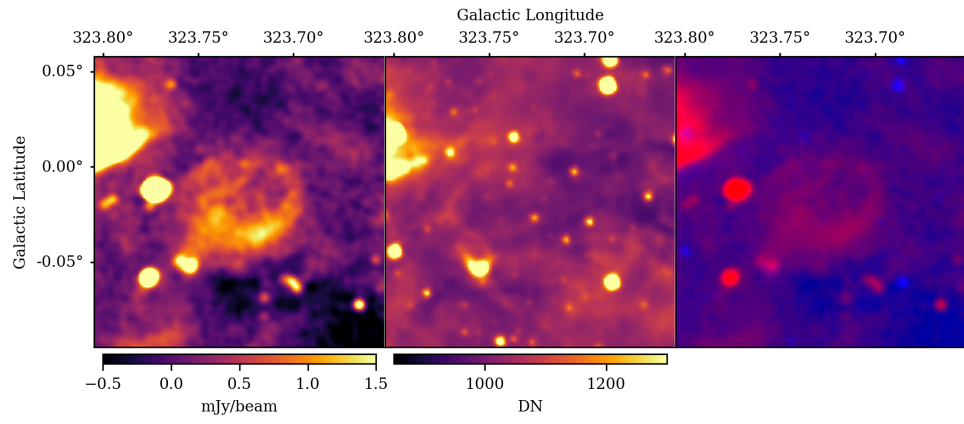


Figure B.3: G323.7+0.0

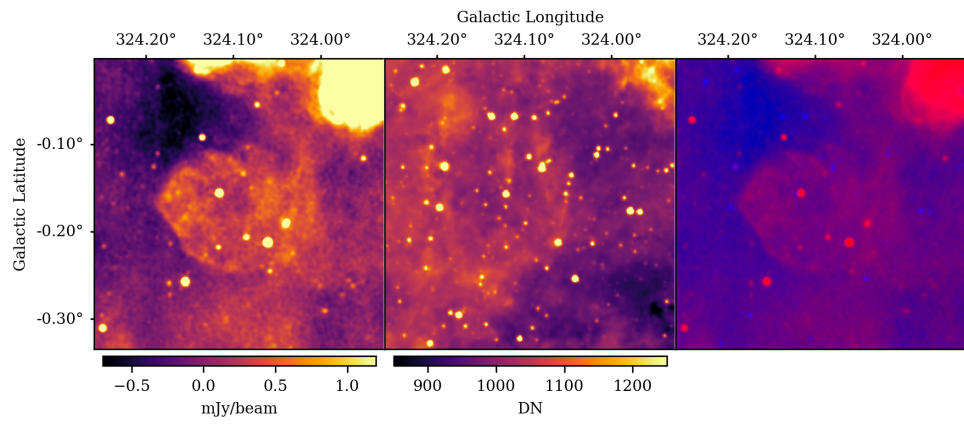


Figure B.4: G324.1-0.2

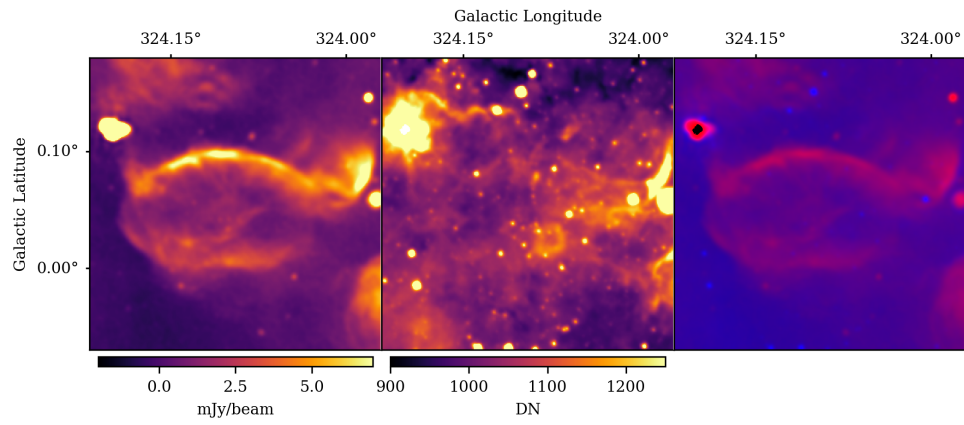


Figure B.5: G324.1+0.0

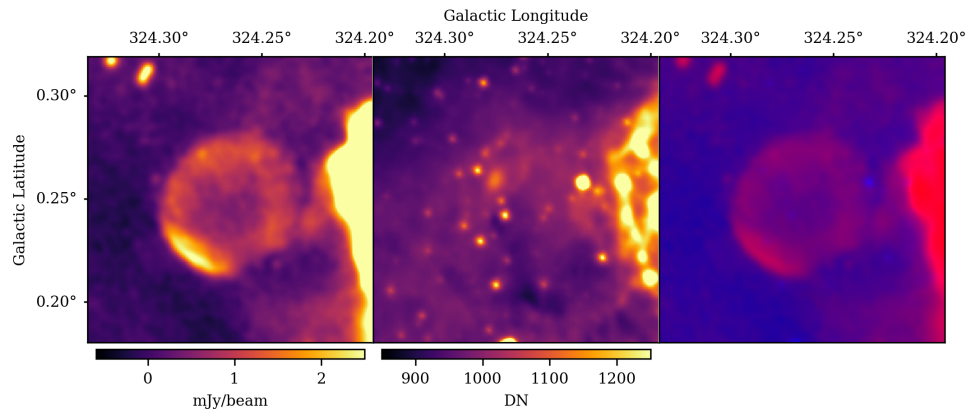


Figure B.6: G324.3+0.2

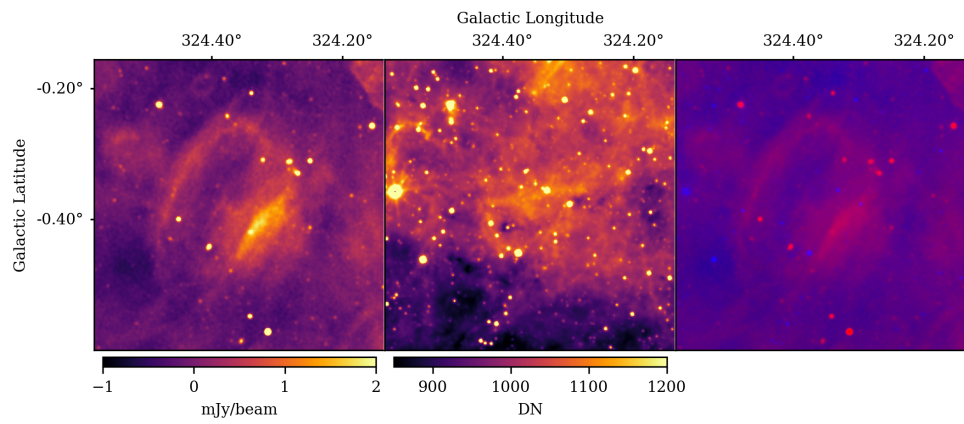


Figure B.7: G324.4-0.4

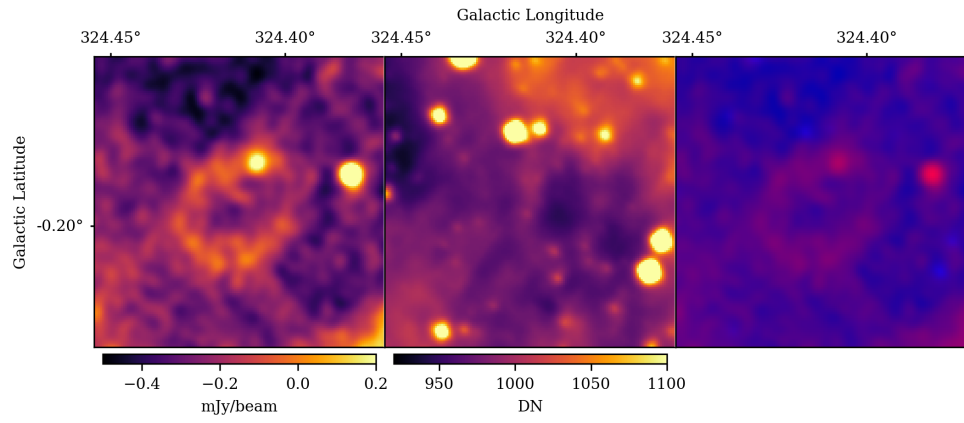


Figure B.8: G324.4-0.2

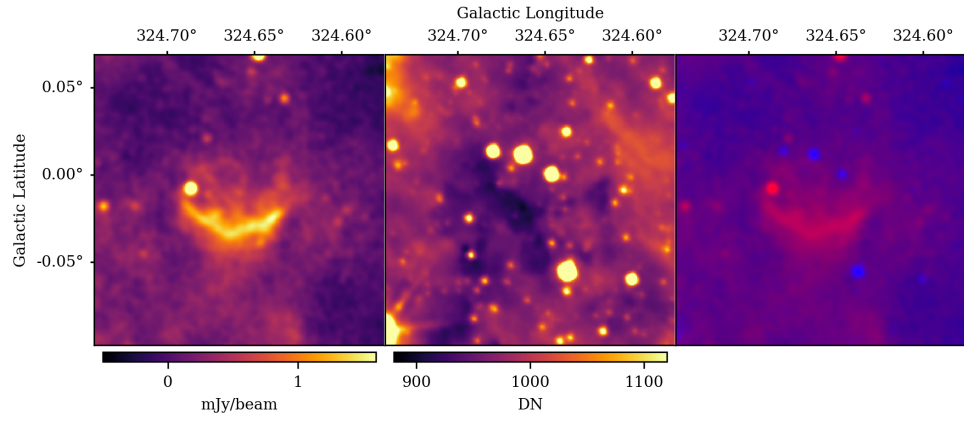


Figure B.9: G324.7+0.0

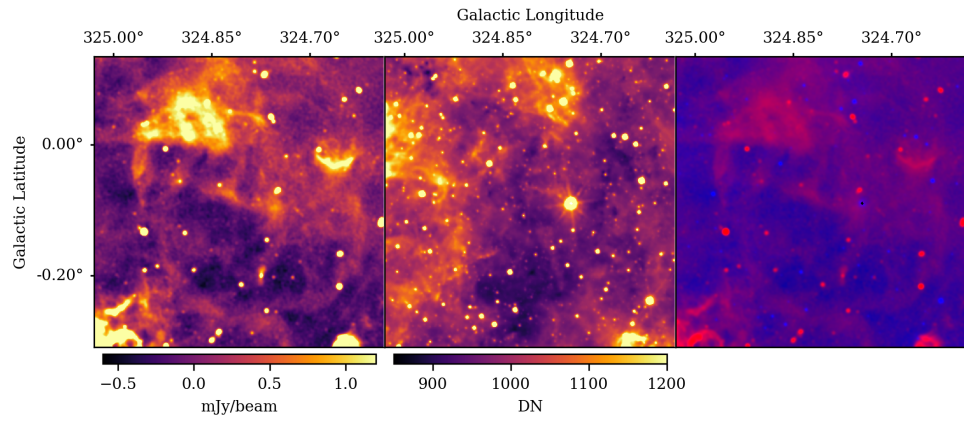


Figure B.10: G324.8-0.1

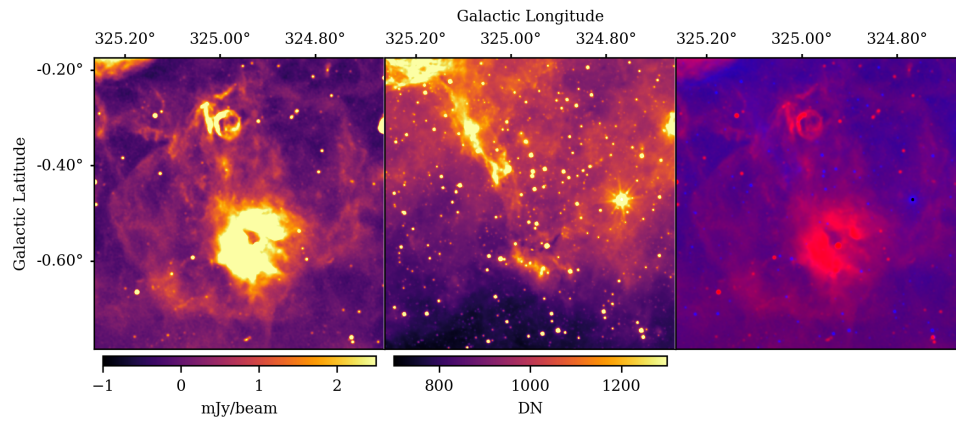


Figure B.11: G325.0-0.5

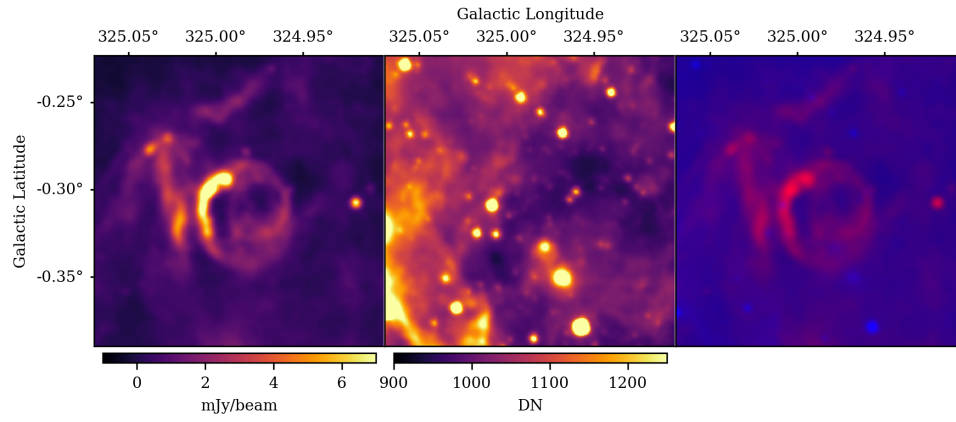


Figure B.12: G325.0-0.3

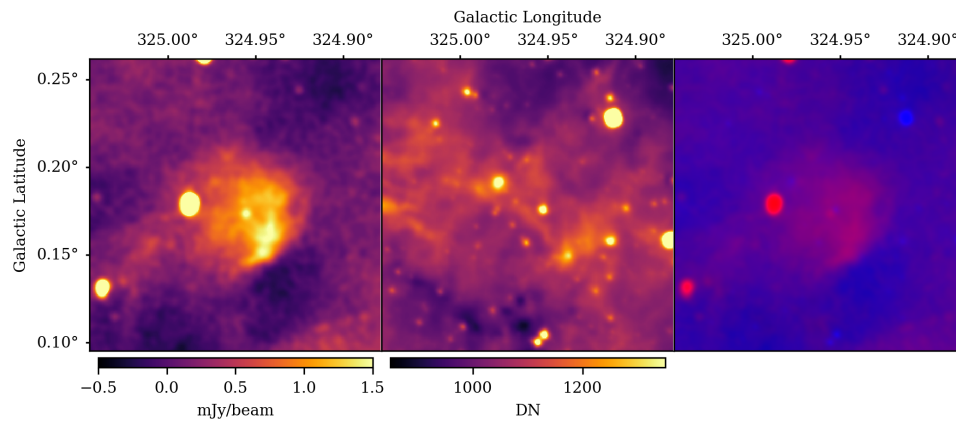


Figure B.13: G325.0+0.2

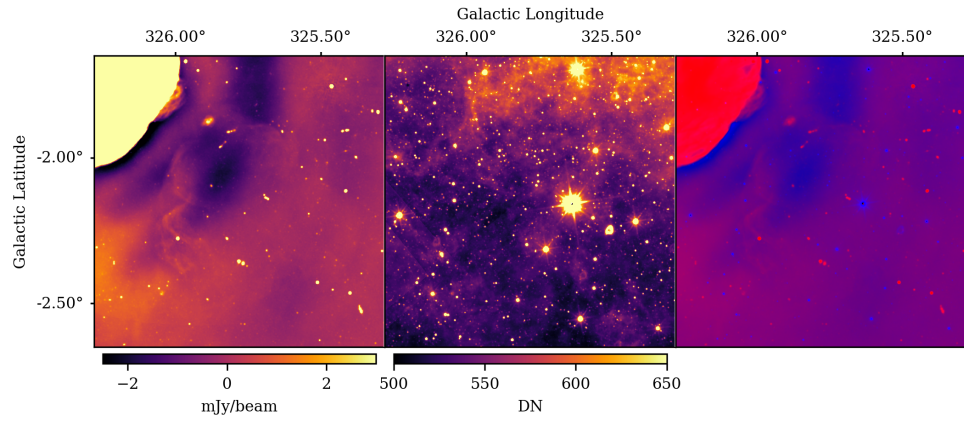


Figure B.14: G325.8-2.1

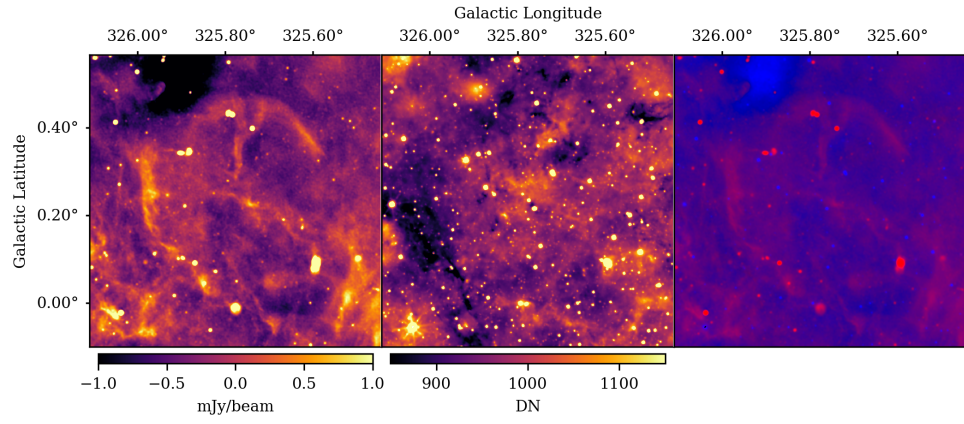


Figure B.15: G325.8+0.3

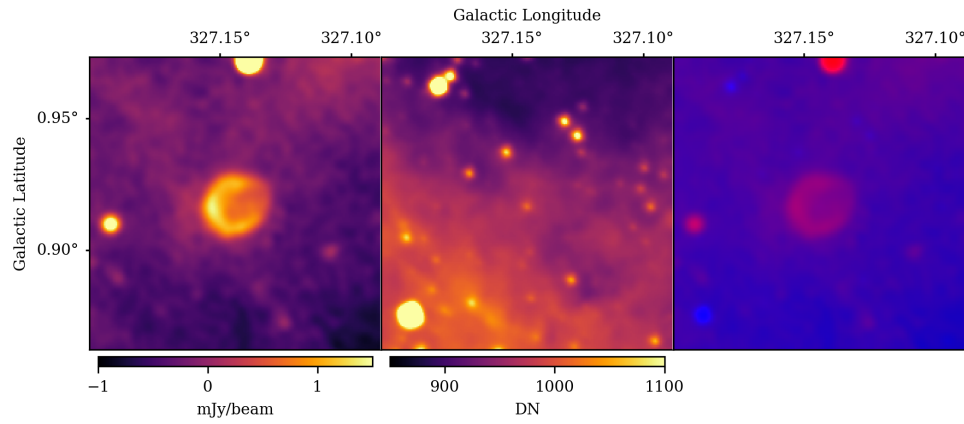


Figure B.16: G327.1+0.9

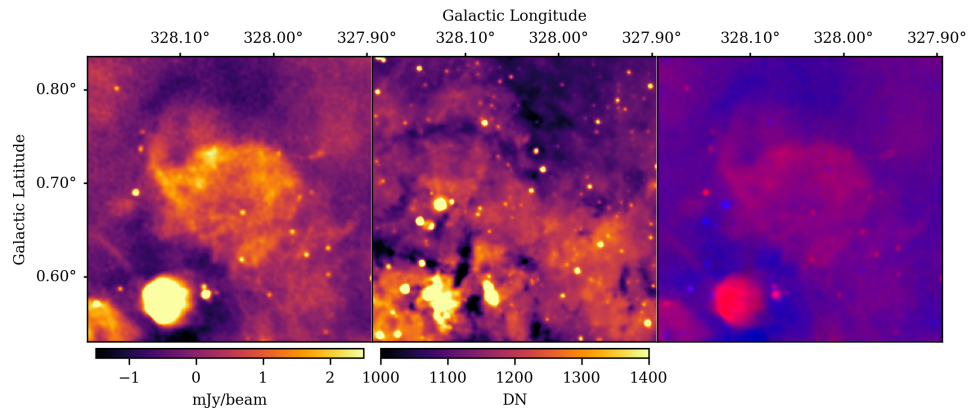


Figure B.17: G328.0+0.7

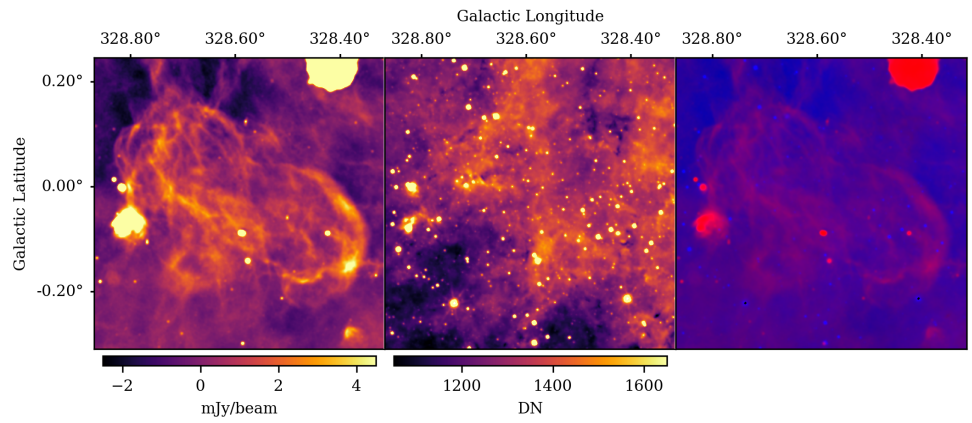


Figure B.18: G328.6+0.0

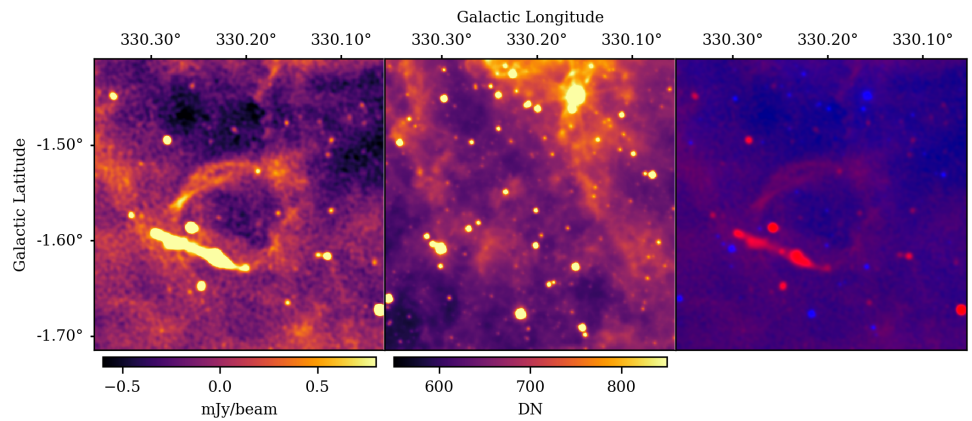


Figure B.19: G330.2-1.6